

Chapter 6

Electronic Effects in Metal-Support Interaction of Pt Catalysts under Reaction Conditions and the Nature of the Active Site of D₂-Ethene Reaction

Transition metal oxide supports have been used as a carrier of the dispersed metal particles in order to stabilize the small clusters. Achieving stabilization and high surface area have been two main roles of the carriers so far. It is, however, inevitable that an interaction which could influence the catalysis should arise from the combination of two phases. One of the most manifesting discovery of this kind of interactions is the strong metal-support interaction (SMSI) for the noble metal on easily reducible oxides such as TiO_2 , Nb_2O_5 , Ta_2O_5 and V_2O_5 . It has originally reported as complete suppression of hydrogen adsorption without significant particle enlargement. [1, 2] There are several other kinds of metal-support interactions in the literature whose origin, appearance and the effect on catalysis have provided many topics in the field. [3-5] According to Bond, metal-support interactions could be classified into three groups.[3] That is, strong (SMSI), medium (MMSI) and weak (WMSI) metal-support interactions. The criteria of this classification is not precise and he exemplified TiO_2 and Nb_2O_5 for the first class, zeolite for the second class and SiO_2 for the third class.

The alternation of the electronic structure accompanied by the support effect should be always taken into account since the metal particles of a supported catalyst are not bare metal particles but inevitably contacts with the different phase. In this meaning, the modification of metal electronic state is the most essential and universal effect brought about by the support. Thus it could be a convenient scale for the metal-support interaction.

The reducibility of the support has been showing its possibility to control the catalysis which is attained by

changing reduction temperature of catalyst and it has been one of the topics gathering most attention. One good example is SMSI catalysts and other supports --- V_2O_5 [6,7], ZrO_2 [8], rare-earth oxides [9, 10] and so on --- have been reported to be reduced under some reduction condition and to influence on the adsorption mode, activity or selectivity. These supports are usually less reducible than TiO_2 and the literature is smaller so far. Mode of interaction between metal particles and reduced support could be a coverage of the metal surface with partially reduced support oxide or electron donation from cation center. For SMSI system both characteristics have been reported.

For the small particle system, X-ray adsorption near edge structure (XANES) is preferable to X-ray photoemission spectroscopy (XPS) in terms of uncoupling the final state change from initial state change. Further, it is measurable even with the reaction gas in the system so that the *in situ* measurement is possible. White lines appearing at the edge position of Pt have been widely used for determining the density of unoccupied d-state of Pt catalysts. It is sensitive enough to monitor the change in d-state which arises from the support [11-13], particle size [12] and adsorption [14, 15]. This chapter intends to elucidate the electronic state of reducible oxide supported Pt catalyst to present a new criterion of support effects. In addition to the vacuum environment, the influence on the elementary steps of ethene hydrogenation is investigated with XANES measurement under reaction condition to compare with that brought by sodium of Na/Pt/SiO₂ in chapter 5. The electronic state of Pt surface should be perturbed by reactant adsorption and the perturbation will have an effect on other steps of the catalytic reaction. In this way, the measurement of electronic

state under reaction condition is essential for the elucidation of the support effect on the catalysis.

The active site and the environment are defined not only by the electronic state but also their microscopic structural feature. Reaction mechanism of the catalysis often involves essence of the nature of the active site. D_2 -ethene reaction has been investigated in terms of the reflection of the structural characteristics of the catalyst as demonstrated in chapter 3, 4, 5 and ref 15. The advantage of this method is measuring the dynamic state of the surface.

6.1 Experimental

Pt/TiO₂, Pt/Nb₂O₅, Pt/Y₂O₃, Pt/V₂O₅ and Pt/ZrO₂ catalysts were prepared by incipient wetness method of TiO₂ (Nippon Aerosil P-25, surface area: 80 m²·g⁻¹), Nb₂O₅ (Soekawa Chemical Co.,Ltd., 99.5%), Y₂O₃ (Soekawa Chemical Co.,Ltd. 99.99%), V₂O₅ (Soekawa Chemical Co., Ltd., 99%) and ZrO₂ (Soekawa Chemical Co.,Ltd., 99%), respectively, with aqueous solution of H₂PtCl₆·6H₂O (Soekawa Chemical Co.,Ltd. research grade). Each sample was allowed to stand for 24 h and then removed water at 320 K and dried at 393 K before calcination at 773 K. The catalysts thus obtained were stored in the desiccator. The loading of platinum metal was 2.3 % for all catalysts. The small amount of them were mounted in a closed circulating system which can be evacuated below 10⁻⁴ Pa. Then it was oxidized with O₂ at 673 K and reduced at each temperature before catalytic reactions and hydrogen adsorption experiments.

XANES spectra were recorded at BL-7C of Photon Factory, National Laboratory for High Energy Physics (KEK-PF) in the

transmission mode. The samples were prepared in the closed circulating system and transferred with or without gases under consideration to the in-situ X-ray absorption cell.

Data analyses of $L_{2,3}$ edges followed chapter 5.

$\text{CH}_2=\text{CH}_2$ (Takachiho Trading Co., Ltd., 99.9%) was purified by freeze-thaw cycles before use. Hydrogen (Takachiho Trading Co., Ltd. research grade) was purified through a trap at 77 K. $\text{D}_2-\text{CH}_2=\text{CH}_2$ reaction was carried out in the closed circulating system mentioned above and the products were analyzed by gas chromatography. The separation column was VZ-10. No subreactions other than hydrogen addition were observed by mass chromatograph. No catalytic reaction proceeded without hydrogen.

6.2 Results

The amount of the hydrogen adsorbed on the catalysts after the several kinds of pretreatments were summarized in Table 6.1. These values were quite different each other even at low temperature reduction (LTR) in spite of the same loading of the metal. The increase of the reduction temperature T_R caused the decrease of H/Pt. The typical case for this tendency is Pt/TiO₂ which is well-known SMSI catalysts. The value changed from 0.750 at 373 K to 0.001 at 773 K. That of Pt/ZrO₂ was fairly (0.75 at 373 K to 0.60 at 773 K) and Pt/Y₂O₃ was slightly (0.199 at 473 K and 0.185 at 773 K) decreased. The behavior of Pt/V₂O₅ is complicated; once decreased (0.241 to 0.13) then increased (0.13 to 0.193) through the local maximum and finally decreased (0.193 to 0.14).

The reversibility of the high temperature reduction (HTR) was examined by 773 K reduction followed by 673 K oxidation before

373 K reduction. H/Pt were completely reproduced in Pt/V₂O₅ and almost completely in Pt/TiO₂ and partly in Pt/ZrO₂. Pt on Y₂O₃ was not reduced at 373 K. The state of Pt was an oxide as elucidated by XANES spectra mentioned after. This state of the catalyst was also reversible after 773 K reduction - 673 K oxidation - 373 K reduction cycle.

In order to investigate the origin of the H/Pt suppression, kinetical experiment for H/Pt was carried out. Figure 6.1 illustrates the reduction time-dependent profile of the H/Pt for Pt/TiO₂ and Pt/V₂O₅, which showed the significant suppression of hydrogen adsorption through the high temperature reduction. The decrease of H/Pt for both catalysts was proportional to the square root of the reduction time (t_R).

X-ray adsorption edge spectra in the XANES region of Pt/ZrO₂, Pt/TiO₂ and Pt/V₂O₅ the catalysts with several reduction treatment are compared in Figure 6.2 and the calculated parameter f_d is plotted versus reduction temperature of the catalysts (T_R) in Figure 6.3. The unoccupied d-density of Pt in the low temperature region was highest in supported Y₂O₃ catalyst and lowest in V₂O₅. f_d of all these catalysts had decreasing tendency to T_R but the degree was quite different from support to support. The catalysts which showed the large difference in f_d ($\Delta f_d = f_d(\text{LTR}) - f_d(\text{HTR})$) were Y₂O₃ and ZrO₂, and that of moderate difference of f_d were TiO₂ and Nb₂O₅. Little alternation could be observed for Pt/V₂O₅. f_d for Pt/Y₂O₃ reduced at 373 K was 2.39 which is the value comparable to Pt oxides.

Arrhenius plots of ethane formation are shown in Figure 6.4 and kinetic parameters such as activation energy derived from the slope in Figure 6.4 and coefficients in the rate equation 5.5, $r =$

$k_{D_2} P_{D_2} / (1 + K_E P_E)$, were listed in Table 6.2. The rate of formation over all catalysts were fitted well to the equation. Activation energy did not depend on the catalyst and reduction temperature for TiO_2 and Y_2O_3 (ca. 40 kJ·mol⁻¹). Whereas the activation energy of Pt/ZrO₂ for both reduction temperature conditions was significantly large (ca. 120 kJ·mol⁻¹). The change in the coefficients were different in this catalyst, i.e. K_E showed almost no change and k_{D_2} increased when the reduction temperature was high. K_E increased and k_{D_2} decreased for the others. The absolute order for ethene adsorption did not vary much, K_E ranging from $1 \cdot 10^{-4}$ to $1 \cdot 10^{-5}$. The variation of k_{D_2} was more sensitive to the catalyst and the reduction temperature, e.g., ranging from $3.4 \cdot 10^{-3}$ (Y_2O_3) to $6.3 \cdot 10^{-5}$ (TiO_2) for 773 K reduction and from $2.9 \cdot 10^{-4}$ (393 K) to $8.7 \cdot 10^{-4}$ (773 K) for ZrO₂. This suggests that k_{D_2} could be a better probe for the surface state of the catalyst.

Figure 6.5 shows the f_3 of Pt particles on the support under ethene gas. The surface of the catalysts are suggested to be covered with ethene since the kinetics of the reaction followed equation 5.5. Thus the ethene in the gas phase is a good model for the steady-state reaction condition of the catalyst surface. With ethene in the gas phase, f_3 in Pt/ZrO₂ increased and the difference was larger as the reduction temperature was higher while f_3 in Pt/TiO₂ and Pt/Y₂O₃ decreased and the difference was smaller as the reduction temperature was higher. f_4 for Pt/V₂O₅ was the same as in vacuum.

The contents of the formed ethane is listed in Table 6.3. The order of the isotopes was regularly smeared as $d_2 > d_1 > d_0$ for Pt/TiO₂ and Pt/V₂O₅ reduced at 393 K, and Pt/Y₂O₃ and Pt/ZrO₂ reduced at both temperatures. It was not smeared and population

was concentrated in d_2 for Pt/V₂O₅ at 773 K reduction. Unusual distribution, $d_2 \geq d_0 > d_1$, was observed in Pt/TiO₂ reduced at 773 K.

The exchange reaction between H of ethene and deuterium occurred during ethane formation and the rates are presented with that of ethane formation in Table 6.4. The rates were normalized with the number of the surface Pt atoms which were estimated by H/Pt except 773 K-reduced Pt/TiO₂. Exchange reaction was suppressed by the high temperature reduction in all catalysts but the relative rate to the ethane formation was increased in Pt/V₂O₅ and Pt/TiO₂. Both exchange and deuteration reaction was drastically slow on 773 K reduced Pt/V₂O₅ comparing to the other catalysts.

Figure 6.6 illustrates the reduction time dependence of the d_1 -ethane formation rate for Pt/TiO₂. d_1 -ethane and d_2 -ethane formation showed the square root-dependence of reduction time of the catalyst (t_R) similarly to the H/Pt in Figure 6.1. On the contrary, d_0 -ethane has the maximum at $t_R = 22$ min and, consequently, the rate as a function of t_R had the term of $t_R^{-1/2}$ ($\propto 1/2$) in addition to $t_R^{1/2}$.

6.3 Discussion

(i) Electronic effects of the support and the classification of the metal-support interactions

The electronic state of platinum is easily influenced by the environment of the particle. One of the most easily and effective method to control it is to change the chemical state of the support. The supports in this study are reducible and the

oxidation number of the metal composing the supports is controllable by the reduction condition of the catalysts. Other effects also can be brought about, which are to be illustrated as chemical or structural transformation of the particle. It is sometimes more notable than electronic modification. The suppression of hydrogen adsorption by high temperature reduction (at around 773 K) has been studied especially in so-called SMSI catalysts, such as TiO_2 , Nb_2O_5 and V_2O_5 . The origin of hydrogen adsorption suppression has been agreed to be the decoration of the metal with the reduced support-oxide. One of the criteria of the migration of the support to metal surface is the thermal diffusion of the support to the metal surface, which reflects H/Pt decreasing as a square root of reduction time. Figure 6.1 shows the well fitted linear relation between H/Pt and $t_R^{1/2}$ as for $\text{Pt}/\text{V}_2\text{O}_5$ and Pt/TiO_2 . Thus the H/Pt decrease of $\text{Pt}/\text{V}_2\text{O}_5$ and Pt/TiO_2 by the high temperature reduction in Table 6.1 is attributed to the migration of support oxide. The reducibility of the support in terms of the decoration of the metal surface is different. That of $\text{Pt}/\text{Nb}_2\text{O}_5$ is faster than these supports even at 500 K reduction as shown in Figure 8.1. Thus for supported Pt , $\text{Nb}_2\text{O}_5 > \text{TiO}_2 > \text{V}_2\text{O}_5$ is derived from Figure 6.1 and Table 6.1. These catalysts satisfy the reversibility of hydrogen adsorption capacity after 773 K reduction - oxidation - 393 K reduction, which is commonly observed in SMSI catalysts.

For Y_2O_3 and ZrO_2 , the suppression of hydrogen adsorption is slight, comparing to SMSI supports. It is agreed with the literature and it has often been treated as medium metal-support interaction --- hydrogen adsorption or the catalysis are significantly changed by the high temperature reduction. Reduction of the support has been reported in Pt/ZrO_2 [9] to form

Pt-Zr bond at higher temperature than in this study. It is, however, ambiguous whether the decrease of H/Pt results from the decoration of the metal surface because of the small difference between LTR and HTR. The complicated reduction profile of Pt/V₂O₅ agrees with the literature in which its origin has been attributed to the formation of the vanadium bronze [7].

f_d depends on the particle size of Pt as demonstrated in chapter 5. Thus the comparison of f_d for different particle size, such as Pt/Y₂O₃ and Pt/ZrO₂ has serious limitation. The focus should be on the effect of the reduction temperature because the particle size did not change significantly even when T_R was high. The difference of f_d between LTR and HTR ($\Delta f_d = f_d$ (LTR) - f_d (HTR)) is understandable in terms of the reducibility of the supports. The supports in the discussion can become more or less metallic when reduced and, consequently, the charge can delocalize between two phases. V₂O₅ is metallic without reduction (resistibility: $\rho/\Omega\text{cm} = 1 \cdot 10^{-3}$ at 300 K [16]) and it remains in metallic state through V_nO_m ($\rho = 1 \sim 3 \cdot 10^{-3}$ except V₅O₁₁ when $2m > n > 1.5m$). Thus the electrons may easily delocalize between d-state of Pt particles and V₂O₅ and the degree does not change through the reduction temperature examined. ZrO₂ is an insulator ($\rho = 1 \cdot 10^{12}$, monoclinic) and the reducibility has been reported to make an alloy with Pt on Pt/ZrO₂ at high temperature [9]. The stoichiometry at 773 K reduction was not measurable and, consequently, the extent of the reduction is suggested to be within the vicinity of the Pt particles. Thus the electrons transferred from the support to metal particles should be restricted in the region where the reduction extended. The charge should be strongly localized. It is suggested that large Δf_d observed for Pt/ZrO₂ results from the

charge donation of the reduced zirconium oxide covering the bottom of Pt particle. Y_2O_3 may belong to the same class. TiO_2 is also an insulator ($\rho = 1.2 \cdot 10^{10}$ at 800 K, for rutile) but it is well known that it is easily reduced to be TiO_n ($n < 2$) and the extent of reduction is measurable with evolving H_2O during catalyst preparation. Most of all TiO_n are metallic at room temperature. Thus the state of the support oxide surrounding Pt particles is the middle between V_2O_5 and ZrO_2 , that is, the reduced region spreads to some extent and the charge extends to it. This might result in Δf_d variation for Pt/ TiO_2 . Nb_2O_5 is likely in the same class.

Metal-support interactions arises from the variation of the reduction temperatures can be reasonably classified into three classes. First, covering the metal particles with support oxide with no f_d changes (Pt/ V_2O_5), second, large change of f_d without coverage of the metal particles (Pt/ ZrO_2 , Pt/ Y_2O_3) and last, covering the metal particles with f_d changes (Pt/ TiO_2 , Pt/ Nb_2O_5). They are originated from the extent of the reduction of the support and the migration of the support.

(ii) The nature of the active site for D_2 -ethene reaction

Correlation between electronic state of the catalyst surface and its catalysis is not so simple that the change in the electronic state can anticipate the reaction kinetics or mechanism. The density of unoccupied d-state of platinum of both Pt/ ZrO_2 and Pt/ Y_2O_3 decreased without decoration of the support oxides through high temperature reduction, *i.e.*, these catalysts quite resemble in metal-support interaction. On the other hand, the changes in kinetic parameters were different. The activation

energy of ethane formation was virtually independent of the reduction temperature. The increase of K_F , observed in Pt/ Y_2O_3 in Table 6.2, implies the promotion of ethene adsorption. And the increase of $k_{0,2}$, observed in Pt/ ZrO_2 , suggests the promotion of deuterium dissociative adsorption which is the rate-determining step for ethane formation.

It is likely that these kinetical alteration is related with the electronic state during the reaction, that is, the density of unoccupied d-state of Pt under reaction condition decreased on Pt/ ZrO_2 and increased on Pt/ Y_2O_3 (Figure 6.5). This modification must be caused by donation or acceptance of electron by ethene π -state. Ethene on Pt/ Y_2O_3 must donate electron to Pt rather than accept and is suggested to have positive charge. Similarly, ethene on Pt/ ZrO_2 must accept electron and is suggested to have negative charge during the reaction. Chapter 5 showed the suppression of ethene adsorption by over π -backdonation of electron by Na through Pt surface. This explanation is applicable to the case of ZrO_2 . On the contrary, on Pt/ Y_2O_3 , donating electron to Pt might cause the strong adsorption of ethene comparing to D_2 . This might be caused by the adsorption site on Pt difference (e.g. atomic arrangement of the site and/or the atomic coordination number of site) between them.

It is shown that the electronic modification of catalysts in vacuum cannot tell the influence on the catalyses. In fact, ZrO_2 and Y_2O_3 had the same kind of high temperature reduction effect, electron donating to platinum particle, but the kinetics of ethane formation changes differently. What is related with the kinetics of ethane formation is not only the static state of Pt but also the electronic state under the reaction condition.

The rate of exchange reaction were suppressed by 773 K

reduction for Pt/Y₂O₃ which might result from the strong adsorption of ethene which is difficult to desorb. The activation energies and the isotope distribution of ethane were rather insensitive to the electronic modification of the catalysts.

The profile of the isotope distribution for high temperature-reduced Pt/V₂O₅ represents the character of the oxide catalysts where almost 90 % of the isotopes was d₂-ethane (Table 6.3). Thus it is suggested that the active site of Pt/V₂O₅ has oxide nature of VO and the surface of Pt particle is completely covered with support oxide. Another possibility, that there is bare Pt but the electronic state of the Pt particle makes the Pt surface completely inactive, should be excluded because the f_d is similar to that of 773 K-reduced Pt/ZrO₂ which has sufficient activity. The low activity, whose suppression is higher than that of SMSI-Pt/TiO₂ (Table 6.4), of this catalyst supports this model. It is most likely that the no change in f_d under reaction in Figure 6.5 was caused by not only the delocalization of the charge but also little adsorption of ethene. And the abnormal enhancement of the exchange reaction might be caused by the completely different nature of the active site.

Isotope distribution of formed ethane in high temperature-reduced Pt/TiO₂ was unusual but was similar to Rh/Nb₂O₅ and Ir/Nb₂O₅ (chapter 3). The deuterium distribution are controlled by the quasi-equilibrium between half-hydrogenated state and associative adsorbed state and the surface H/D ratio in steady-state of the reaction. Thus the isotopes should be statistically distributed with a peak at d₂-ethene or, alternatively, d₀-ethene. Appearance of two peaks at d₀- and d₂-ethanes strongly suggests two kinds of reaction site and reaction environments

with different H/D ratio. This is confirmed by the controlling the number of each active site. The surface area of Pt of Pt/TiO₂ decreases according to square root of reduction time, $t_R^{1/2}$, as shown in Figure 6.1 while the boundary of TiO₂ and Pt surface should increase with $t_R^{1/4}$ dependence at the initiation of the migration. The rate of each isotope of ethane should be a polynomial of t_R for Pt/TiO₂ as is demonstrated in Figure 6.6. Only d₀-ethane has $t_R^{1/4}$ term in it and, consequently, it is concluded that only this species generates at the peripheral site in the boundary of TiO₂ on the Pt surface. This is the characteristics of TiO₂ support which differentiate from the other SMSI support. It is unlikely that d₁- and d₂-ethane also formed on site II (peripheral site) but follow the rate equation including $[S_1]^n$ ([bare metal site]ⁿ).

The small difference in f_d under the reaction condition on Pt/TiO₂ (Figure 6.5) may come from the poor availability of the Pt surface because of the decoration by the support suboxide. Thus the correlation between f_d and kinetic parameters cannot be elucidated similarly to Pt/V₂O₅.

6.4 Summary

The electronic modification of the density of 5d-state of Pt by the reduction temperature strongly depends on the support. ZrO₂ and Y₂O₃ donates charge according as increasing reduction temperature without migration of the support oxides. It is more dramatically than TiO₂ and Nb₂O₅ which are known as SMSI supports. This might be because the region the reduction extends is restricted in the vicinity of the Pt particles. V₂O₅ is independent of the reduction temperature but the decoration by

the support oxide occurs. The active site of D₂-ethene reaction is characterized with kinetic parameters and isotope distributions. Ethene is negatively charged on Pt/ZrO₂ while it is positively charged on Pt/Y₂O₃. Pt/TiO₂ reduced at 773 K has two kinds of active site with different surface H/D ratio in D₂-ethene reaction --- one is the bare metal site of Pt producing d₂-ethane mainly and the other is the peripheral site of TiO₂ producing d₀-ethane. The active site of Pt/V₂O₅ reduced at 773 K has oxide nature, that is, Pt particles may be completely covered with support oxide.

References

1. S.J.Tauster, S.C.Fung, R.L.Garten, *J. Am. Chem. Soc.*, **100**, 170 (1978).
2. S.J.Tauster, S.C.Fung, *J. Catal.* **55**, 29 (1978).
3. G.C.Bond, in "Metal-Support and Metal-Additive Effects in Catalysis", (B.Imelik, C.Naccache, G.Coudurier, H.Praliaud, P.Meriaudeau, P.Gallezot, G.A.Martin, J.C.Vedrine, eds.) Elsevier, 1982; Chapter 1.
4. S.J.Tauster, in "Strong Metal-Support Interactions", ACS Symp.Ser, 298, American Chemical Society, Washington DC, 1986.
5. G.L.Haller, D.E.Resasco, *Adv.Catal.*, **36**, 173 (1989).
6. G.C.Bond, M.A.Duarte, *J.Catal.*, **111**, 189 (1988).
7. Y.J.Lin, D.E.Resasco, G.L.Haller, *J.Chem.Soc., Faraday Trans. 1*, **83**, 2091 (1987).
8. C.Dall'Agnol, A.Gervasini, F.Morazzoni, F.Pinna, G.Strukul, L.Zanderighi, *J.Catal.*, **106**, 96 (1985).
9. R.Szymanski, H.Charcosset, P.Gallezot, J.Massardier, L.Tournayan, *J.Catal.*, **97**, 366 (1986).

10. J.S.Rieck, A.T.Bell, *J.Catal.*, **99**, 278 (1986).
11. B.J.McHugh, G.Larsen, G.L.Haller, *J.Phys.Chem.* submitted.
12. D.R.Short, A.N.Mansour, J.W.Cook,Jr., D.E.Sayers, J.R.Katzer, *J.Catal.*, **82**, 299 (1983).
13. P.Gallezot, R.Weber, R.A.Dalla Betta, M.Boudart, *Z. Naturforschung*, **A34**, 40 (1979).
14. T.Fukushima, J.R.Katzer, D.E.Sayers, J.W.Cook,Jr., Proceedings of 10th Int.Congr.Catal., vol. IV, 1984; p.79.
15. P.Nazario, A.Brenner, Proceedings of 10th Int.Congr.Catal. 1988, p.1020.
16. R.C.Weast, "*Handbook of Chemistry and Physics*", CRC Press, 1980.

Table 6.1 H/Pt of Pt particle of the catalysts reduced at several temperature.

T_R / K	373	473	573	673	773	773-673ox-373
Pt/ Y_2O_3		0.199	0.188	0.186	0.185	
Pt/ ZrO_2	0.75	0.71	0.68	0.63	0.60	0.73
Pt/ V_2O_5	0.241	0.13	0.173	0.193	0.14	0.240
Pt/ TiO_2	0.750		0.607		0.001	0.699

773-673ox-373 is 773 K reduction followed by 673 K oxidation and 373 K reduction. The reduction time of the catalyst was 60 min and the hydrogen adsorption experiments were carried out at room temperature. The state of Pt on Y_2O_3 reduced at 373 K was a oxidewhich was evaluated from f_4 and it was reproduced after 773 K reduction followed by 673 K oxidation and 373 K reduction. The other blanks of the table were not measured.

Table 6.2 Kinetic parameters for ethene hydrogenation.

	T_R / K	$E / kJ \cdot mol^{-1}$	K_E / Pa^{-1}	$k_{D_2} / Pa^{-1} \cdot min^{-1}$
Pt/Y ₂ O ₃	573	43	$4.0 \cdot 10^{-4}$	$3.8 \cdot 10^{-3}$
	773	40	$8.7 \cdot 10^{-4}$	$3.4 \cdot 10^{-3}$
Pt/ZrO ₂	373	119	$2.2 \cdot 10^{-4}$	$2.9 \cdot 10^{-4}$
	773	119	$2.0 \cdot 10^{-4}$	$8.7 \cdot 10^{-4}$
Pt/TiO ₂	373	36	$1.6 \cdot 10^{-4}$	$9.5 \cdot 10^{-4}$
	773	39	$1.0 \cdot 10^{-3}$	$6.3 \cdot 10^{-5}$

T_R is the reduction temperature of the catalyst. E is activation energy and K_E and k_{D_2} are the coefficients in equation (4).

Reactions are carried out at around 245 K for Pt/Y₂O₃, 215 K for Pt/ZrO₂ and Pt/TiO₂. The initial pressure of each reactant is $P_{C_2H_2} = P_{D_2} = 1.3$ kPa for the activation energy measurement.

Table 6.3 Percentage distributions of ethane formed in D_2 - $CH_2=CH_2$ reaction on platinum catalyst of several supports with some reduction temperatures (T_R).

	T_R/K	d_0	d_1	d_2	d_3	d_4	d_5	d_6	$\Sigma id_i / 6 \Sigma d_i$
Pt/ Y_2O_3	573	13	35	52	0	0	0	0	23
	773	13	35	52	0	0	0	0	23
Pt/ ZrO_2	373	15	19	48	9	6	3	0	30
	773	16	20	49	8	5	2	0	27
Pt/ V_2O_3	373	14	28	50	6	2	0	0	26
	773	3	5	87	4	1	0	0	33
Pt/ TiO_2	373	12	22	51	12	3	0	0	28
	773	33	13	49	4	1	0	0	21

The reactions were carried out at 223 K and $P_{CH_2=CH_2} = P_{D_2} = 1.3$ kPa. T_R is the reduction temperature of the catalyst.

Table 6.4 The rate of formation of the products in D_2 - $CH_2=CH_2$ reactions.

	T_K / K	r_{ethane}	$r_{d_1} + 2r_{d_2}$	$r_{d_1} + 2r_{d_2} / r_{\text{ethane}}$
Pt/ Y_2O_3	573	0.16	0.12	0.72
	773	0.16	0.026	0.16
Pt/ ZrO_2	393	0.74	0.096	0.13
	773	1.63	0.083	0.051
Pt/ V_2O_5	393	0.31	0.092	0.30
	773	0.0070	0.0091	1.3
Pt/ TiO_2	393	0.63	0.22	0.35
	773	0.025	0.020	0.80

The unit of the rates is min^{-1} which are normalized by the number of surface Pt atoms estimated by H/Pt. The reactions were carried out at 223 K and $P_{C_2H_2=CH_2} = P_{D_2} = 1.3$ kPa. The exchange reaction between deuterium and the hydrogen in $CH_2=CH_2$ were assessed with the rate for the number of deuterium atoms which were found in ethene. Thus it were estimated by the sum of the rate of d_n -ethenes. *: observed at 333 K. **: normalized by H/Pt of 393 K reduced Pt/ TiO_2 .

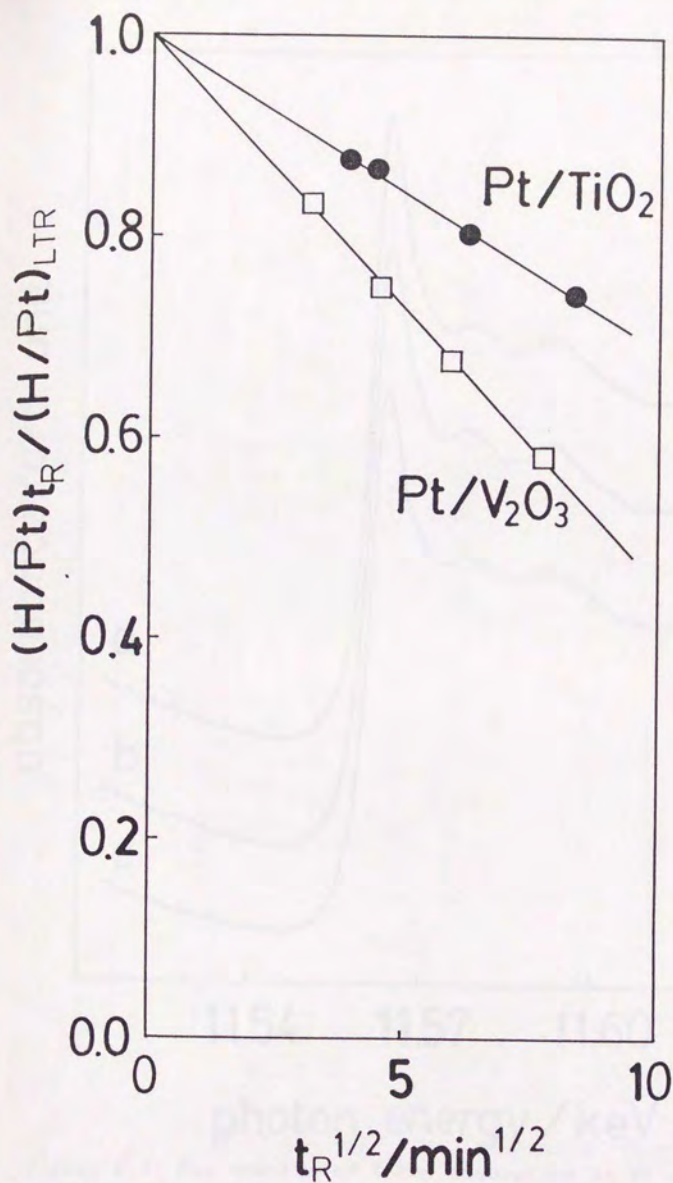


Figure 6.1 The amount of hydrogen adsorption against the reduction time. The ratio to the H/Pt in 373 K reduction is plotted as a function of the square root of reduction time, t_R . ● : Pt/TiO₂ reduced at 623 K, □ : Pt/V₂O₃ reduced at 773 K. Hydrogen adsorption was performed in $P_{\text{H}_2} = 15.0$ kPa at room temperature.

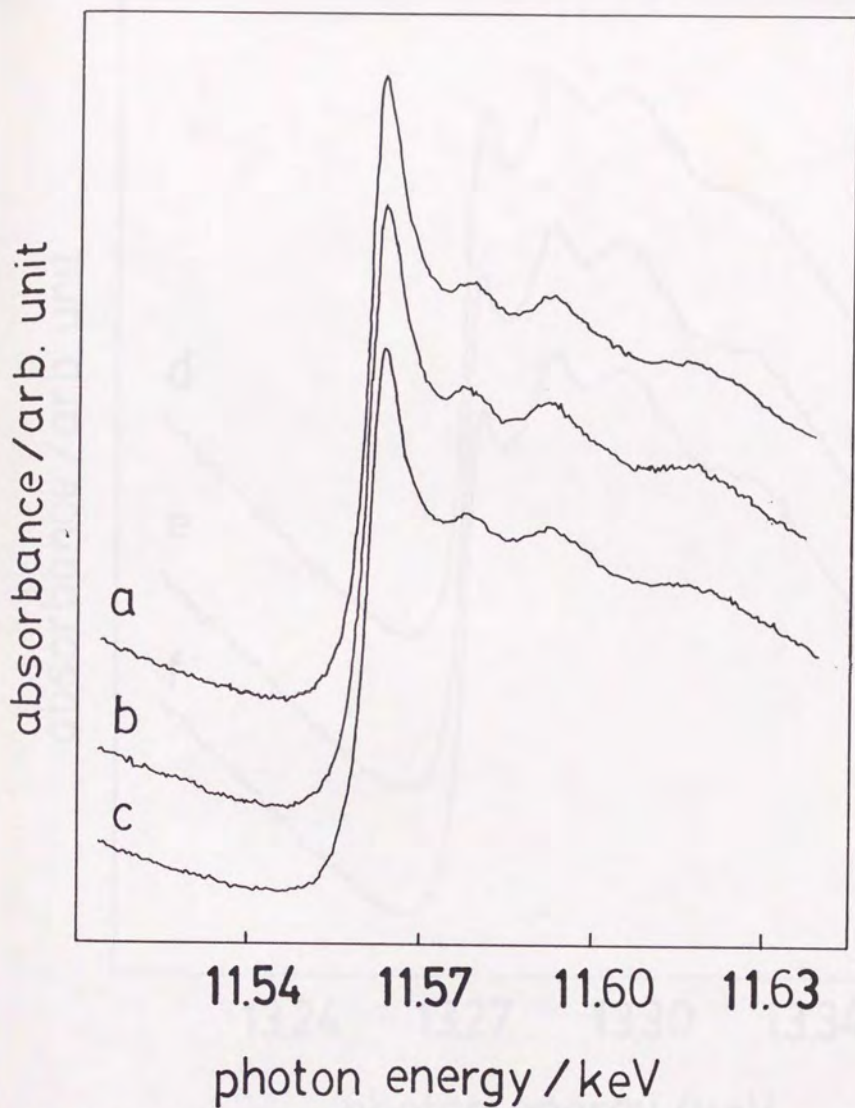


Figure 6.2 Raw spectra of X-ray adsorption in Pt edge region of Pt/ZrO₂ catalysts in vacuum. a: L₃ edge reduced at 373 K, b: L₃ edge reduced at 573 K, c: L₃ edge reduced at 773 K. The photon energy was not adjusted.

absorbance / arb. unit

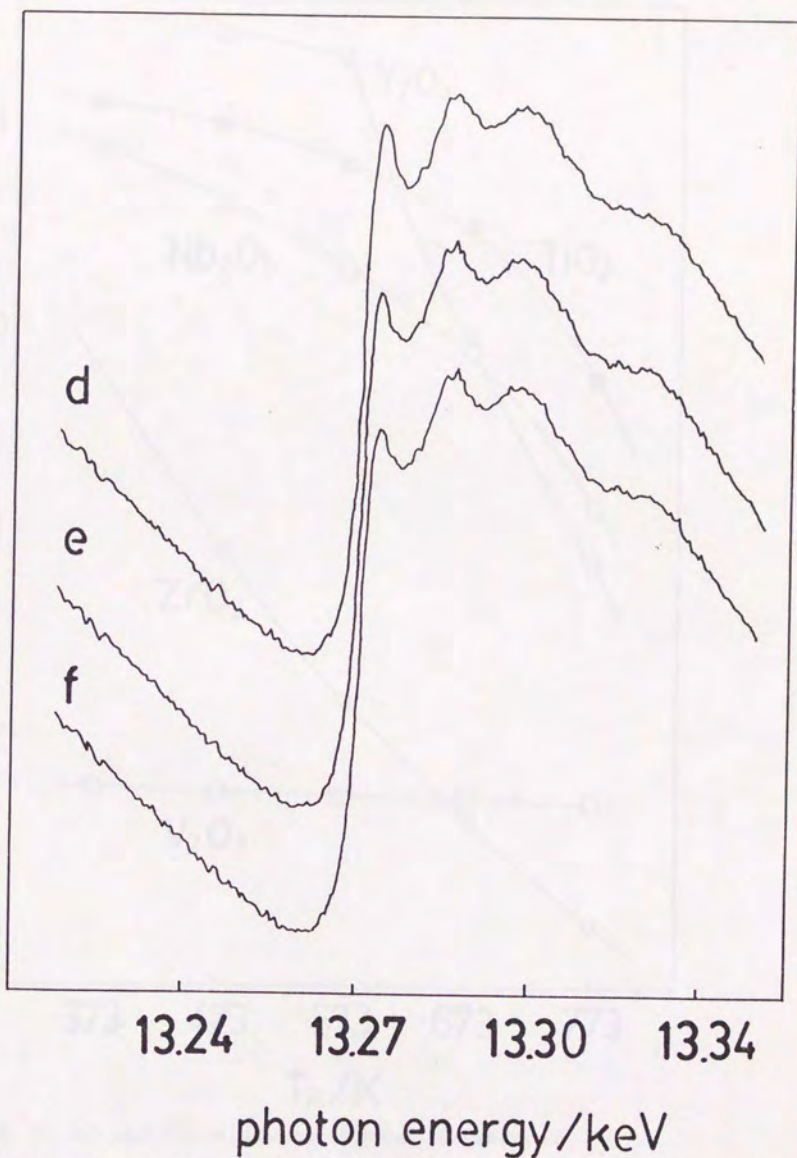


Figure 6.2 Raw spectra of X-ray adsorption in Pt edge region of Pt/ZrO₂ catalysts in vacuum. d: L₂ edgereduced at 373 K, e: L₂ edge reduced at 573 K, f: L₂ edge reduced at 773 K. The photon energy was not adjusted.

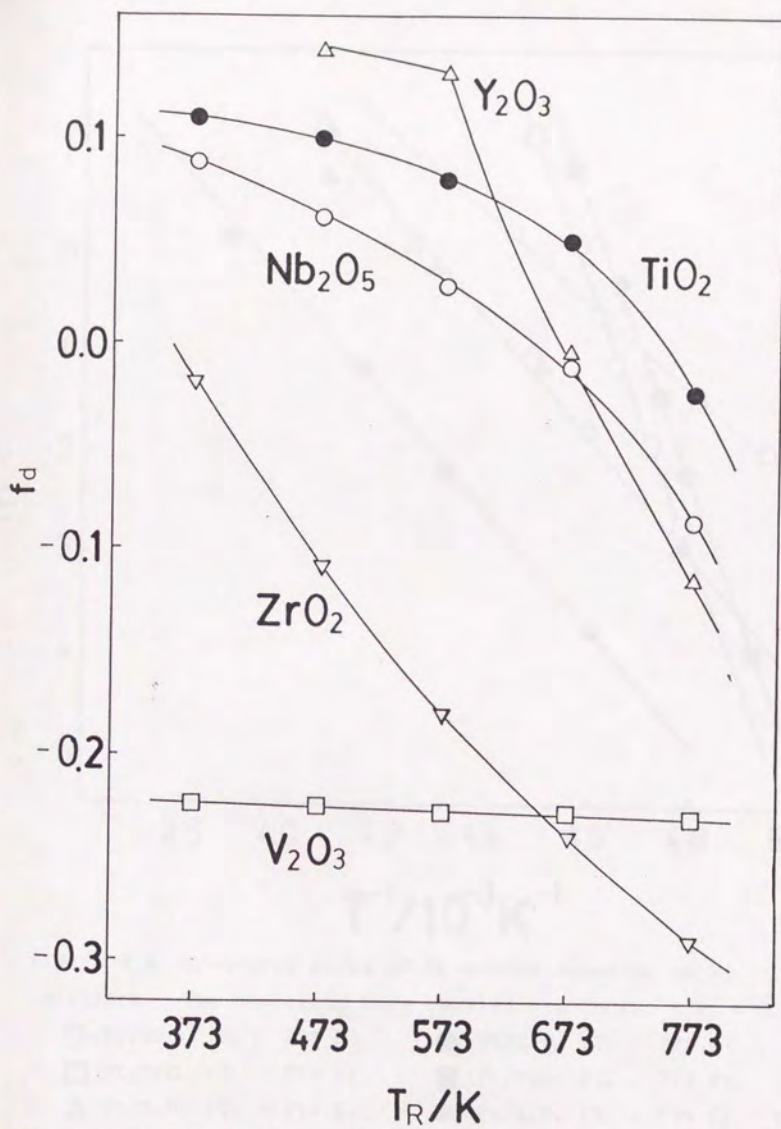


Figure 6.3 f_d of the Pt catalysts reduced at several temperatures, T_R . The catalysts were in vacuum.

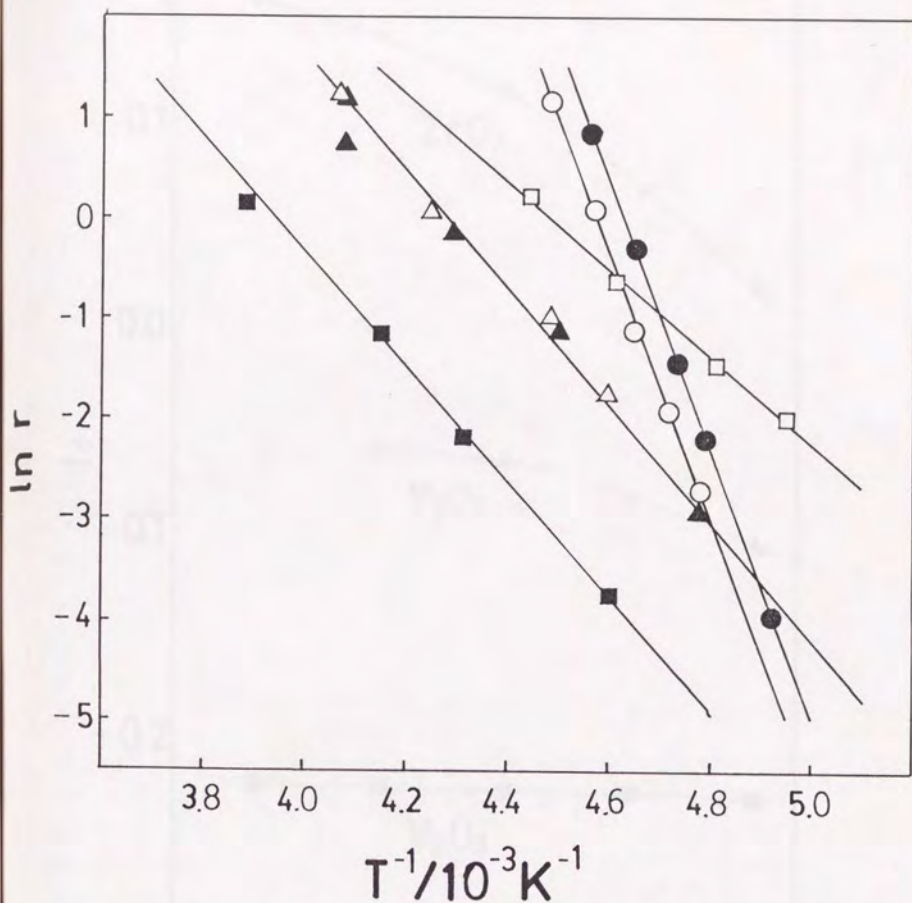


Figure 6.4 Arrhenius plots of D_2 -ethene reaction on Pt catalysts. The reactions were carried out in $P_{D_2} = P_E = 1.3$ kPa.

○:Pt/ZrO₂ ($T_R = 373$ K), ●:Pt/ZrO₂ ($T_R = 773$ K),
 □:Pt/TiO₂ ($T_R = 373$ K), ■:Pt/TiO₂ ($T_R = 773$ K),
 △:Pt/Y₂O₃ ($T_R = 573$ K), ▲:Pt/Y₂O₃ ($T_R = 773$ K). The rates are normalized with H/Pt of the catalyst reduced at 373 K (for ZrO₂ and TiO₂) or 573 K (for Y₂O₃) and expressed with min⁻¹.

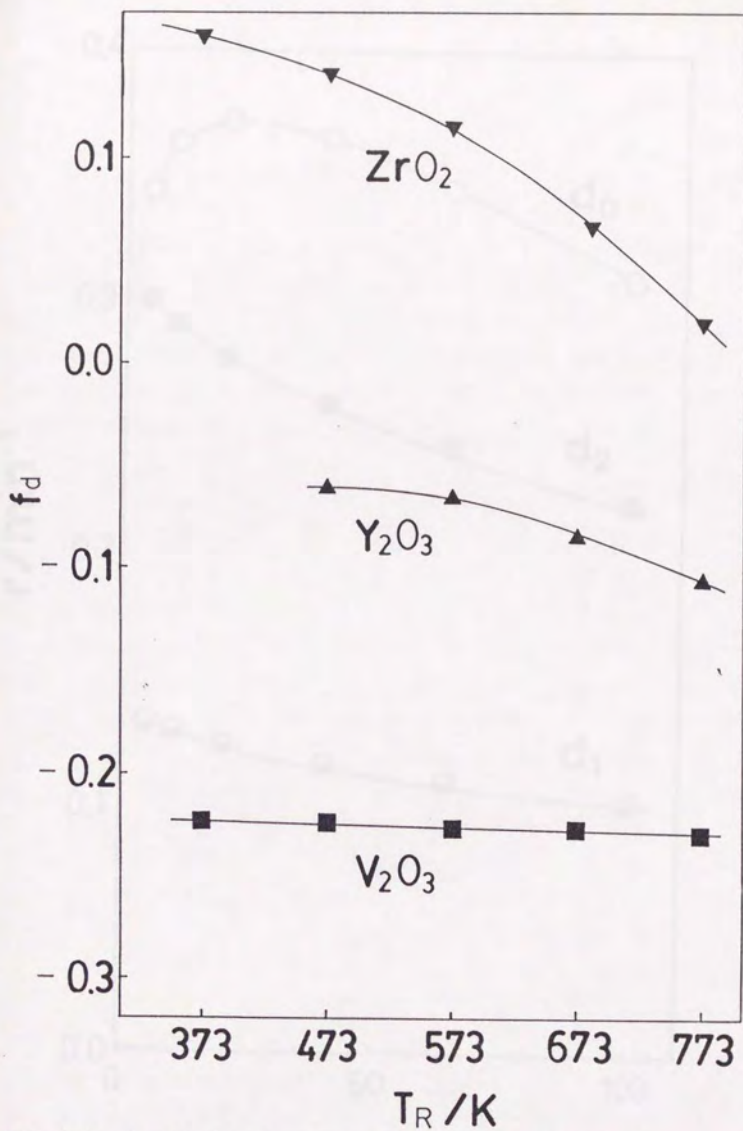


Figure 6.5 f_d of the Pt catalysts reduced at several temperatures, T_R . The catalysts were in 1.3 kPa of ethene in gas phase.

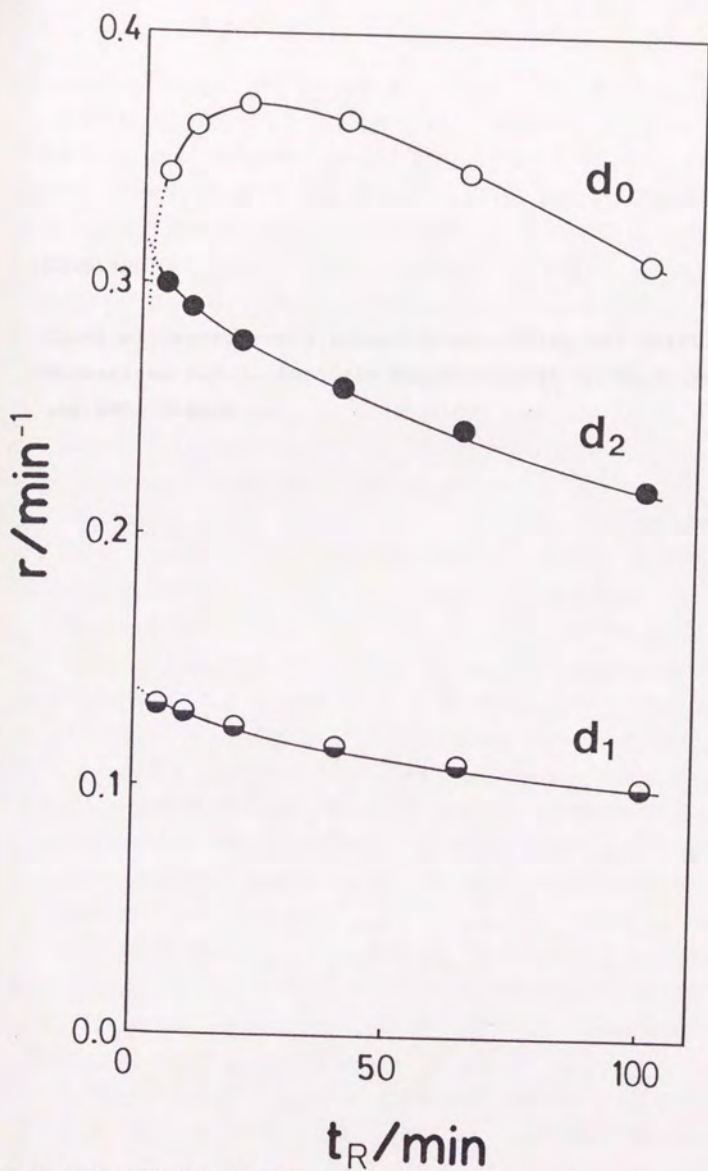


Figure 6.6 The formation rate of ethane isotopes versus reduction time of Pt/TiO₂. The catalyst reduction temperature was 623 K. The catalytic reactions carried out in $P_{D_2} = P_E = 1.3$ kPa at 223 K. The rates are normalized with $H/Pt = 0.750$.

Chapter 7

Chemical Environments around Active Sites and Reaction Mechanisms for D₂-Acrolein Reaction over Ir/Nb₂O₅ in Normal and SMSI States

In previous chapters, the properties of the chemical environments around active sites in the working state of various catalysts of D_2 -ethene reaction were presented. SMSI-Rh/Nb₂O₅, Ir/Nb₂O₅ and Pt/TiO₂ catalysts were manifesting among these catalysts. Two kinds of active sites and deuterium atomspheres generates in the reflecting the structural singularity of SMSI catalyst. SMSI catalysts are also good systems for investigating the genesis of promoting/poisoning effects in metal catalysis because the comparison with the corresponding non-SMSI catalyst (non-promoted catalyst having almost the same metal-particle size) is easy and the degree of the migration of support suboxides is controllable with reduction temperature and time.

To confirm the existence of these sites for the other reaction and to investigate the chemical nature of these two sites, D_2 -acrolein reaction is studied in chapter 7 and 8.

Acrolein is the simplest molecule in the unsaturated carbonyl compounds and regarded as a good probe for the exploration of selectivity in hydrogenation over a variety of promoted catalysts as discussed in chapter 1. It is an attractive molecule also in terms of the mechanism of its hydrogenation. Hydrogenation of unsaturated aldehydes or ketones is usually described as an associative mechanism for the alternative hydrogenation of C=C and C=O double bonds. However, for conjugated system there could be a mutual influence of these groups. [1-5] Thus the mechanism of acrolein hydrogenation may be markedly affected by modification of surface by promoters, supports and particle size. In other words, acrolein hydrogenation may be considered as a good indicator of changes in active sites and their chemical environments which are closely related to reaction mechanisms.

The surface of SMSI catalysts includes heterogeneous

environments which influence or determine the reaction path and the transport of adspecies. The mechanism for acrolein hydrogenation over SMSI catalysts may consequently provide useful factors of activation for promoted metal catalysts. This chapter deals with hydrogenation/deuteration of acrolein over Ir/Nb₂O₅, where the SMSI metal surface is characterized in the working state of catalyst and the relation with reaction mechanism is discussed.

7.1 Experimental

Nb₂O₅-supported Ir catalysts were prepared by similar way as chapter 3. Acrolein (research grade) purchased from Tokyo Kasei Co., Ltd., was further purified by freeze-thaw cycles. Hydrogen and deuterium gases of research grade were purified through a 5A molecular sieve trap at 77 K.

The reaction of H₂-acrolein and D₂-acrolein were carried out in a closed circulating system. The products in the H₂-acrolein reaction were analysed by gas chromatography; propanal, allyl alcohol, 1-propanol and acrolein were separated on a 2 m PEG-1500 column at 333 K and hydrocarbons on a 2 m VZ-10 column at 333 K. In the D₂-acrolein reaction the deuterated product were separated by the column and analysed by a mass spectrometer. Data analysis in detail was described in chapter 2.

7.2 Results and Discussion

(i) Kinetic Behavior

The main products were always propanal and allyl alcohol in the

initial stage of the reaction. 1-Propanol was a secondary product because it was formed after a certain induction period. Some decomposition products such as ethane, ethene propane, propene and carbon monoxide were observed, but the amount of these products was within 2 mol% of the total products over low-temperature reduced catalyst and 0.1 mol% over high-temperature reduced catalyst. The break of an SMSI state as is often observed in H_2 -CO reactions was not observed.

Figure 7.1 shows Arrhenius plots of the initial rates of the formations of allyl alcohol and propanal over both LTR and HTR catalyst. Activation energies for both products were the same ($12 \text{ kJ}\cdot\text{mol}^{-1}$) in the case of LTR, whereas those for HTR catalyst were different, that is, $5 \text{ kJ}\cdot\text{mol}^{-1}$ for allyl alcohol and $35 \text{ kJ}\cdot\text{mol}^{-1}$ for propanal. The dependence of the rates on temperatures over LTR catalyst also indicates that the formation of propanal was dominant over the whole range of temperature ($353 - 433 \text{ K}$), but the preferential formation of allyl alcohol was observed at the lower temperature like 353 K over HTR catalyst. The disagreement of the apparent activation energy between products suggests that the rate-determining step and/or the active sites are different for the two products over SMSI-Ir/Nb₂O₅. The decrease in the activation energy of SMSI-Ir/Nb₂O₅ is also observed in ethene deuteration in chapter 3. Rate-determining step of these reactions likely to include certain similarities. On the contrary, the increase of activation energy for propanal formation suggests different phenomena like the shift of rate-determining step.

(ii) Isotope Distributions in Products and Reaction Intermediates

Percentage isotopic distributions in each product at the initial stage of the $D_2 - CH_2=CHCH=O$ reaction are summarized in Tables 1-3. Less deuterated products than d_3 species were observed.

Table 7.1 summarizes the populations of deuterated acrolein formed in the H-D exchange reaction between D_2 and $CH_2=CHCH=O$. Aldehydic hydrogen was mainly exchanged over LTR catalyst. This suggests that acrolein is adsorbed with aldehydic carbon and the exchange reaction is most likely to proceed mainly via interconversion between $\eta^2(C-O)$ and $C-C-C-O^*$ as illustrated in Scheme 7.1(a). On the other hand, over the HTR catalyst the terminal hydrogen was exchanged in addition to the aldehydic hydrogen. Two possible exchange schemes are reasonable. One is the conversion of $\eta^2(C-C)$ into *iso*-species and the other is the conversion of $\eta^4(C-C-C-O)$ species into $\eta^3(C-C-C)$. It is not impossible to distinguish these schemes from the isotope distribution. Thus two schemes are illustrated in scheme 7.1(b).

The density of d-state of Pt/TiO_2 increases according to the reduction temperature as demonstrated in chapter 6. Electron withdrawing character of $\eta^4(C-C-C-O)$ is higher than $\eta^2(C-C)$ species. In addition, as shown in Figure 1.1, one of the terminal C-H bonds of $\eta^4(C-C-C-O)$ is significantly longer than the other vinyl C-H and it suggests the high reactivity of terminal H. The scheme through $\eta^4(C-C-C-O)$ is, therefore, more probable than it seems. But there is no reason for excluding the associative exchange reaction of C-C bond for $3-d_1$ -acrolein formation.

Deuterium were found on the oxygen ($o-d$) and α -carbon ($1-d$) in allyl alcohol on the LTR catalyst and no deuterium was incorporated on the γ -carbon ($3-d$) and β -carbon ($2-d$), shown in Table 7.2, which depicts a typical profile of the associative

mechanism of C=O double bond hydrogenation of acrolein. $\eta^2(\text{C-O})$ converts into *iso*- or *o*- σ -adspecies and turns back as illustrated in Scheme 7.2(a). It is suggested that the former is more easily than the latter, by comparing the population of *o*- d_1 - and *1*- d_1 -allyl alcohol.

o- d_1 - and *3*- d_1 -allyl alcohols were main products among d_1 -species for HTR catalyst unlike to LTR catalyst. The *o*- d_1 formation could be the same way as LTR catalyst but the formation of *3*- d_1 -species can not be explained by simple associative mechanism of C-O bond. The most reasonable explanation of the formation is intrahydrogen shift reaction of $\eta^4(\text{C-C-C-O})$ into $\eta^3(\text{C-C-C})$ through the substitution of terminal hydrogen by surface deuterium as is demonstrated in Scheme 7.2(b). No deuterium found on α -carbon in Table 7.2 suggests the lack of associative deuteration of C-O on HTR catalyst.

Isotope distribution of propanal are shown in Table 7.3. The amount of *1*- d_1 -species was small to be neglected. Propanal formation is likely to be dominated by associative mechanism. *3*- d_1 -Propanals was superior to *2*- d_1 -propanal on LTR catalyst, while *2*- d_1 was predominantly formed over *3*- d_1 on HTR catalyst. This difference reasonably explained by the reflection of the difference in the reactivity of half-hydrogenated (or deuterated) species on the two catalysts. As for LTR catalyst, *2*- σ -adspecies contributes much but, for HTR catalyst, dominant species shifts to *3*- σ -adspecies. This is illustrated in scheme 7.3.

(iii) Location and Reaction Environment of Active Sites

The amount of deuterium incorporated into the both deuterated products, $\sum id_i / 8\sum d_i$, decreased on HTR catalyst as listed in Table

7.2 and 7.3. Moreover, on LTR catalyst, this almost agreed between two products but, on HTR catalyst, allyl alcohol is much lower than propanal. In other words, surface D/H ratio in reaction steady state is significantly lower around the active site for allyl alcohol than that for propanal. In this context two kinds of active sites should be distinguished for D₂-acrolein reaction on SMSI-Ir/Nb₂O₅ like D₂-ethene reaction on Rh/Nb₂O₅, Ir/Nb₂O₅ and Pt/TiO₂. Less-deuterated ethanes are formed on the peripheral site of migrated support oxide in these catalysts and it is natural to infer that this site contributes allyl alcohol formation. This analogy should be tested through the rate variation by catalyst reduction time, t_r. The results are shown in two graphs of Figure 7.2.

Rates of allyl alcohol formation and propanal formation is plotted in Figure 7.2 (a) where allyl alcohol has an optimum rate around t_r = 50 min. On the contrary, propanal and H₂-D₂ exchange under the reaction condition were decreasing monotonously. From the discussion in previous chapters, allyl alcohol formation is attributed to the peripheral site (site II) and the propanal formation and D₂ dissociative adsorption do not include influence of the peripheral site, assuming that the number of sites is rate-dominating. The damping of the graph shape observed in allyl alcohol formation might result from an increasing electronic modification at higher coverage of NbO₂.

The rate for 1-d₁-acrolein and 3-d₁-acrolein are plotted as a function of t_r in Figure 7.2 (b) where the former is the decreasing convex function and the latter has an maximum at 50 min. This suggests that terminal hydrogen exchange occurs on site II and supports the assign of the formation of η⁴(C-C-C-O) intermediate on this site.

It is likely that all paths in the deuterium-acrolein reaction over LTR catalyst (normal state) proceed competitively on bare metal sites with homogeneous surface hydrogen isotope ratio because of the similar isotope density in propanal and allyl alcohol and the similar activation energy for both products. The heterogeneity of metal surface caused by SMSI not only brings about changes in the reaction kinetics, rate-determining step and reaction intermediates, but also generates the different local environments around active sites. A schematic model for acrolein deuteration and hydrogen-exchange reactions is illustrated in Figure 7.3. On SMSI surface, site I acts as a kind of deuterium reservoir for site II.

7.3 Summary

Chemical environments around active sites of Ir/Nb₂O₅ in LTR and HTR states were investigated in a working state of catalyst by kinetics and a tracer study in relation to the chemoselectivity of the acrolein deuteration and the structural feature of SMSI catalysts.

Propanal and allyl alcohol were produced in acrolein hydrogenation on both LTR and HTR catalysts, but the selectivity was very different between these catalysts.

The activation energy for the formation of allyl alcohol decreased from 12 kJ·mol⁻¹ for the normal state to 5 kJ·mol⁻¹ for the SMSI state, while that for propanal formation increased from 12 to 35 kJ·mol⁻¹, suggesting the presence of electronic perturbation of iridium surface by migrated NbO₂ on Ir-metal catalysis.

Each reaction on LTR catalyst proceeded in similar surface

environments, whereas on HTR catalyst there were two kinds of active sites in different reaction environments, one being bare metal sites (site I) and the other the peripheral sites of migrated NbO₂ islands (site II).

The rate for reaction on site I decreased monotonously with the reduction time of the catalyst, but that on site II went through maximum. It is suggested that deuterium dissociation and propanal formation proceed on site I, while allyl alcohol was formed through η^{π} -species on site II, and, further, 1-d₁-acrolein was formed on site I in D₂-acrolein reaction, whereas 3-d₁-acrolein was produced on site II. The two active sites (site I and II) with different reaction environments are characterized with different D/H concentration ratio around them during catalytic reaction.

References

1. D.Cornet, F.G.Gault, *J.Catal.*, **7**, 140 (1967).
2. S.Teratani, K.Tanaka, H.Ogawa, K.Taya, *J.Catal.*, **51**, 372 (1978).
3. K.Hirota, R.Touroude, M.Miyasaka, C.Matsumura, *J.Res.Inst. Catal., Hokkaido Univ.*, **25**, 37 (1977).
4. G.W.Smith, J.F.Deany, *J.Catal.*, **6**, 14 (1966).
5. R.Touroude, *J.Catal.*, **65**, 110 (1980).

Table 7.1 Percentage distributions of acrolein in the initial stage of deuterium-acrolein reaction.

	LTR	HTR
$\text{CH}_2 = \text{CHCHO}$	97	95
$\text{CH}_2 = \text{CHCDO}$	3	3
$\text{CH}_2 = \text{CDCHO}$	0	0
$\text{CHD} = \text{CHCHO}$	0	2

Reaction temperatures are 373 K for LTR and 413 K for HTR. These distributions are at 2 % of conversion to the deuterated products. $P_{\text{ac}} = 1.3$ kPa and $P_{\text{D}_2} = 5.3$ kPa.

Table 7.2 Percentage distributions of allyl alcohol in the initial stage of deuterium-acrolein reaction.

	LTR	HTR
$\text{CH}_2 = \text{CHCH}_2\text{OH}$	23	48
$\text{CH}_2 = \text{CHCH}_2\text{OD}$	28	27
$\text{CH}_2 = \text{CHCHDOH}$	10	0
$\text{CHD} = \text{CHCH}_2\text{OH}$	0	25
$\text{CH}_2 = \text{CHCHDOD}$	39	0
$\Sigma i d_i / 6 \Sigma d_i$	19	9

Reaction temperatures are 393 K. These distributions are at 0 % of conversion through the extrapolation of initial distributions. $P_{\text{ac}} = 1.3$ kPa and $P_{\text{D}_2} = 5.3$ kPa.

Table 7.3 Percentage distributions of propanal in the initial stage of deuterium-acrolein reaction.

	LTR	HTR
CH ₃ CH ₂ CHO	22	31
CH ₃ CH ₂ CDO	4	6
CH ₃ CHDCHO	9	30
CH ₂ DCH ₂ CHO	23	10
CH ₂ DCHDCHO	20	12
CHD ₂ CH ₂ CHO	22	5
CH ₃ CD ₂ CHO	0	6
$\Sigma i d_i / 6 \Sigma d_i$	20	15

Reaction temperatures are 393 K. These distributions are at 0 % of conversion through the extrapolation of initial distributions. $P_{H_2} = 1.3$ kPa and $P_{D_2} = 5.3$ kPa.

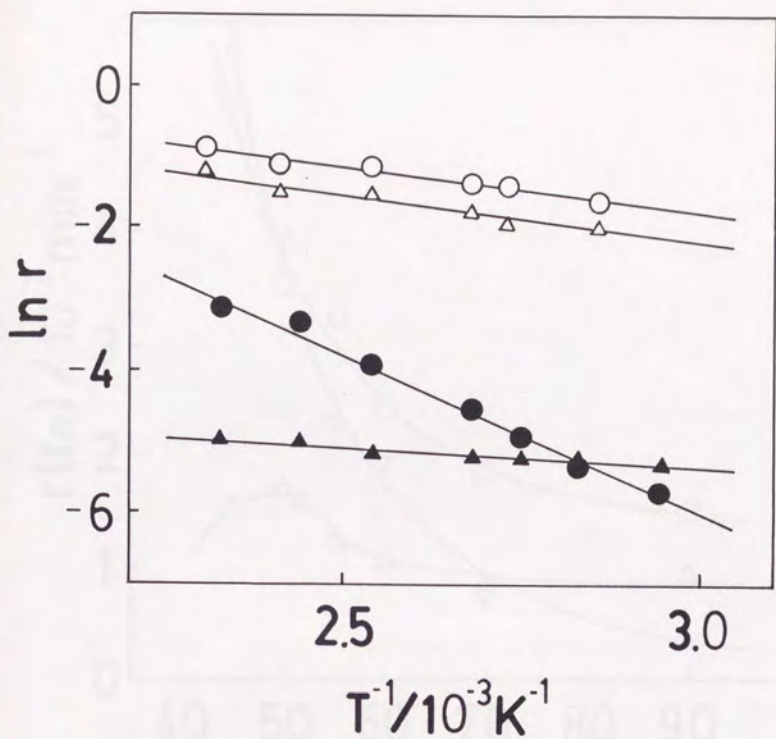


Figure 7.1 Arrhenius plots of the initial rates of acrolein hydrogenation over Ir/Nb₂O₅ reduced at 473 K (for LTR) and 773 K (for HTR). Δ , formation of allyl alcohol (LTR), $E = 12 \text{ kJ}\cdot\text{mol}^{-1}$; \circ , formation of propanal (LTR), $E = 12 \text{ kJ}\cdot\text{mol}^{-1}$; \blacktriangle , formation of allyl alcohol (HTR), $E = 5 \text{ kJ}\cdot\text{mol}^{-1}$; \bullet , formation of propanal (HTR), $E = 35 \text{ kJ}\cdot\text{mol}^{-1}$. $P_{\text{ac}} = 1.3 \text{ kPa}$ and $P_{\text{D}_2} = 5.3 \text{ kPa}$.

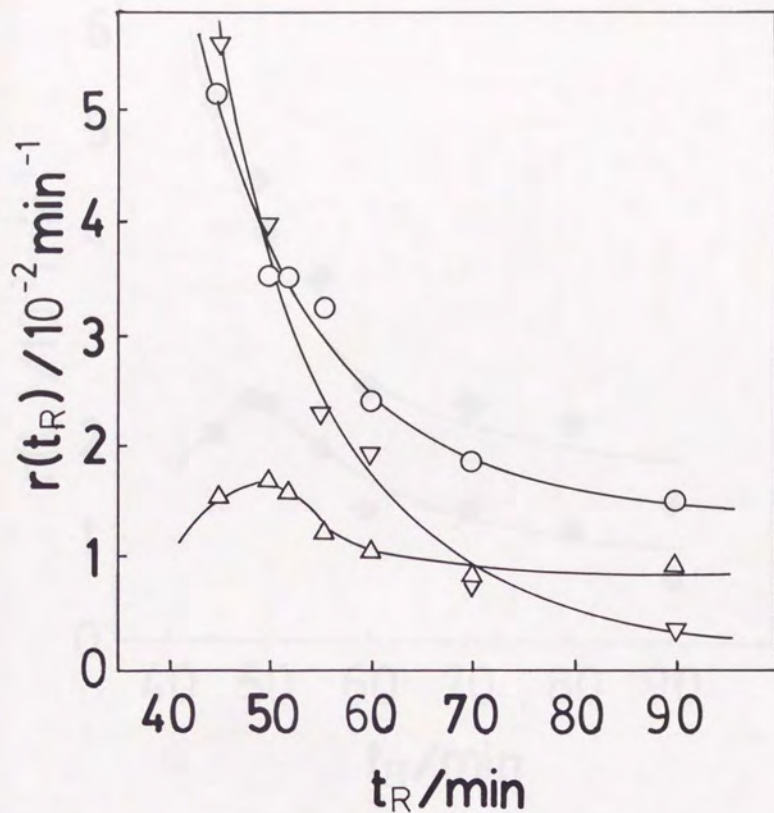


Figure 7.2 (a) Variation reaction rates, $r(t_R)$, for each product at 423 K with reduction time, t_R , of Ir/Nb₂O₆ at 673 K. Δ , allyl alcohol formation; \circ , propanal formation; $P_{wC} = 1.3$ kPa and $P_{D_2} = 5.3$ kPa. HD formation; $P_{wC} = 1.3$ kPa and $P_{D_2} = P_{H_2} = 2.7$ kPa.

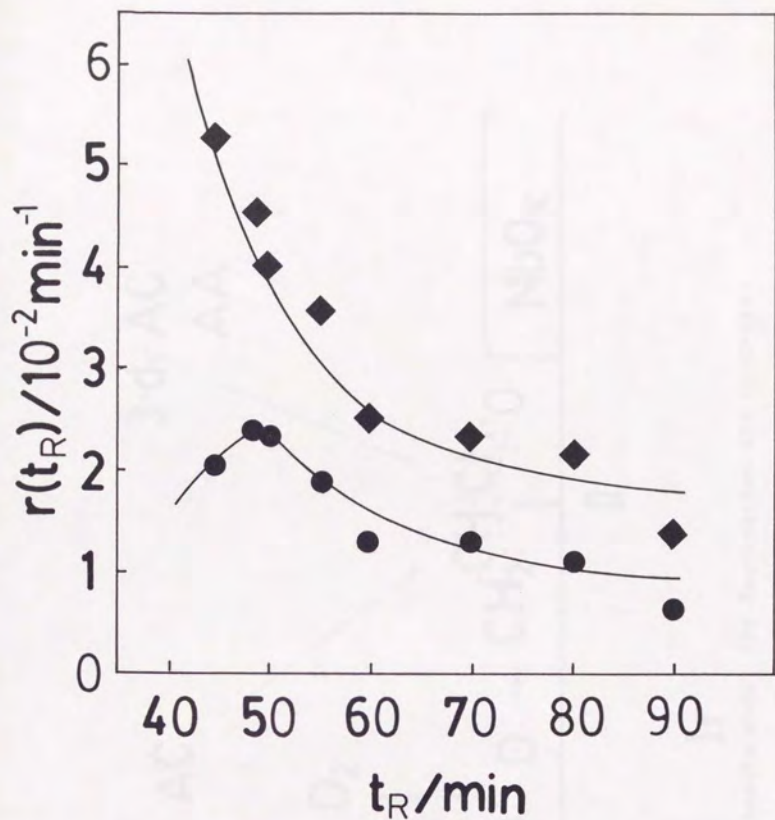


Figure 7.2 (b) Variation of reaction rates, $r(t_R)$, for each product with reduction time t_R of $\text{Ir}/\text{Nb}_2\text{O}_5$ at 423 K. \blacklozenge , *t-d*₁-acrolein formation; \bullet , *3-d*₁-acrolein, $P_{\text{ac}} = 1.3$ kPa and $P_{\text{D}_2} = 5.3$ kPa.

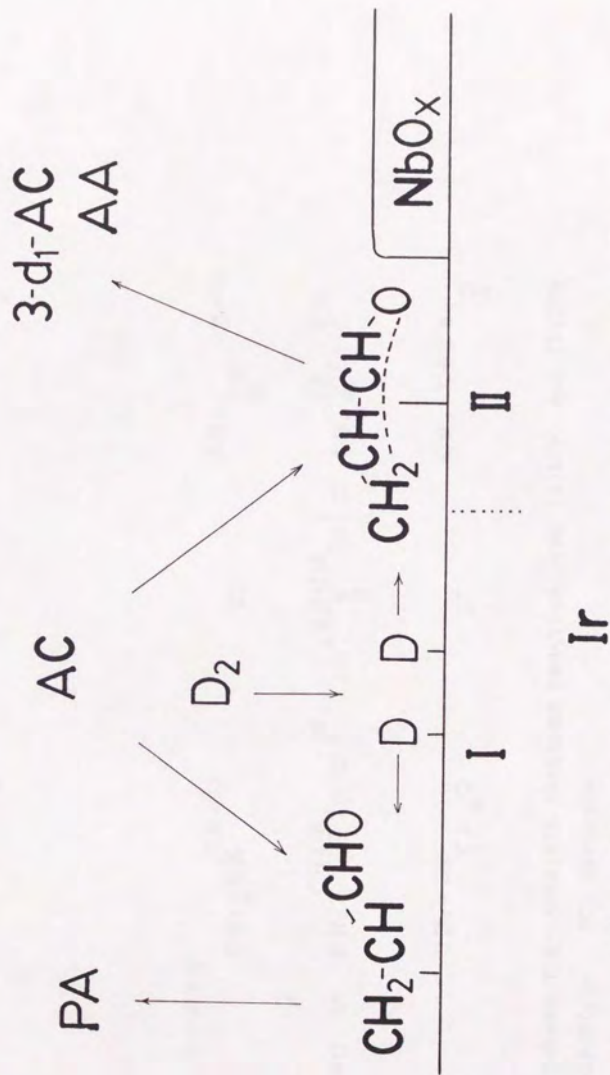
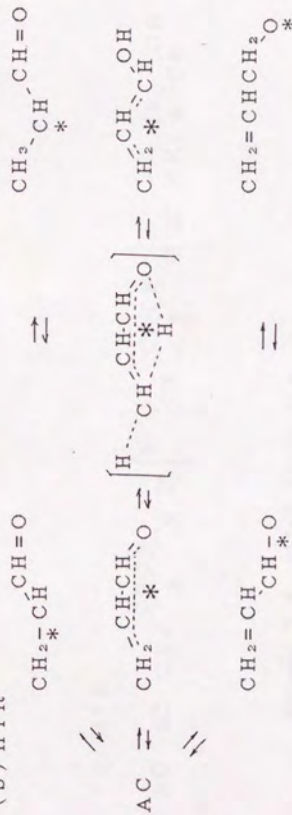


Figure 7.3 A schematic model for deuteration and hydrogen exchange of acrolein over SMSI-Ir/Nb₂O₅. AA, allyl alcohol; PA, propanal; AC, acrolein.

(a) LTR

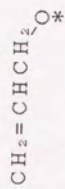
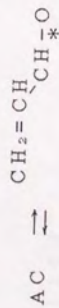


(b) HTR

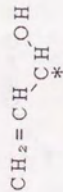


Scheme 7.1 Acrolein exchange reaction over (a)LTR- and (b)HTR-Ir/Nb₂O₅. AC: acrolein.

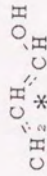
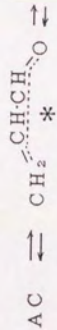
(a) LTR



AA



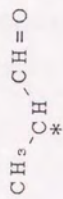
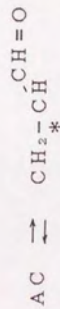
(b) HTR



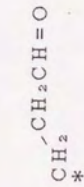
AA

Scheme 7.2 Allyl alcohol formation over (a) LTR- and (b) HTR-Ir/Nb₂O₅. AC: acrolein, AA: allyl alcohol.

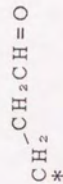
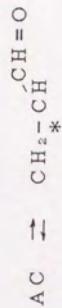
(a) LTR



PA



(b) HTR



PA

Scheme 7.3 Propanal formation over (a) LTR- and (b) HTR-Ir/Nb₂O₆.

AC: acrolein, PA: propanal.

Chapter 8

Cooperative Behavior of Two kinds of Reaction Sites and
Reaction Mechanisms for Deuteration of Acrolein on SMSI-
Pt/Nb₂O₅ Catalyst

SMSI catalysts can be regarded as a model of additive/promotor effects because their catalysis includes both poisoning and promoting phenomena, which may be derived from the migration of suboxides accompanied with perturbation of metal electronic state. Suppression of adsorption capacity by SMSI is believed to result in the decrease in the rates of almost catalytic reactions. But their extent is not constant even among the same kinds of hydrogenations. [1] In contrast, methanation reaction has been reported to be enhanced in SMSI state [2-17], which has often been attributed to the relatively small suppression of H_2 chemisorption and the activation of CO adsorbed at metal-support (or suboxide) interface. It may be of great importance to investigate the catalytic reaction mechanism involving the behavior of adsorbed species rather than the static profiles like adsorption in order to understand the genesis or origin of supported metal catalysis and the role of promoters. The kinetic studies on hydrogenation of benzene [18, 19], acetone [20] and crotonaldehyde [21] has been reported, which showed that SMSI changes not only catalytic activity but also reaction path.

Previous chapters describe deuteration mechanisms of ethene and acrolein on Rh/Nb_2O_5 , Ir/Nb_2O_5 and Pt/TiO_2 by kinetics and isotope tracing methods in order to clarify the microscopic behavior of reaction sites, their chemical environments, and the factors for activation of molecules in SMSI state, which could be made clear only under dynamic reaction conditions. The mechanism of acrolein deuteration and the deuterium distribution can be a sensitive probe of the nature and change of reaction sites on metal surfaces. In chapter 8, this test molecule is used for the investigation of the synergistic behavior of active sites and the reaction mechanism of deuteration on Pt/Nb_2O_5 in normal and SMSI

states.

8.1 Methods

Nb_2O_5 -supported platinum catalyst was prepared by a conventional impregnation method with aqueous solution of $\text{H}_2\text{PtCl}_6 \cdot 6\text{H}_2\text{O}$ (Soekawa Chemical) and subsequently dried for 3 h at 393 K and calcined for 2 h at 773 K in air. Commercially available Nb_2O_5 (Soekawa Chemical; BET surface area: $5\text{m}^2 \cdot \text{g}^{-1}$) was used as support. The metal loading was 2.5 wt %. The catalyst thus obtained was placed in a closed circulating system (dead volume: 130 cm^3). Then it was treated with oxygen for 1 h at 673 K, followed by evacuation for 30 min, and reduced for 1 h at 393 K (LTR) or 773 K (HTR), followed by evacuation for 30 min before each catalytic reaction. The particle size of platinum metal was determined to be 3.9 nm by transmission electron microscopy.

Acrolein (purchased from Tokyo Kasei), *d*₆-acrolein (MSD isotopes) and 3,3,3-trifluoropropene (99.5 %, Japan Halon Co.) were further purified by freeze-thaw cycles. Hydrogen and deuterium gases of research grade were purified through a 5A molecular sieve trap at 77 K. Typical reaction gas pressure was 1.3 kPa for acrolein and 5.3 kPa for deuterium (or a mixture of deuterium and hydrogen). The deuterated products of reactions were analyzed by gas chromatography with a TCD detector or by a mass spectrometer after the separation by the column; propanal, allyl alcohol (prop-2-en-1-ol), 1-propanol and acrolein were separated on a 2 m PEG-1500 at 333 K and 3,3,3-trifluoropropene and 1,1,1-trifluoropropane on a 2 m VZ-10 at 343 K.

8.2 Results

The amounts of hydrogen adsorbed on Pt/Nb₂O₅ reduced at various temperatures are illustrated in Figure 8.1. Each measurement was conducted on the same sample after oxidation (673 K) - reduction treatments. The reversibility of H/M in oxidation-reduction treatments was confirmed. The H/M versus square root of reduction time ($t_R^{1/2}$) plots were extrapolated to the same point of H/M = 0.375 at $t_R = 0$ which agrees with H/M for LTR catalyst, (H/M)_{LTR}. (H/M)_{LTR} did not change with $t_R^{1/2}$. H/M for HTR (773 K reduced) catalyst, (H/M)_{HTR}, was below the detection limit (< 0.01). H/M curves were proportional to square root of t_R . No significant sintering of Pt particles occurring during HTR treatment was observed by TEM.

The initial rates and activation energies for the deuteration of acrolein and 3,3,3-trifluoropropene are listed in Table 8.1. The selectivities to propanal, allyl alcohol and propanol in *d*₀-acrolein deuteration on LTR catalyst are 58 %, 17 % and 25 %, respectively, while those on HTR catalyst are 30 %, 70 % and 0 % as demonstrated in Table 8.1. On Pt/SiO₂ only propanal was formed under the same condition. Hydrogenolysis is negligible and no acceleration of rates was observed, which is often found in CO-H₂ reaction. Significant isotope effect in acrolein-hydrogen for allyl alcohol formation was observed with HTR catalyst on which the rate for D₂ - CH₂=CHCHO was 10 times higher than that for D₂ - CD₂=CDCDO, while negligible isotope effects were observed as for propanal formation on both LTR and HTR catalysts and for allyl alcohol formation on LTR catalyst.

The activities and the activation energies for H₂-D₂ exchange reaction on LTR catalyst under acrolein deuteration

conditions are the same as those for the deuteration of acrolein. On the other hand, they are different for HTR catalyst.

The comparison of C=C hydrogenation rate between acrolein and 3,3,3-trifluoropropene offers an influence of the conjugation on this reaction. On LTR catalyst the rate of 1,1,1-trifluoropropane formation is higher by a factor of 1.6 than that of propanal formation but on HTR catalyst lower by a factor of $5.1 \cdot 10^{-3}$. H_2-D_2 exchange reaction under the condition of 3,3,3-trifluoropropene deuteration showed the same feature as that under acrolein deuteration.

There is a possibility of the secondary reaction of allyl alcohol under reaction conditions; allyl alcohol is the most unstable product among the three (allyl alcohol (AA) : $\Delta H_f = -124.2 \text{ kJ}\cdot\text{mol}^{-1}$, propanal (PA) : $\Delta H_f = -187.4 \text{ kJ}\cdot\text{mol}^{-1}$, propanol (PO) : $\Delta H_f = -254.8 \text{ kJ}\cdot\text{mol}^{-1}$). The deuteration of a mixture of acrolein (AC) and allyl alcohol was carried out at $P_{H_2} + P_{H_2O} = 1.3 \text{ kPa}$ and $P_{H_2O} = 5.3 \text{ kPa}$ and the rate was normalized by r_0 (rate at $P_{H_2O} = 0 \text{ kPa}$) as shown in Figure 8.2. Allyl alcohol is converted to propanol mainly by further hydrogenation and suppresses acrolein consumption on LTR catalyst, while it is converted to propanal mainly through isomerization on HTR catalyst. This behavior is consistent with the time profile for the product formation in $D_2 - CH_2=CHCHO$ reaction on both catalysts; allyl alcohol formation rate saturates on both catalysts, and propanol or propanal has no saturation in the formation on LTR or HTR catalyst, respectively.

Isotope distributions of the products in $D_2 - CH_2=CHCHO$ reaction are listed in Tables 8.2-8.4. Exchange of hydrogen between AC and D_2 occurs at aldehydic hydrogen (7 %) and terminal hydrogen (3 %) on LTR catalyst, while it was observed mainly at

the latter position on HTR catalyst as shown in Table 8.2. The exchange yield is not different between the two catalysts.

Deuterium was observed on β - and γ -carbon atoms in propanal for both catalysts as shown in Table 8.3. The ratio γ -d₁ : β -d₁ = 14 : 9 for LTR and 31 : 4 for HTR, *i.e.* terminal carbon is preferable in deuterium addition for both catalysts but the selectivity is much larger with HTR catalyst. The amount of deuterium incorporated in the produced propanal ($\sum id_i / n \sum d_i$; n is the number of intrahydrogens related to the reaction) is much lower for HTR than for LTR catalyst, which reflects the surface D/H ratio under reaction condition.

Deuterium addition for allyl alcohol formation on LTR catalyst occurred at C=O double bond as shown in Table 8.4. In contrast, the main position of deuterium incorporation was the terminal carbon for HTR catalyst. The $\sum id_i / n \sum d_i$ value is lower with HTR than with LTR catalyst likely to the case of propanal.

The significant difference between the two catalysts in the deuterium distribution in 1,1,1-trifluoropropane formed in D₂ - 3,3,3-trifluoropropene reaction is the amount of deuterium incorporated in Table 8.5 where it is much lower with HTR catalyst than for LTR catalyst. The profile of $\sum id_i / n \sum d_i$ is similar to that of propanal.

Deuteration rates for each product were measured in the course of the generation of SMSI state at different reduction temperatures as a function of reduction time in Figure 8.3. Each measurement was done on the same sample after the oxidation-reduction treatments, showing good reproducibility in the data. All rates are normalized by H/M = 0.375. At 393 K reduction the rates are constant against reduction time t_R of catalyst. On the other hand, at 473 K reduction, propanol had a maximum at ca. t_R

= 40 min. The rates of allyl alcohol and propanal formations on the catalyst prerduced at 623 K showed the maximum at ca. $t_R = 20$ min while they were almost constant against t_R for 773 K reduced catalyst. The behavior of the rates for allyl alcohol and propanal formations in Figure 8.3 are same except the absolute value. Figure 8.3 (a) and (b) also demonstrate that the choice of reduction temperature for LTR ($T_R = 393$ K) and HTR ($T_R = 773$ K) was adequate. The H_2 - D_2 exchange in $H_2 + D_2 \rightarrow CH_2=CHCHO$ reaction was also monitored against t_R at 623 K reduction in Figure 8.3(c). The rate decreased monotonously unlike to propanal and allyl alcohol formations.

In order to explore the origin of the isotope effect in deuteration of $CH_2=CHCHO$ and $CD_2=CDCDO$, two kinds of transient isotope tracing experiments were done as shown in Figures 8.4 and 8.5 and Table 8.6. $CH_2=CHCHO$ was introduced during the course of $D_2 - CD_2=CDCDO$ reaction in Figure 8.4. The profile of allyl alcohol formation is characterized with the rate enhancement with the induction period after the emergence of $CH_2=CHCHO$ in gas phase. The propanal formation also increased a little after $CH_2=CHCHO$ addition. In Figure 8.5 H_2 was introduced during the course of $D_2 - CD_2=CDCDO$ reaction. HD formation is hundred times as rapid as propanal and allyl alcohol formations. The rate of allyl alcohol is remarkably enhanced without induction period, while the enhancement for propanal was a little. The isotope distributions in allyl alcohol in the initial stage of transient reaction are listed in Table 8.6.

Table 8.7 shows the result of another kind of transient isotope tracing study which offer the information on active sites for allyl alcohol isomerization under $D_2 - CD_2=CDCDO$ reaction conditions. d_0 -allyl alcohol was introduced to the $D_2 -$

CD₂=CDCDO system. All propanals were produced in the initial stage of the isomerization of allyl alcohol.

8.3 Discussion

(i) Hydrogen adsorption

It is widely believed that the suppression of hydrogen adsorption by high temperature reduction (HTR) of TiO₂ - or Nb₂O₅ - supported metal catalysts is due to the migration of partially-reduced support-oxide onto the metal surfaces. Square root dependence of hydrogen adsorption on t_k in the reduction temperature range $T_k < 623$ K (Figure 8.1) is consistent to the SMSI catalysts of previous chapters. It is likely that the migration of the suboxides onto metal surfaces is subjected to thermal diffusion process. The activation energy of the process on Pt/Nb₂O₅ was determined to be 94 kJ·mol⁻¹. On the other hand, H/M for the reduction temperatures $T_k \geq 623$ K was not the case. It may be due to the repulsion of NbO_x islands and/or the change of the growth mode, e.g. two dimensional to three dimensional.

(ii) Kinetic Properties

The suppression of the catalytic activity by SMSI has been reported to depend on the type of the reaction and the metal. [1] In previous chapters, the deuteration of ethene or acrolein over Rh/Nb₂O₅ or Ir/Nb₂O₅ catalysts was observed to be suppressed by a factor of 10-100 by HTR. In this meaning, it is important to choose carefully a standard of reaction for the comparison of activity and the exploration of the genesis of catalysis.

Acrolein having C=C and C=O double bonds is a probe molecule to investigate the dynamic behavior of adspecies and reaction sites. In most cases the hydrogenation occurs preferentially on C=C double bond. Carbonyl bond seems to have no interaction with metal surface. On the contrary, the Nb₂O₅-supported Pt catalyst produces significant amount of C=O hydrogenated molecules. Particularly SMSI-Pt/Nb₂O₅ showed the selective formation of allyl alcohol as shown in Table 8.1. Vannice et al. reported the hydrogenation of crotonaldehyde (CH₃CH=CHCHO) to form the corresponding unsaturated alcohol on Pt/TiO₂, while no alcohol was formed on Pt/SiO₂ [21]. A drastic improvement of selectivity often includes a mechanistic change.

The activation energy (5 kJ·mol⁻¹) for H₂-D₂ exchange is coincident with those for propanal and allyl alcohol formations on LTR-Pt/Nb₂O₅ catalyst as shown in Table 8.1. The initial rates of propanal and allyl alcohol formations were nearly proportional to the hydrogen pressure. The similar kinetic parameters suggest that the reaction environments for the formation of both products on LTR catalyst are similar and that both reactions involve a common rate-determining step which is also common to that for H₂-D₂ exchange in the presence of acrolein, and hence that the rate-determining step is the dissociative adsorption of hydrogen which is similar to the result observed with Ir/Nb₂O₅. On the SMSI catalyst, however, the rate of HD formation is significantly higher than those for both deuterated products, and the activation energy is much lower for HD formation (19 kJ·mol⁻¹) than for both products (46 and 45 kJ·mol⁻¹). The rate-determining step is thought to shift to the other step. Isotope effect between D₂ - CH₂=CHCHO and D₂ - CD₂=CDCDO reactions observed in Table 8.1 suggests that the rate-

determining step for allyl alcohol formation on HTR catalyst is the C-D (C-H) bond breaking rather than hydrogen addition to acrolein. The increase of the activation energy for H_2 -D₂ exchange (from 5 kJ·mol⁻¹ for normal state to 19 kJ·mol⁻¹ for SMSI state) is a reverse phenomenon to the case of Ir/Nb₂O₅.

-CHO is an electron withdrawing group with $\sigma_m = 0.36$ (σ_m : Hammett's parameter). The influence of the conjugation of C=C and C=O in acrolein can be examined by the comparison with C=C bond hydrogenation of non-conjugated molecule with a group having a similar Hammett's parameter instead of -CHO group. The HOMO and LUMO levels are summarized in Table 8.8 [22]. From the energy levels of vinyl compounds in Table 8.8, the electronic state of C=C bond in CH₂=CHCF₃ well imitates that of CH₂=CHCHO. Thus the conjugation effects can be extracted in hydrogenation of C=C bond by the comparison of the reaction of both reactants. In fact, the activation energies for both reactants in Table 8.1 were not much different and $\Sigma id_i / n \Sigma d_i$ values where n is the number of hydrogen concerning to hydrogenation/exchange in Table 8.3 and 8.5 were similar for propanal (= 0.42) and 1,1,1-trifluoropropane (= 0.47) as for LTR catalyst. Interaction of acrolein C=C bond with Pt is a little stronger than that for 3,3,3-trifluoropropene, judging from their LUMO energies. Then, hydrogen which competes with the unsaturated substrate in adsorption more readily adsorbs on Pt in hydrogen/3,3,3-trifluoropropene system than in hydrogen/acrolein system, resulting in the rapid formation of 1,1,1-trifluoropropane as compared with the formation of propanal.

In contrast, C=C hydrogenation on SMSI-Pt/Nb₂O₅ was much slower for 3,3,3-trifluoropropene than for acrolein as shown in Table 8.1. The difference between the two reaction rates is

$5 \cdot 10^2$, while $\Sigma id_i / n \Sigma d_i$ values are not so much different. Considering that the rate-determining step is not hydrogen dissociation on HTR catalyst for both products, the difference in the kinetic parameters indicates the different reaction intermediates for the hydrogenation of $CH_2=CHCHO$ and $CH_2=CHCF_3$ on SMSI catalyst. To summarize, the mechanism for both reactions is suggested to be similar over LTR catalyst (through the associative adsorption at C=C bond) but different over HTR catalyst.

(iii) Propanol formation

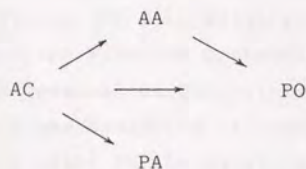
Propanol forms from the initial stage over LTR catalyst but it is produced after a certain induction period over SMSI catalyst. It is clear that allyl alcohol formed during deuteration of acrolein is easily converted to propanol over LTR catalyst as shown in Figure 8.2. But all the propanol is not to be derived from allyl alcohol because of the absence of the induction period and the different behavior of propanol and allyl alcohol in Figure 8.3(a) in which propanol did not follow allyl alcohol. It is suggested that propanol formation requires the metal ensemble like hydrogenolysis of methylcyclopentane since it is more sensitive to the coverage of NbO_x than simple hydrogenations like propanal or allyl alcohol formation. The paths are summarized in scheme 8.1.

(iv) Reaction Intermediates

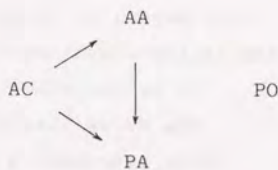
The difference to be noted between LTR and HTR catalysts in Tables 8.2 - 8.4 is the population of deuterium atom on the

terminal carbon in the products. A drastic difference is observed for allyl alcohol in Table 8.4. γ -hydrogen in d_1 - and d_2 -allyl alcohol was selectively deuterium-exchanged on HTR catalyst unlike on LTR catalyst where α -deuterium and alcoholic deuterium were observed as expected from a usual 1,2-deuterium addition. This feature of deuterium distribution in allyl alcohol was also observed with Ir/Nb₂O₅ in chapter 7. This suggests the attack of surface deuterium to terminal carbon. η^3 (C-C-C)-, η^2 (C-C)- or η^4 (C-C-C-O)-type bonding has been reported for transition metal-acrolein complexes. [23-25] Several reaction intermediates and schemes including η^2 , η^3 or η^4 -intermediates have been proposed for the hydrogenation of α, β -unsaturated carbonyl compounds. [26-28] Allyl alcohol is likely to be produced via η^4 (C-C-C-O)-intermediate on the HTR catalyst where surface hydrogen (deuterium) attacks the terminal(γ) carbon of acrolein with the resultant 1,4-hydrogen transfer as illustrated in scheme 8.2.

(a) LTR



(b) HTR



Scheme 8.1. Reaction paths of acrolein hydrogenation on Pt/Nb₂O₅

In addition to the main formation of $\text{CHD}=\text{CHCH}_2\text{OH}$ in d_1 -allyl alcohol (Table 8.4), the large isotope effect in acrolein deuteration ($\text{CD}_2=\text{CDCDO}/\text{CH}_2=\text{CHCHO} = 10$ in Table 8.1) which is attributed to hydrogen abstraction in the rate-determining step confirms the previous reaction mechanism for allyl alcohol formation involving 1,4-hydrogen transfer in η^4 -intermediate induced by the attack of surface hydrogen atom to the terminal carbon as shown in scheme 8.1. This is also in coincidence with the selective formation of $\text{CHD}=\text{CHCHO}$ in deuterated acrolein on SMSI catalyst in Table 8.2. The other possible mechanisms never fit the present kinetic data and isotope distributions.

The induction period observed when d_0 -acrolein was added during the course of d_4 -acrolein deuteration in Figure 8.4(c) is attributable to a slow rate of the d_0 -acrolein by replacement with the preadsorbed d_4 -acrolein. Since the HD formation under the reaction conditions in Figure 8.5 was faster by a factor of hundred than hydrogenation, the dissociative adsorption of hydrogen on HTR catalyst must be fast as compared with the deuterium addition to acrolein-adsorbed species. Therefore, the isotope distribution of allyl alcohol formed after H_2 introduction to the $\text{D}_2 - \text{CD}_2 = \text{CDCDO}$ reaction in Figure 8.5(c) reflects the push-pull reaction from A_1 to B_2 in scheme 8.1. Thus the relative probability of the hydrogen/deuterium attack to the terminal carbon $((1-x)/x)$ and of the 1,4-transfer of hydrogen/deuterium $((1-y)/y)$ can be estimated, which are equivalent to the relative concentration of hydrogen atom/deuterium atom at the metal surface (site I as discussed hereinafter) and that on the terminal carbon of η^4 -intermediate. The relative rate of the steps and the deuterated allyl alcohols are deduced as follows:

step	relative rate	product
D-attack and D-transfer	$x * y * 0.1$	$CD_2 = CD_2 CD_2 OD$
H-attack and D-transfer	$(1-x) * y * 0.1$	$CHD = CD_2 CD_2 OD$
D-attack and H-transfer	$x * (1-y)$	$CD_2 = CD_2 CD_2 OH$
H-attack and H-transfer	$(1-x) * (1-y)$	$CHD = CD_2 CD_2 OH$
normalization factor	$1 - 0.9 y$	

The factor 0.1 is the value from the isotope effect in Table 8.1. The values, $x = 0.55$ and $y = 0.8$, give the calculated distribution of above products which is in good agreement with the observed distribution as shown in Table 8.6. The value of $x = 0.55$ implies that surface deuterium is quickly shuffled with hydrogen before the reaction with the η^a -intermediate.

The deuterium atom in deuterated propanal formed in D_2 -acrolein reaction was preferentially incorporated to the terminal carbon as shown in Table 8.3; $CH_2 DCH_2 CHO : CH_3 CHDCHO = 31 : 4$ and $CHD_2 CD_2 CHO : CH_3 CD_2 CHO = 29 : 3$. It is most likely that both allyl alcohol and propanal are formed through the same kind of the intermediate on SMSI catalyst because of the similarity of incorporation of deuterium on γ -carbon. The easy conversion of allyl alcohol to propanal (Figure 8.2) also indicates a close relation between the mechanisms for both product formations on HTR catalyst. On the other hand, allyl alcohol was not transformed to propanal on LTR catalyst in Figure 8.2. The ratio of (C-D in γ -carbon)/(C-D in β -carbon) in deuterated propanal on LTR catalyst is 1.5, showing no selective incorporation of deuterium on γ -carbon. Again, LTR catalyst showed the different

isotope distribution in allyl alcohol between both catalysts in Table 8.4; on LTR catalyst deuterium was observed on the C-0 position. The hydrogenation of acrolein to form propanal and allyl alcohol on LTR catalyst can be well explained by the Horiuti-Polanyi mechanism involving the associative adsorption of C=C and C=O, respectively, followed by the hydrogenation (3,4- and 1,2-addition) as shown in Scheme 8.2. There was no evidence for the coupling of C=O and C=C hydrogenation on LTR catalyst. The preferable half-hydrogenated species is B₃ rather than B₄ because D on γ -carbon is more than D on β -carbon.

The rate-determining step of propanal formation on SMSI catalyst is attributable to the hydrogen addition to B₁ to form C₁. Because the A₁ to B₁ step is thought to be fast for the following reasons; (1) d₀-allyl alcohol (12 %) was formed in the deuteration of d₀-acrolein with D₂, which implies the easy abstraction of methyl hydrogen (B₁ to A₁) to form surface hydrogen atom, (2) the step of A₁ to B₂ was found to be the rate-determining step for allyl alcohol formation, and (3) H on the terminal carbon has been observed when the species A₁ is attacked by surface hydrogen/deuterium to form B₂ in Table 8.6 ((1-y) = 0.2). Furthermore, the rate of propanal formation on HTR catalyst was smaller than that of allyl alcohol as shown in Table 8.1. Then the step of B₁ to C₁ must be rate-determining for propanal formation. Vinyl alcohol CH₂=CHOH is not stable enough to be observed and it isomerizes to propanal quickly.

(V) *The location of reaction site*

The identification of the location of active sites can be obtained by the reaction rate as a function of reduction time of

catalyst (t_R). There are three kinds of surfaces on Pt/Nb₂O₅, that is, bare Pt metal surface, periphery of NbO_x island, which are chemically different. The activities of Nbⁿ⁺ oxides (n = 3 - 5) for hydrogenation under the present conditions were negligible in comparison with Pt [29]. The present attention is, consequently, focused on bare metal site (site I) and periphery of NbO_x (site II).

The reaction rate profiles as a function of t_R were similar for the formations of both propanal and allyl alcohol in Figure 8.3, suggesting that both reactions proceed on the same type of reaction sites. SMSI generates gradually by increasing reduction temperature (T_R). At $T_R = 623$ K, the rate-determining step shifted from the dissociative adsorption of hydrogen to the addition of surface hydrogen to adspecies as HD formation in Figure 8.3 is one order of magnitude higher than propanal and allyl alcohol formations. Thus, the characteristic reaction rate profile at $T_R = 623$ K in Figure 8.3(b) is suggested to be due to the change in the number of sites (site I and site II) by SMSI generation similarly to the features observed with SMSI-Rh/Nb₂O₅ and Ir/Nb₂O₅.

The number of site I and site II changes as a function of t_R as follows;

$$S_I = S_0 - \alpha t_R^{1/2}, \quad S_{II} = \beta t_R^{1/4}$$

where S_0 is the number of site I on LTR catalyst without the migration of NbO_x, and α , β are constants. The site I decreases linearly with $t_R^{1/2}$ by the blocking due to the thermal migration (diffusion) of NbO_x onto metal surface, while the periphery of NbO_x islands (site II) increases with $t_R^{1/4}$ at the initial stage.

The reaction rate has a maximum at certain t_s when site II plays a significant role in catalysis or both sites contribute to the reaction in a cooperative manner as discussed in previous chapters. In the data at $T_R = 623$ K for HD formation in Figure 8.3 (c), the rate for H_2 - D_2 exchange decreased monotonously with an increase of t_s whereas the rates of the formations of propanal and allyl alcohol showed the maximum in Figure 8.3(b). Consequently, hydrogen dissociates on bare metal site (site I) while acrolein is suggested to adsorb to react with the hydrogen on the periphery site (site II). Ir/ Nb_2O_5 that propanal is, however, formed on site I via a different intermediate from that for allyl alcohol formation which proceeds on site II. On Pt/ Nb_2O_5 both propanal and allyl alcohol are produced on the same site II as already mentioned, hydrogen atom being produced on site I as illustrated in Figure 8.6.

The H/M in Figure 8.1 decreased from 0.375 to below 0.01 by SMSI, but the rate of H_2 - D_2 exchange during acrolein hydrogenation/deuteration decreased only from 1.32 to 0.406 min^{-1} as shown in Table 8.1. From these results the H_2 - D_2 exchange reaction per Pt surface metal is evaluated to be enhanced more than 100 times by SMSI. The above picture explains the increase in the rate of H_2 - D_2 exchange which is prevented by the competitive adsorption of acrolein on LTR catalyst. The picture also explains the decrease of $\Sigma id_i / n \Sigma d_i$ in both deuterated propanal and allyl alcohol on SMSI catalyst. $\Sigma id_i / n \Sigma d_i$ reflects surface $[H]/[D]$ ratio. Surface deuterium formed by D_2 dissociation is generally diluted by the hydrogen produced by interconversion between π -intermediate (A species in Schemes 8.1 and 8.2) and half-hydrogenated intermediate (B species) during the deuteration of d_0 -acrolein. If the hydrogen atoms freely

diffuse on both site I and site II, they would be exchanged with deuterium in gas phase and as a result $\sum d_i / n \sum d_i$ on SMSI catalyst would not be different from that on LTR catalyst having only bare metal site. The significant difference in $\sum d_i / n \sum d_i$ between both catalysts in Tables 8.3 and 8.4 implies some restriction for the movement of surface hydrogen into site II, probably due to the crowdedness of adsorbed acrolein on site II.

Isotope distribution in propanal in Table 8.7 suggests the identity of chemical environments of active sites for the isomerization of allyl alcohol to propanal and the deuteration of acrolein. If the isomerization and C=C hydrogenation occur on different kinds of sites, d_3 , d_4 and d_5 -propanals should not be produced. This is also consistent with Scheme 8.1.

(Vi) The microscopic behavior of active sites during the reaction

As for metal-semiconductor junction, the Fermi-level of the metal and the semiconductor must be equal at the interface [1, 30, 31]. If the work function of TiO_2 or NbO_5 is smaller than that of metal, electrons will flow from the suboxides to the metal. Since the screening distance in metal is usually quite short, it is possible that specially electronically modified sites appear at the interface. Theoretical calculations indicate that the electronic perturbation is screened out within two atomic distances or < 0.5 nm [32-36]. This area may correspond to site II on SMSI catalyst.

Deuteration of acrolein on SMSI-Pt/ Nb_2O_5 occurs by the cooperative work of site I and site II as illustrated in Figure 8.6. Site I dissociates D_2 and site II adsorbs acrolein as A_1 species which appears to turn its oxygen atom to Nb_2O_5 island.

Because deuterium can be supplied only from site I and the isotope distributions in propanal and allyl alcohol show the singular population on D on the γ -carbon. The addition of D atom to η^4 -adsorbate(A_1) produces B_1 and B_2 species, followed by further addition of deuterium or hydrogen to form propanal and allyl alcohol. Singular populations of hydrogen on β -carbon in propanal and α -carbon in allyl alcohol suggest the second addition of H much more than D which may be due to the spatial restriction of D atom availability. Deuterium population is higher on site I. This difference in "deuterium atmosphere" of reaction sites on SMSI Pt/Nb₂O₅ is similar to D₂-acrolein reaction on Ir/Nb₂O₅ and D₂-ethene reaction on Rh/Nb₂O₅ or Ir/Nb₂O₅.

The difference in the deuteration mechanisms among Pt, Ir and Rh catalysts are summarized in Table 8.9. Appearance of two kinds of reaction sites by SMSI is common for three metals. While Rh was not electronically modified apparently, the other two metals weremodified, judging from the difference of activation energies between LTR and HTR catalysts. This reason might be explained by their Fermi-levels. The work functions of three metals decrease in the order 5.65, 5.27 and 4.98 eV, for Pt, Ir, and Rh, respectively. It is difficult to estimate the work function of junctive NbO₂ due to unknown x and unknown structure. Titanium oxide after high temperature reduction has been reported to have 4.6 eV [37] and reduced niobium oxide may be assumed to have a similar value. All of the work functions of Pt, Ir and Rh are higher than this value and hence the electrons would flow into the metal. It is possible that acrolein is adsorbed as three kinds of intermediates, η^2 (C-C), η^2 (C-O) on site I and η^4 (C-C-C-O) on site II; the former two were observed

on both normal Ir/Nb₂O₅ and Pt/Nb₂O₅, and the last one was observed on site II of SMSI-Pt/Nb₂O₅, but on SMSI-Ir/Nb₂O₅ the three kinds of intermediates were observed. The η^4 -type adsorption may be advantageous on electron-rich metal in terms of the delocalization of electron (indirect interaction). Nbⁿ⁺ (n < 5) is also possible to coordinate directly to the oxygen atom of CHO group of acrolein (direct interaction).

8.4 Summary

(1) The structures and microscopic behaviors of reaction sites for acrolein hydrogenation/deuteration on SMSI Pt/Nb₂O₅ catalyst were studied by kinetics and isotope distributions.

(2) The selectivity to allyl alcohol formation was enhanced on HTR catalyst.

(3) The acrolein hydrogenation on LTR catalyst follows the conventional associative mechanism involving η^2 (C-C) or η^2 (C-O) species.

(4) In contrast, on HTR catalyst both propanal and allyl alcohol are formed through η^4 -(C-C-C-O) intermediate.

(5) Hydrogen dissociates on bare metal sites (site I), while acrolein adsorbs to react with the hydrogen atoms on the periphery sites of NbO₂ islands (site II) on HTR catalyst. Accordingly, the acrolein hydrogenation proceeds by the cooperative behavior of the two kinds of reaction sites on HTR catalyst.

(6) The comparison with the hydrogenation of CH₂=CHCF₃ having CF₃ group with a similar Hammett's parameter to CHO group of acrolein showed the contribution of the conjugation of C=C and C=O in acrolein molecule to the adsorption and hydrogenation reaction on

SMSI surface.

(7) The hydrogen-induced γ -C-H breaking mechanism for the hydrogenation of acrolein to allyl alcohol was presented on the basis of a large isotope effect in the rate and the isotope distribution on the γ -carbon of allyl alcohol.

(8) The η^4 -(C-C-C-O) intermediate was suggested to be stabilized at the conjunction area of metal-NbO_x (site II) by electronic effects.

(9) The D/H ratio of surface concentration in D₂-acrolein reaction is lower on site II than on site I.

(10) The reaction rate profiles as a function of reduction time of catalyst, the comparison of HTR and LTR catalysts in the HD formation (H₂+D₂+acrolein), the values $\Sigma id./n\Sigma d.$, and the reaction rates of acrolein and 3,3,3-trifluoropropene hydrogenations, and the cooperative reaction mechanism discriminate two different reaction sites in the working state.

(11) While the value of H/M decreased from 0.375 to below 0.01 by SMSI, the site I (bare metal sites) worked as active sites for hydrogen chemisorption and H₂-D₂ exchange reaction, which suggests the heterogeneous distribution of large NbO_x islands on Pt surfaces rather than the uniform and high dispersion of small NbO_x clusters on Pt surface.

References

1. R.Burch, in *Hydrogen Effects in Catalysis* (Zoltan, P., and Menon, P.G., eds.) Marcel Dekker Inc., New York, 1988.
2. R.Burch, A.R.Flambard, *J.Catal.*, **78**, 389 (1982).
3. M.A.Vannice, R.L.Garten, *J.Catal.*, **66**, 242 (1980).
4. C.C.Kao, S.C.Tsai, Y.W.Chung, *J.Catal.*, **73**, 136 (1982).

5. M.A.Vannice, R.L.Garten, *J.Catal.*, **56**, 236 (1979).
6. C.H.Bartholomew, R.B.Pannell, J.L.Butler, *J.Catal.*, **65**, 335 (1980).
7. Y.W.Chung, G.Xiang, C.C.Kao, *J.Catal.*, **85**, 237 (1984).
8. M.A.Vannice, R.L.Garten, *J.Catal.*, **63**, 255 (1980).
9. A.Erdohelyi, F.Solymosi, *J.Catal.*, **84**, 446 (1983).
10. F.Solymosi, I.Tombacz, A.Erdohelyi, *J.Catal.*, **75**, 78 (1982).
11. J.D.Bracy, R.Burch, *J.Catal.*, **86**, 384 (1984).
12. Y.A.Ryndin, R.F.Hicks, A.T.Bell, *J.Catal.*, **70**, 287 (1981).
13. S.J.Wang, S.H.Moon, M.A.Vannice, *J.Catal.*, **71**, 167 (1981).
14. M.A.Vannice, C.Sudhakar, *J.Phys.Chem.*, **88**, 2429 (1984).
15. E.I.Ko, J.M.Hupp, N.J.Wagner, *J.Catal.*, **86**, 315 (1984).
16. K.Kunimori, H.Abe, E.Yamaguchi, S.Matsui, T.Uchijima, 8th Inter.Congr.Catal., (Berlin), V, 251 (1984).
17. T.Iizuka, Y.Tanaka, K.Tanabe, *J.Mol.Catal.*, **17**, 381 (1982).
18. D.E.Resasco, R.J.Fenoglio, M.P.Suarez, J.O.Cechini, *J.Phys.Chem.*, **90**, 4330 (1986).
19. P.Chou, M.A.Vannice, *J.Catal.*, **107**, 129 (1987).
20. B.Sen, M.A.Vannice, *J.Catal.*, **113**, 52 (1988).
21. M.A.Vannice, B.Sen, *J.Catal.*, **115**, 65 (1989).
22. S.D.Kahn, C.F.Pan, L.E.Overman, W.J.Hehre, *J.Am.Chem.Soc.*, **108**, 7381 (1986).
23. W.T.Hendrix, F.G.Cowherd, J.L.Rosenberg, *J.Chem.Soc., Chem. Commun.*, 98 (1968).
24. T.Yamamoto, J.Ishizu, A.Yamamoto, *J.Am.Chem.Soc.*, **103**, 6863 (1981).
25. H.P.Fritz, G.N.Schrauzer, *Chem.Ber.*, **94**, 65 (1961).
26. G.C.Bond, "Catalysis by Metals", Academic Press, London, (1962).
27. R.Touroude, *J.Catal.*, **65**, 110 (1980).

28. G.W.Smith, J.F.Deany, *J.Catal.*, **6**, 14 (1966).
29. M.Nishimura, K.Asakura, Y.Iwasawa, *J.Chem.Soc., Chem.Commun.*, 1660 (1986).; *Chem.Lett.*, 573 (1987).
30. W.Schottky, *Z.Phys.*, **113**, 367 (1939).
31. L.J.Brillson, *Appl.Surf.Sci.*, **11/12**, 249 (1982).
32. R.W.Joyner, J.B.Pendry, D.K.Saldin, S.R.Tennison, *Surf. Sci.*, **95**, 1 (1984).
33. J.R.Smith, F.J.Arlinghaus, J.G.Gay, *Phys.Rev.*, **B26**, 1092 (1982).
34. D.J.Feibelman, D.R.Hamann, *Surf.Sci.*, **149**, 48 (1985).
35. J.M.MacLaren, J.B.Pendry, R.W.Joyner, *Surf.Sci.*, **178**, 856 (1986).
36. J.M.MacLaren, J.B.Pendry, R.W.Joyner, P.Meehan, *Surf.Sci.*, **175**, 263 (1986).
37. Y.W.Chung, W.J.Lo, G.A.Somorjai, *Surf.Sci.*, **64**, 588 (1977).

Table 8.1 Initial rates and activation energies for the deuteration of $\text{CH}_2=\text{CHCHO}$ and $\text{CH}_2=\text{CHCF}_3$, and for the H_2 - D_2 exchange reaction.

reaction	product	r_{LTR}^{**}	E_a^{LTR}	r_{HTR}^{**}	E_a^{HTR}	$r_{\text{HTR}}/r_{\text{LTR}}$
$\text{D}_2 + \text{CH}_2 = \text{CHCHO}$ (373 K)	PA	0.737	5	0.041	46	$5.6 \cdot 10^{-2}$
	AA	0.224	5	0.094	44	$4.2 \cdot 10^{-1}$
	PO	0.318	7	0.000		0.0
$\text{D}_2 + \text{CD}_2 = \text{CDCDO}$ (373 K)	PA	0.740		0.040		$5.4 \cdot 10^{-2}$
	AA	0.201		0.009		$4.5 \cdot 10^{-2}$
	PO	0.288		0.000		----
$\text{H}_2 + \text{D}_2 + \text{CH}_2 = \text{CHCHO}$ (373 K)	HD	1.32	5	0.406	19	$3.1 \cdot 10^{-1}$
$\text{D}_2 + \text{CH}_2 = \text{CHCF}_3$ (273 K)	EtCF ₃	1.18	9	$2.1 \cdot 10^{-4}$	9	$1.7 \cdot 10^{-4}$
$\text{H}_2 + \text{D}_2 + \text{CH}_2 = \text{CHCF}_3$ (273 K)	HD	1.20	8	0.376	17	$3.1 \cdot 10^{-1}$
Pt/SiO ₂						
$\text{D}_2 + \text{CH}_2 = \text{CHCHO}$ (373 K)	PA	0.132	6			
	AA	0.00				
	PO	0.00				

* PA, AA and PO represent propanal, allyl alcohol and propanol, respectively. The other products such as ethane, carbon monoxide are less than 1 %. ** r_{LTR} and r_{HTR} represent the initial rates (min^{-1} , normalized by $\text{H}/\text{M} = 0.375$) for LTR and HTR catalyst, respectively. E_a stands for the activation energies ($\text{kJ} \cdot \text{mol}^{-1}$). Reaction temperature is between 333 K and 393 K. $\text{CH}_2 = \text{CHCHO}$, $\text{CD}_2 = \text{CDCDO}$, $\text{CH}_2 = \text{CHCF}_3$: 1.3 kPa, total hydrogen (H_2 , D_2 or $\text{H}_2 + \text{D}_2$) : 5.3 kPa.

Table 8.2 Percentage distributions of deuterated acrolein in the initial stage of D_2 -acrolein reaction at 373 K.

product	catalyst	
	LTR	HTR
d_0 $CH_2=CHCHO$	90	91
d_1 $CHD=CHCHO$	3	8
$CH_2=CDCHO$	0	1
$CH_2=CHCDO$	7	0
$100 \sum d_i / 4 \sum d_i$	2.5	2.3

Values at 8% conversion of deuteration.

$CH_2=CHCHO$: 1.3 kPa, D_2 : 5.3 kPa.

Table 8.3 Percentage distributions of deuterated propanal in the initial stage of D_2 -acrolein reaction at 373 K.

	product	catalyst	
		LTR	HTR
d_0	$CH_3CH_2CH=O$	0	13
d_1	$CH_2DCH_2CH=O$	14	31
	$CH_3CHDCH=O$	9	4
d_2	$CHD_2CH_2CH=O$	23	29
	$CH_2DCHDCH=O$	16	20
	$CH_3CD_2CH=O$	11	3
d_3	$CD_3CH_2CH=O$	10	0
	$CHD_2CHDCH=O$	7	0
	$CH_2DCD_2CH=O$	5	0
d_4	$CD_3CHDCH=O$	4	0
	$CHD_2CD_2CH=O$	1	0
100 $\Sigma id_i / 6\Sigma d_i$		35(42)	23(28)

Values in the bracket are 100 $\Sigma id_i / 5\Sigma d_i$. $\Sigma id_i / 5\Sigma d_i$ is reasonable parameter as for LTR catalyst because the hydrogen in $-CH=O$ is not concerning with the hydrogenation of $C=C$ and, consequently, it is comparable with Table 5. See text. The values are ones at the extrapolation to 0 % conversion. $CH_2=CHCHO$: 1.3 kPa, D_2 : 5.3 kPa.

Table 8.4 Percentage distributions of deuterated allyl alcohol in the initial stage of D₂-acrolein reaction at 373 K.

	product	LTR	HTR
d ₀	CH ₂ =CHCH ₂ OH	16	12
d ₁	CH ₂ =CHCH ₂ OD	4	4
	CH ₂ =CHCHDOH	29	2
	CHD=CHCH ₂ OH	0	62
d ₂	CH ₂ =CHCHDOD	41	0
	CHD=CHCH ₂ OD	0	3
	CD ₂ =CHCH ₂ OH	0	17
d ₃	CH ₂ =CHCD ₂ OD	10	0
100 Σid _i /6Σd _i		24(48)	18(36)

Values in the bracket is 100 Σid_i/3Σd_i. The values are ones at the extrapolation to 0 % conversion. CH₂=CHCHO : 1.3 kPa, D₂ : 5.3 kPa.

Table 8.5 Percentage distributions of deuterated 1,1,1-trifluoropropane and 3,3,3-trifluoropropene in the initial stage of D_2 - $CH_2=CHCF_3$ reaction at 310 K.

product	LTR	HTR
d_0 $CH_3CH_2CF_3$	4	21
d_1 $CH_2DCH_2CF_3$	19	33
d_2 $CHD_2CH_2CF_3$	28	38
$CH_2DCHDCF_3$	9	8
d_3 $CD_3CH_2CF_3$	15	0
CHD_2CHDCF_3	8	0
d_4 CD_2CHDCF_3	8	0
$CHD_2CD_2CF_3$	6	0
d_5 $CD_3CD_2CF_3$	3	0
$\Sigma id_i / 5 \Sigma d_i$	47	25
d_0 $CH_2=CH_2CF_3$	98	98
d_1 $CHD=CH_2CF_3$	2	2

The values are ones at the extrapolation to 0 % conversion for deuterated products and 8 % conversion to exchanged products.

$CH_2=CHCHO$: 1.3 kPa, D_2 : 5.3 kPa.

Table 8.6 Isotope distribution in allyl alcohol formed in 10 min after H_2 introduction to the $D_2/CD_2=CDCDO$ system on HTR catalyst. $CD_2=CDCDO$: 1.3 kPa, D_2 : 5.3 kPa.

	exper.	calc. ^a
d_6 $CD_2=CDCD_2OD$	19	16
d_5 $CHD=CDCD_2OD$	10	13
$CD_2=CDCD_2OH$	37	39
d_4 $CHD=CDCD_2OH$	35	32

a : See text

Table 8.7 Isotope distribution in propanal formed by d_0 -allyl alcohol addition during the course of d_4 -acrolein deuteration on HTR catalyst.

	d_0	d_1	d_2	d_3	d_4	d_5	d_6
relative amount/%	10	13	36	5	6	8	22

$CD_2=CDCDO$, $CH_2=CHCH_2OH$: 1.3 kPa, D_2 : 5.3 kPa.

Table 8.8 HOMO and LUMO levels of vinyl compounds.

	orbital energy / eV		σ_n
	HOMO	LUMO	
$\text{CH}_2 = \text{CHNO}_2$	-11.63	1.3	0.71
$\text{CH}_2 = \text{CHCHO}$	-10.9	2.6	0.36
$\text{CH}_2 = \text{CHCF}_3$	-11.6	3.6	0.43
$\text{CH}_2 = \text{CHSiH}_3$	-10.4	4.0	
$\text{CH}_2 = \text{CH}_2$	-10.3	5.1	0
$\text{CH}_2 = \text{CHCH}_3$	-9.9	5.3	-0.07

Table 8.9 The Comparison of three (Rh, Ir and Pt) SMSI catalysts in ethene and acrolein deuteration.

metal (ϕ)	reaction (E_{η})	adsorption and deuteration	
		site I	site II
Rh (4.98eV)	$\text{CH}_2=\text{CH}_2+\text{D}_2$ ($E_{\text{LTR}}=E_{\text{HTR}}$)	D_2 (g) * D (ad) C_2H_4 * $\eta^2(\text{C-C})(\text{ad})$ d_2 -ethane, formed.	C_2H_4 * $\eta^2(\text{C-C})(\text{ad})$ d_0 -ethane, formed.
	$\text{CH}_2=\text{CHCH}=\text{O}+\text{D}_2$ ($E_{\text{LTR}} < E_{\text{HTR}}$; PA) ($E_{\text{LTR}} > E_{\text{HTR}}$; AA)	D_2 (g) * D (ad) AC * $\eta^2(\text{C-C})(\text{ad})$ $\eta^2(\text{C-O})(\text{ad})$.	AC * $\eta^4(\text{C-C-C-O})(\text{ad})$. d_2 -PA + d_2 -AA, formed. d_0 -AA, formed.
Pt (5.65eV)	$\text{CH}_2=\text{CHCH}=\text{O}+\text{D}_2$ $E_{\text{LTR}} < E_{\text{HTR}}$	D_2 (g) * D (ad) none, formed.	AC * $\eta^4(\text{C-C-C-O})(\text{ad})$. d_1, d_2 -AA + d_1, d_2 -PA formed.

E_{LTR} and E_{HTR} represent the activation energy for LTR and HTR catalysts, respectively. AC, PA and AA are acrolein, propanal and allyl alcohol, respectively.

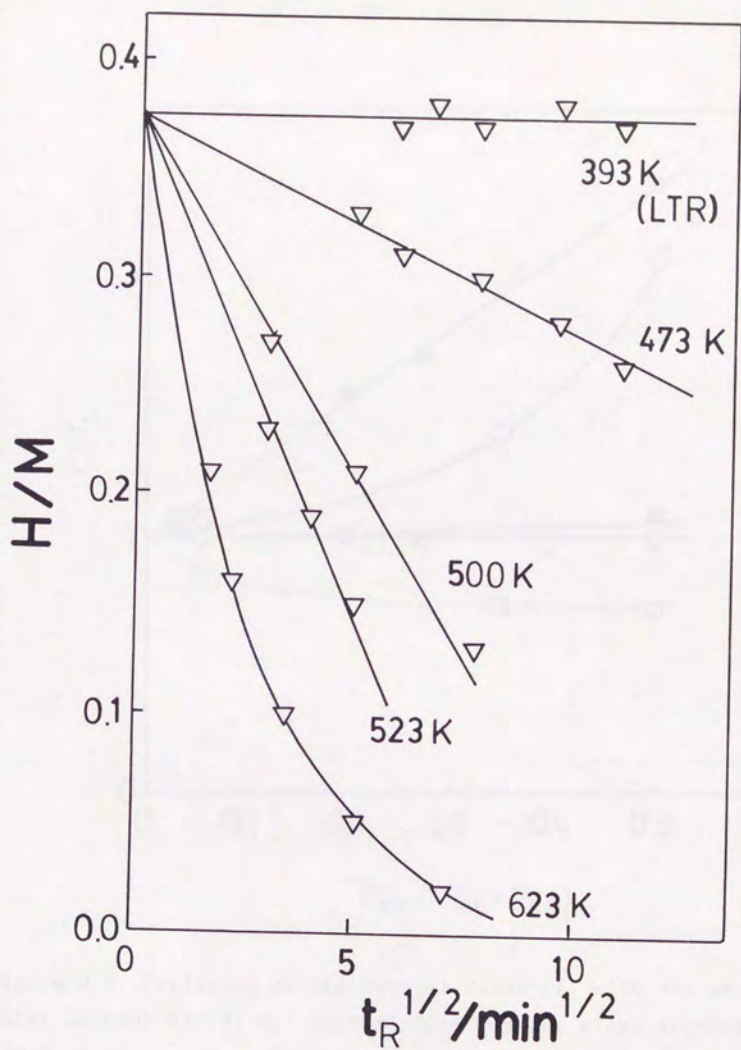


Figure 8.1 H/M versus reduction time of catalyst at several temperatures.

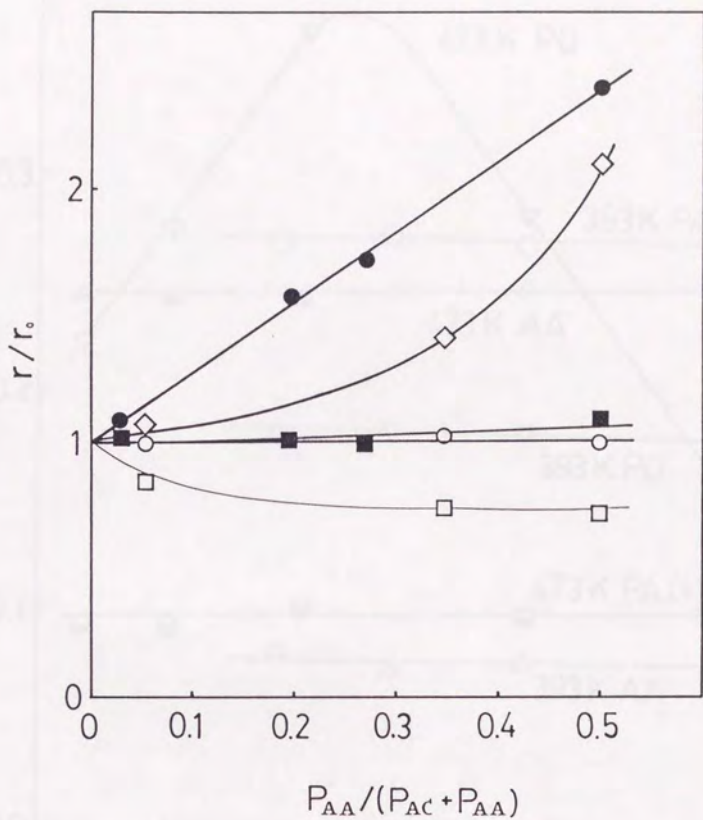


Figure 8.2 Variation of the initial rates (r) with the amount of allyl alcohol added; r_0 : initial rate without allyl alcohol added.

LTR catalyst: ○ : propanal, ◇ : propanol, □ : acrolein,
 HTR catalyst: ● : propanal, ■ : acrolein.

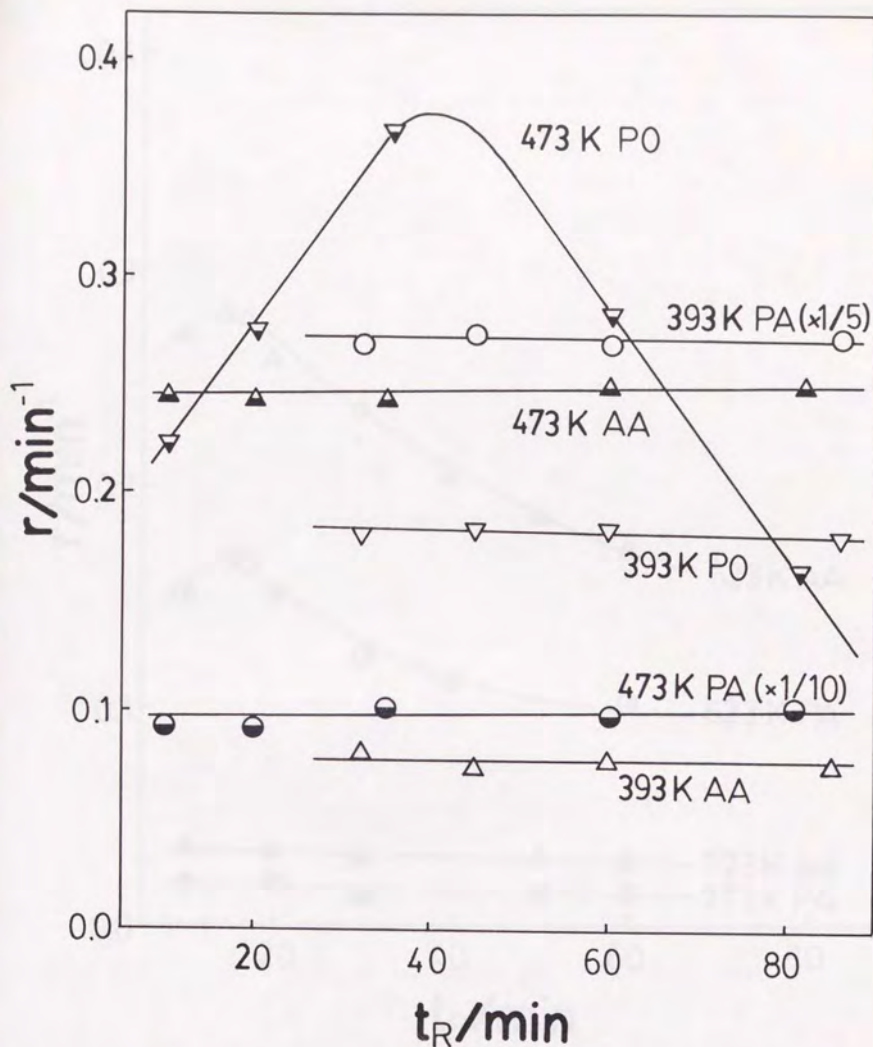


Figure 8.3(a) Rates (turnover frequencies :TOF) of the product formations at 373 K versus reduction time (t_R) of catalyst at 393 and 473 K; acrolein : 1.3 kPa, D_2 : 5.3 kPa.

TOF was calculated by using $H/M = 0.375$.

○●: propanal, △▲: allyl alcohol, ▽▽: propanol.

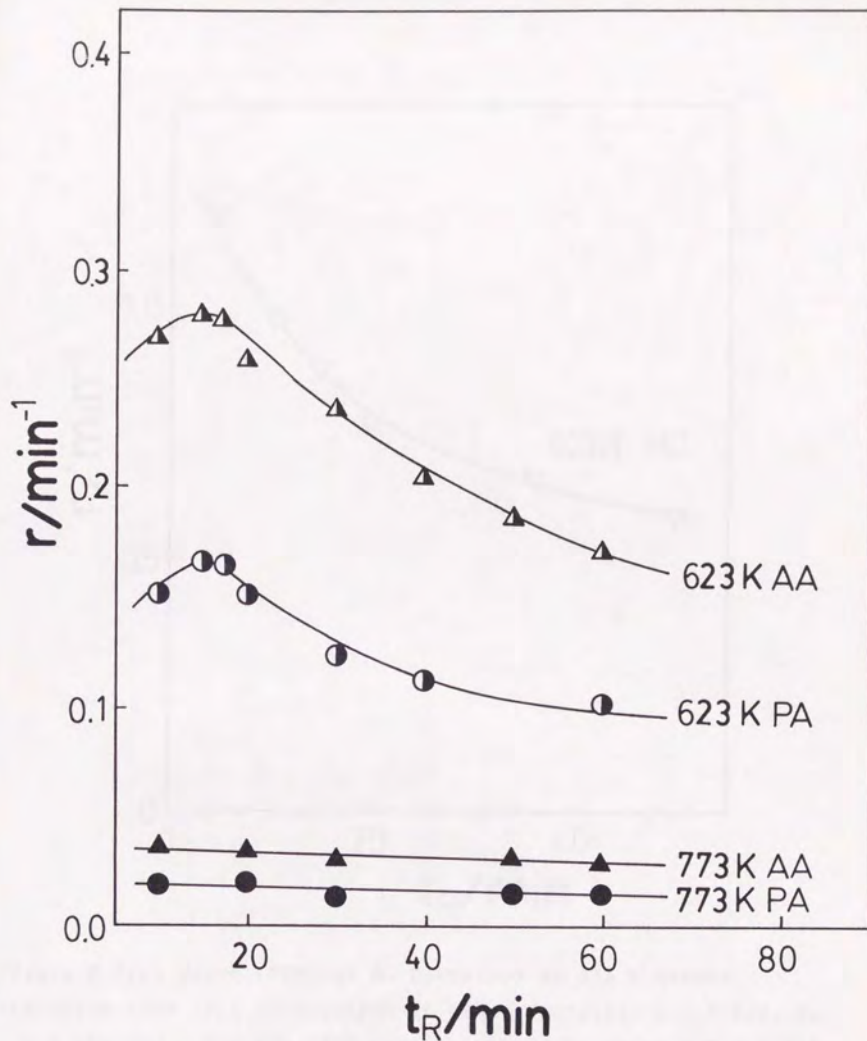


Figure 8.3(b) Rates (TOF) of the product formations at 373 K versus reduction time (t_R) of catalyst at 623 and 773 K; acrolein : 1.3 kPa, D_2 : 5.3 kPa. TOF was calculated by using $H/M=0.375$. \circ \bullet : propanal, \triangle \blacktriangle : allyl alcohol.

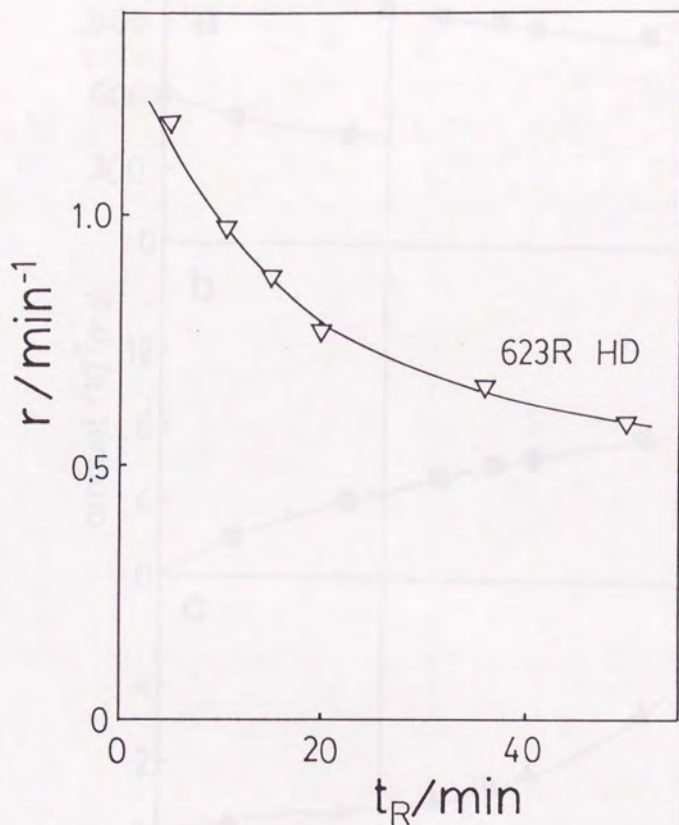


Figure 8.3(c) Rates (TOF) of HD formation at 373 K versus reduction time (t_R) of catalyst at 623 K; acrolein : 1.3 kPa, H_2 : 2.6 kPa, D_2 : 2.6 kPa. TOF was calculated by using $\text{H}/\text{M} = 0.375$.

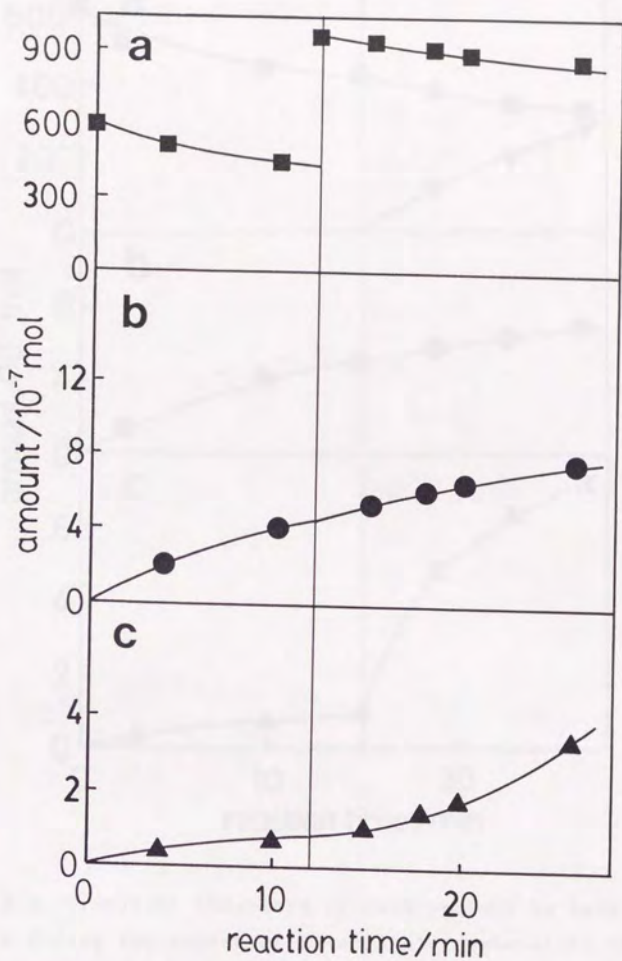


Figure 8.4 Transient behaviors of (a): acrolein, (b): propanal, and (c): allyl alcohol produced by *d*₀-acrolein addition during the course of *d*_s-acrolein deuteration on SMSI-Pt/Nb₂O₅ catalyst at 373 K; *d*_s-acrolein : 1.3 kPa, D₂ : 5.3 kPa, *d*₀-acrolein : 1.3kPa. *d*₀-acrolein was added at t = 12 min.

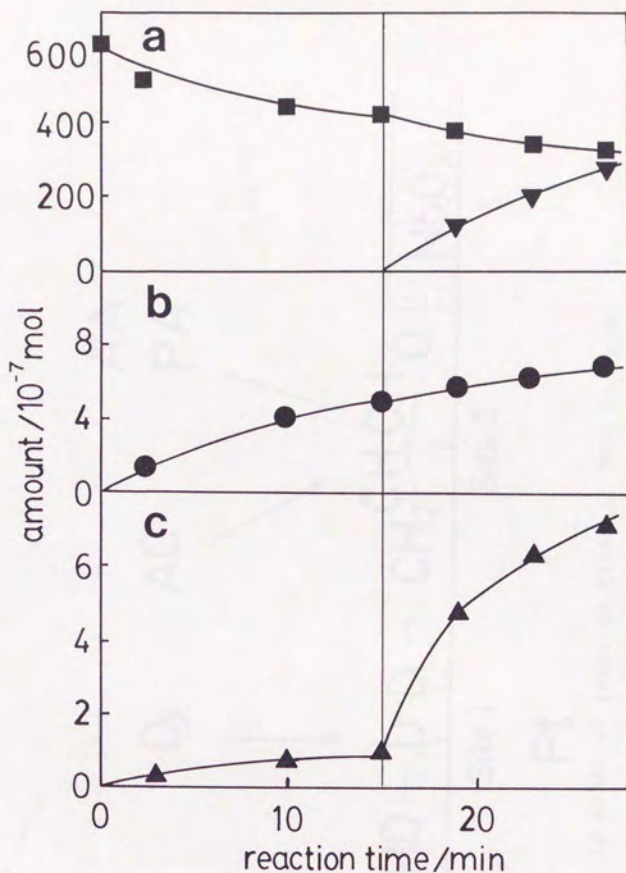


Figure 8.5 Transient behaviors of each product by hydrogen addition during the course of d_4 -acrolein deuteration on SMSI catalyst at 373 K; d_4 -acrolein : 1.3 kPa, D_2 : 5.3 kPa, H_2 : 5.3kPa. H_2 was added at $t = 15$ min.

(a) ■ : acrolein, ▼ : HD; (b) propanal; (c) allyl alcohol.

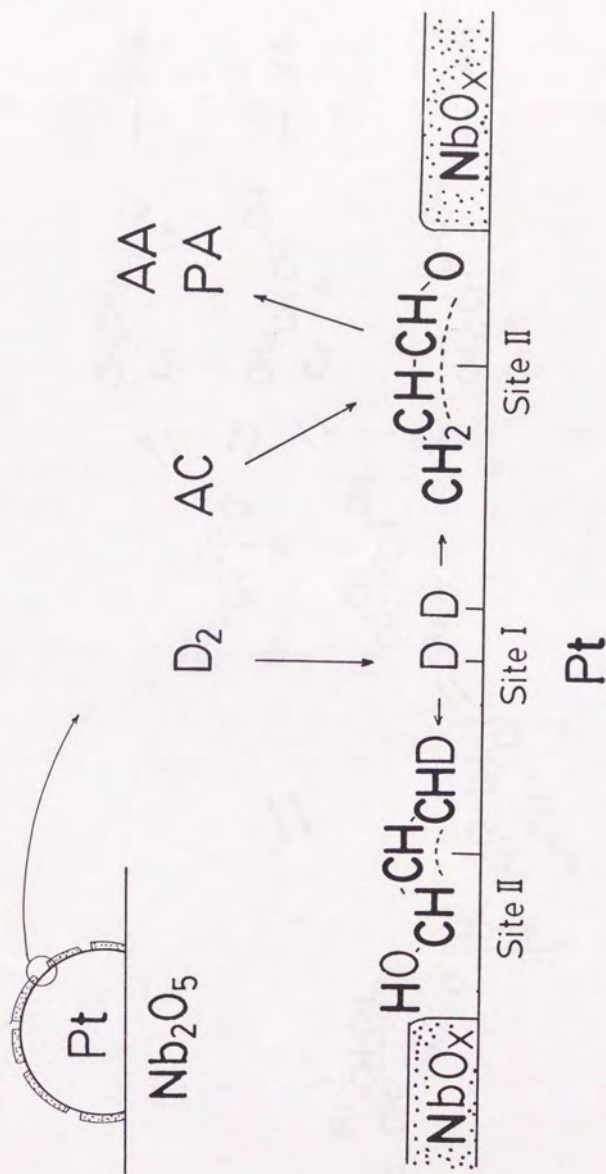
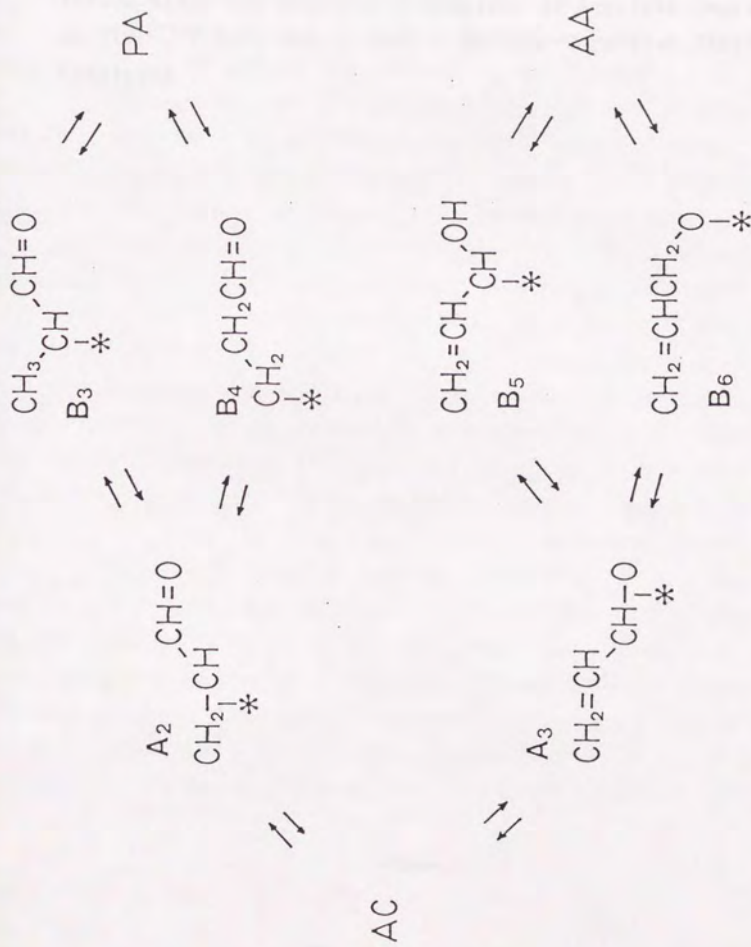


Figure 8.6 A schematic model of reaction sites of SMSI Pt/Nb₂O₅ for acrolein deuteration.



Scheme 8.2. Reaction paths and Intermediates for acrolein hydrogenation/deuteration on LTR-Pt/Nb₂O₅. AC: acrolein, PA: propanal, AA: 2-propene-1-ol.

Chapter 9

Active Sites and Reaction Mechanisms of Acrolein Deuteration on TiO_2 -, Y_2O_3 -, ZrO_2 -, CeO_2 -, Na/SiO_2 -Supported Platinum Catalysts

The conversion of α, β -unsaturated aldehyde into saturated aldehyde or unsaturated alcohol has been a probe reaction for the performance of a given metal catalyst. Olefinic double bond is to be reduced by kinetic and thermodynamic advantages and the yield of unsaturated alcohol has been very small in usual. Thus, from synthetic point of view, it has been usually under discussion in what circumstances carbonyl group is reduced selectively to leave C=C bond unreacted. It has been successfully done to introduce the additives [1-5] or supports [6] as polarized ligands to compose the active site.

2-Propenal(acrolein) is the simplest molecule in this category and is, consequently, preferable to the detailed characterization of the surface in addition to the synthetic performance. Research on its mechanism including the intermediate identification is possible with less difficulties than the other molecules by means of isotope tracing techniques and vibrational spectroscopic methods. And the results would describe the working state of the catalyst surface in detail.

Metal-support interactions in catalysis has been one of the most important topics, especially SMSI, and now the origin of the SMSI came to agreed with the migration of partially reduced support oxide onto the metal surface. Interest has been also gathered on other supports, mainly easily reducible oxides. [7-11] As for Pt/ZrO₂ and Pt/Y₂O₃, the transition of the density of unoccupied d-state by high temperature reduction is larger than Pt/TiO₂ and Pt/Nb₂O₅ which are well known SMSI catalyst as already shown in chapter 6. Pt/CeO₂ has been also demonstrated to show pleasant catalysis accompanied by the partial reduction of the support. [7, 12] In this chapter, acrolein deuteration is applied to these catalysts in addition to Pt/TiO₂. Clarification

of the behavior of active site under catalytic reaction is essential to tracing the genesis of catalysis and gives a key ingredient of future control of metal catalyses. Acrolein deuteration could contribute in the elucidation of the state of the metal surface in a working state, which is modified by the partially reduced support-oxide in the vicinity and the electron transfer between support and the metal particle.

9.1 Methods

2.3%-Pt/TiO₂, Pt/Y₂O₃, Pt/ZrO₂, and Pt/CeO₂ catalysts were prepared by incipient wetness method of TiO₂ (Nippon Aerosil P-25), Y₂O₃ (Soekawa Chemical Co.,Ltd. 99.99%), ZrO₂ (Soekawa Chemical Co.,Ltd. 99%), CeO₂ (Soekawa Chemical Co.,Ltd. 99%), respectively, with aqueous solution of H₂PtCl₆·6H₂O (Soekawa Chemical Co.,Ltd., research grade). Pt/SiO₂ and Na/Pt/SiO₂ catalysts were also prepared by co-impregnation method as described in chapter 4. The catalysts thus obtained were placed in a closed circulating reactor. Then they were treated with oxygen at 473 K for 1 h, followed by evacuation for 30 min and reduced at 373 K ~ 773 K for 1h, followed by evacuation for 30 min before the catalytic reaction. Pt/SiO₂ and Na/Pt/SiO₂ were constantly reduced at 673 K. Acrolein (Tokyo Kasei Co.,Ltd.) were purified by freeze-thaw cycles before use. Deuterium (Takachiho Trading Co.,Ltd., research grade) was purified through a 5A molecular-sieve trap at 77 K.

Typical reaction conditions were $P_{\text{CH}_2=\text{CHCHO}} = 1.3 \text{ kPa}$, $P_{\text{D}_2} = 5.2 \text{ kPa}$ and the temperature $323 \text{ K} \leq T \leq 403 \text{ K}$. The products of D₂ - CH₂=CHCHO reaction were separated and identified by gas chromatograph with molecular sieve 5A, VZ-10 and PEG-1500

columns. The products were analyzed by TCD or mass spectrometer (ANELVA AQA-100R operating with 70 eV electrons) after separation. Hydrogen adsorption for dispersion (H/Pt) measurement were done in the same reactor.

The adsorbates on the catalysts were observed by infrared spectrometer (JASCO FT/IR-7000 with 2 cm^{-1} resolution). The catalysts were molded into self-supporting disks and mounted in the closed circulating reactor mentioned above. Usual procedure was as follows : acrolein adsorption at room temperature and evacuation with increasing temperature up to 353 K (or 333 K), following repetition of H_2 circulation and evacuation at this temperature. The spectra accumulated after each evacuation in a transmission mode.

9.2 Results

Suppression of the hydrogen adsorption by high temperature reduction of Pt/TiO₂, Pt/Y₂O₃, Pt/ZrO₂, and Pt/CeO₂ catalysts is represented again in Table 9.1. The adsorption decreased considerably on Pt/ZrO₂ and Pt/CeO₂ while little on Pt/Y₂O₃. Pt/TiO₂, well known SMSI catalyst, lost adsorption capacity almost completely by 773 K reduction. The loss of H/Pt of all 773 K-reduced catalysts recovered by oxidation-low temperature reduction treatment. Pt/Y₂O₃ could not be reduced at 373 K and 473 K-reduced catalyst was defined as low temperature reduced Pt/Y₂O₃. The regeneration of hydrogen adsorption capacity was also confirmed. H/Pt for Na/Pt/SiO₂ reduced at 673 K were shown in chapter 4, i.e. Pt/SiO₂: 0.31, Na/Pt/SiO₂ (Na/Pt = 0.19): 0.24, Na/Pt/SiO₂ (Na/Pt = 0.75, 1.5, 2.3, 6.1): 0.13.

The reaction rates hereafter was divided by the number of

surface atoms of Pt based on H/Pt of each catalyst. Only 773 K-reduced Pt/TiO₂ was based on H/Pt of 373 K-reduced Pt/TiO₂.

The products of D₂ - acrolein reaction were deuterated acrolein, propanal, and allyl alcohol. Some hydrogenolysis products, such as ethene, ethane, carbon monoxide, were detected over Pt/ZrO₂ and their amount was usually below 3%. No acceleration of formation was observed for 773 K-reduced Pt/TiO₂ and the other catalysts under the condition of the experiments.

Arrhenius plot for the catalysts which converted acrolein into both propanal and allyl alcohol is shown in Figure 9.1 (a)~(d). The slope which represents activation energy did not change by reduction temperature for propanal formations of all catalysts ($E = 40 \text{ kJ}\cdot\text{mol}^{-1}$ for Pt/TiO₂ and Pt/Y₂O₃, and $E = 30 \sim 31 \text{ kJ}\cdot\text{mol}^{-1}$ for Pt/ZrO₂ and Pt/CeO₂). Little activity alternation brought about by the 773 K reduction was observed for Pt/Y₂O₃, Pt/ZrO₂ and Pt/CeO₂. Pt/TiO₂ alone showed clear suppression of the activity by a factor of 6. The slope of allyl alcohol formation varied to increase on Pt/CeO₂ ($4 \text{ kJ}\cdot\text{mol}^{-1}$ to $19 \text{ kJ}\cdot\text{mol}^{-1}$) and to decrease on Pt/TiO₂ ($36 \text{ kJ}\cdot\text{mol}^{-1}$ to $19 \text{ kJ}\cdot\text{mol}^{-1}$) and Pt/ZrO₂ ($43 \text{ kJ}\cdot\text{mol}^{-1}$ to $20 \text{ kJ}\cdot\text{mol}^{-1}$) while it did not change for Pt/Y₂O₃ ($27 \text{ kJ}\cdot\text{mol}^{-1}$). Although the activation energy change made the evaluation and assessment of activity change difficult, the formation rate of allyl alcohol increased manifestingly by 773 K reduction of Pt/CeO₂ and Pt/ZrO₂.

The profile of Na/Pt/SiO₂ was different as in Figure 9.1(e). Detectable amount of allyl alcohol did not form and the activation energy for propanal formation did not depend on the loading of sodium ($41 \text{ kJ}\cdot\text{mol}^{-1}$) while it was $5 \text{ kJ}\cdot\text{mol}^{-1}$ for Pt/SiO₂. The activity changed little over all Na loadings except Na/Pt = 0.0.

The relative ratio of deuterium - H of $\text{CH}_2=\text{CHCHO}$ exchange reaction and the distribution of the products are summarized in Table 9.2 (a) and (b). Deuterium was found in every site of acrolein and d_2 -form was only 2,3- d_2 ($\text{CHD}=\text{CDCHO}$). The rate for the exchange was represented here as a ratio to propanal formation, $r_{\text{ex}}/r_{\text{p.a.}}$. It increased significantly in 773 K-reduced Pt/TiO₂ and Na-added Pt/SiO₂ which showed no loading dependence at Na/Pt \geq 0.75. The population of aldehydic deuterium in Pt/SiO₂ was fairly small and increased as the loading of Na then saturated after Na/Pt \geq 0.75.

The percentage distributions of d -propanals and d -allyl alcohols formed at the initial stage of the reaction are listed in Table 9.3(a), (b) and Table 9.4. Because Na/Pt/SiO₂ did not convert acrolein into detectable amount of allyl alcohol, Table 9.4 lacks this catalyst. Comparing Table 9.3(a) and Table 9.4, the range of isotope distribution was wider in propanal, $d_0 \sim d_2$, than in allyl alcohol, $d_0 \sim d_2$. Na promoted catalyst showed significantly small $\Sigma d_i/6\Sigma d_i$ which is a indicator of D/H picking up ratio and this tendency did not depend on the loading of Na in Na/Pt \geq 0.75. On the contrary, in the other supported catalysts, $\Sigma d_i/6\Sigma d_i$ had no dependence on the reduction temperature. Pt/TiO₂ and Pt/Y₂O₃ were rather higher (37 ~ 39) than the other two (34 ~ 35). The distribution of allyl alcohol was small and, consequently, this make it possible to identify and quantify the species from the mass spectra analysis. 3- d_1 -allyl alcohol ($\text{CHD}=\text{CHCH}_2\text{OH}$) and 3,0- d_2 -allyl alcohol ($\text{CHD}=\text{CHCH}_2\text{OD}$) were formed on Pt/TiO₂ and Pt/Y₂O₃. The population was specially large in Pt/Y₂O₃. The other species, 1- d_1 -, 0- d_1 - and 1,0- d_1 -allyl alcohols, were found all catalysts of all reduction temperatures. d -propanal formed on all catalysts did not include aldehydic

deuterium.

Infrared spectra in carbonyl stretching region of adsorbed acrolein and following H_2 -treatment are shown in Figure 9.2 (a) ~ (h). All of these are plotted after subtraction of the adsorption of catalysts themselves. Pt/CeO₂ was excluded because the clear adsorption band was not observed on it or rather CeO₂ seemed to polymerize acrolein which could not appear in vapor. Pt/CeO₂ of both reduction temperatures gave the growing broad band of 1998 and 1868 cm⁻¹ after H₂ addition.

Three intense peaks, 1722, 1685 and 1658 cm⁻¹, and one weak band 1382 cm⁻¹ were observed on 373 K-reduced Pt/TiO₂ (Figure 9.2 (a)). With addition of H₂, 1685 cm⁻¹ declined fastest and 1658 cm⁻¹ slowest. At 773 K reduction (Figure 9.2(b)), the intensity of adsorption of 1720 and 1686 cm⁻¹ was not changed but the position of 1658 cm⁻¹ was slightly shifted to be 1654 cm⁻¹ and the intensity increased. The rate of disappearance of these peaks was not different between the reduction temperatures. 1382 cm⁻¹ on 373 K reduction shifted a little to 1386 cm⁻¹ and the intensity was increased. 473 K-reduced Pt/Y₂O₃ had three bands, namely, 1672(strong), 1618(shoulder) and 1367 cm⁻¹, which disappeared with H₂ (Figure 9.2(c)). The position, intensities and the rate of disappearance did not change when the reduction temperature was 773 K (Figure 9.2(d)). 1649 cm⁻¹ band observed on 373 K-reduced Pt/ZrO₂ (Figure 9.2(e)) was shifted to 1656 cm⁻¹ in 773 K reduction (Figure 9.2(f)) Hydrogen sensitive band at 1706 cm⁻¹ on 373 K-reduced catalyst was almost disappeared on 773 K-reduced catalyst. 1725 cm⁻¹ band appeared on both reduction temperature and disappearance was slow comparing to the other two bands when H₂ was added. On Pt/SiO₂ (Figure 9.2(g)), only one band was reactive, that is, 1655 cm⁻¹, declined with H₂ addition.

Two active bands, 1663 and 1600 cm^{-1} , were observed on Na/Pt/SiO₂ (Figure 9.2(h)). The former shifted to 1674 cm^{-1} at H₂ atmosphere. 1625 cm^{-1} of Pt/SiO₂ and 1622 cm^{-1} of Na/Pt/SiO₂ were inactive.

9.3 Discussion

One of the common feature noticeable in both alkali metal-doped Pt catalysts and high-temperature reduced Pt/MO_x catalysts (MO_x: TiO₂, Nb₂O₅, Y₂O₃, ZrO₂, etc.) is electron transfer to 5d-state. The density of unoccupied 5d-state of platinum particles decreases when Na loading or reduction temperature increases (chapter 5). The alternation of the total density of unoccupied 5d-state, n_f , is comparable between Na/Pt/SiO₂ and Pt/MO_x catalysts within the preparation condition controlled by present Na loadings and reduction temperature. The net effects of the metal additives and supports on the platinum particles are, roughly speaking, comparable, which do not include the difference in the local structure composed by each support or additive and the particular coordination state of platinum atoms induced. Under the same electron density, the promoted platinum surfaces in a working state is worth of comparing by the acrolein-deuterium reaction in order to analyze the characteristics of each support or additive.

Na/Pt/SiO₂ (and Pt/SiO₂)

The activation energy shifts in Figure 9.1(e) are caused by two possible changes in the elementary steps. One is the shift of rate-determining step and the other is the change in energetic profile of the rate-determining step. The activation energy of

HD formation of $H_2 + D_2 \rightarrow CH_2 = CHCHO$ reaction can be the criterion. It is $5 \text{ kJ}\cdot\text{mol}^{-1}$ for Pt/SiO₂ which is coincident with propanal formation and $10 \text{ kJ}\cdot\text{mol}^{-1}$ for Na/Pt/SiO₂ in all Na/Pt ratio which is significantly smaller than that of propanal ($41 \text{ kJ}\cdot\text{mol}^{-1}$). This result strongly suggests the rate-determining step shift from D₂ dissociation to another.

The surface structure of Na/Pt/SiO₂ is stabilized at Na/Pt > 0.2 as demonstrated in chapter 4. It is consistent to the previous chapters that most reaction characteristics here were constant above Na/Pt \geq 0.75.

The largest modification of intermediates of D₂-acrolein reaction is presented by the occurrence of aldehydic hydrogen exchange (Table 9.2(b)). C=O bond can be activated by Na addition which is not observed on Pt/SiO₂. An active band to hydrogen of 1600 cm^{-1} in infrared spectrum (Figure 9.2(h)) is assigned to C=C stretching of acrolein [13] and this band is attributed to C-O associative chemisorption species. ($\eta^2(\text{C-O})$, Scheme 9.1(b)) Pt/SiO₂ has no adsorption around this region. It is unlikely that the decrease of the unoccupied d-state density of platinum causes more than 20 cm^{-1} shift to bring about the crucial change for the reactivity. Thus the emergence of 1600 cm^{-1} band may reflect the different surface environments induced by Na.

The other effect of Na is the reduction of $\Sigma i d_i / 6 \Sigma d_i$ of propanal formation. It is suggested that the relative rate in quasi-equilibrium between C-C associative species and half-hydrogenated state become slower comparing to the second D/H addition step (to desorb). 1655 cm^{-1} for Pt/SiO₂ and 1663 cm^{-1} for Na/Pt/SiO₂ were attributed to C=O stretching of active $\eta^2(\text{C-C})$. These species likely to have the same environment of active

site with slightly modified electronic state which results in the shift of 8 cm^{-1} and the influence on the stability of this adspecies may be related with the enhancement of the exchange reaction of hydrogen about C=C- skeleton (Table 9.2(b)). 1718 cm^{-1} on Pt/SiO₂ and 1713 cm^{-1} on Na/Pt/SiO₂ are near free carbonyl of acrolein and inactive species.

Propanal formation is likely to follow associative mechanism of C=C bond in the absence of the interaction of C=O bond with surface because all deuterium were found about C=C double bond.

Blue-shift induced by H₂ treatment on Na/Pt/SiO₂ (1663 cm^{-1} to 1674 cm^{-1}) might be resulted from occurrence of the $\eta^2(\text{C-C})$ to half-hydrogenated species. Sudden transformation of the band suggests that half-hydrogenated species is rather stable and $\eta^2(\text{C-C})$ is very active under H₂.

The surface transformation of the intermediates and the reaction mechanisms proposed are illustrated in Scheme 9.1(a) for propanal and *d*-acrolein formation on Pt/SiO₂ and Na/Pt/SiO₂. *l*-*d*-acrolein formation on Na/Pt/SiO₂ should follow scheme 9.1(b).

Pt/TiO₂

f_s of Pt on TiO₂ reduced at 373 K is 0.11 which is comparable to that of Pt/SiO₂, 0.06, and 773 K is -0.08 comparable to -0.08 of Na/Pt/SiO₂ (Na/Pt = 1.5). The electronic state of Pt is almost the same and so-called electronic effects on catalyses should be similar for both pairs. But in fact the catalyses of each pair were totally different and the similarities were rather found in Pt/SiO₂ - Na/Pt/SiO₂ pair and Pt/TiO₂ pair. $\Sigma i d_i / 6 \Sigma d_i$ for propanal formation and IR spectra are alike for both reduction temperature of Pt/TiO₂ in addition to the production of allyl alcohol. Thus, what determines the catalyses is the structural

feature of catalyst surface, for example, composition of active site, rather than the absolute value of the d-density of Pt.

The similarities in activation energy of formation, the D/H picking up ratio, $\Sigma d_i / 6 \Sigma d_i$, of propanal formation, IR adsorption of C=O stretching regions and its reactivity to hydrogen (1722 cm^{-1} to 1720 cm^{-1} and 1685 cm^{-1} to 1686 cm^{-1} , corresponding to two kinds of $\eta^2(\text{C-C})$ species) suggest the identification of the active site for propanal on both reduction temperature and its environment under the reaction. 1722 and 1720 cm^{-1} bands are near gas phase C=O stretching of acrolein, which may come from the adspecies $\eta^2(\text{C-C})$ without net electron donation or acceptance with surface. 1685 and 1686 cm^{-1} shift by ca. 40 cm^{-1} from them and are suggested to include direct chemical interactions of carbonyl, perhaps with suboxide of titanium, Ti^{n+} ($n < 4$). [14]

Propanal formation reasonably follows associative mechanism of C=C bond illustrated in scheme 9.1(a) similarly to Pt/SiO₂ and Na/Pt/SiO₂.

The increase of the relative rate of acrolein exchange reaction (Table 9.2(a)) is notable. The suppression of hydrogen adsorption by 773 K-reduction, the rate of propanal formation and the rate of exchange reaction are by a factor of 750, 6 and 1.7, respectively, that is, the exchange is suppressed little by SMSI state. No or little suppression of hydrogenation and hydrogen exchange reaction have rather commonly been observed in previous chapters and it is probably due to site differentiation, one site for only hydrogen the other site for both, or selective coverage of inactive atoms for hydrogenation (but active for adsorbing hydrogen in H/M measurement) by migrated TiO₂. The latter is more likely for D₂-acrolein reaction on Pt/TiO₂ because no evidence for the isotope distributions and for adsorbates on

surface accompanied by the new kind of site creation.

The disagreement of $\Sigma d_i / 6\Sigma d_i$ between allyl alcohol formation and propanal formation for both reduction temperatures proves the different D/H surface ratio of their creation and suggests the existence of different site for each products. This "surface heterogeneity of deuterium atmosphere" exists on SMSI-Ir/Nb₂O₅ where allyl alcohol formed on less D/H environment. (chapter 7) One feature of allyl alcohol formation, the deuterium observed on terminal carbon of the molecule, has been observed also on Ir/Nb₂O₅ (chapter 7) and Pt/Nb₂O₅ (chapter 8). In the present case of Pt/TiO₂, there are reasonably two paths for the formation, one produces CH₂=CHCHDOD and the other produces CHD=CHCH₂OD. On 373 K-reduced catalyst, the former is advantageous and on 773 K-reduction the latter is advantageous (Table 9.4). η^4 -species is proposed as an intermediate for the latter path and the total mechanism follows Scheme 9.1(b) and (c). The band appears at 1382 cm⁻¹ (373 K-reduced catalyst) and 1386 cm⁻¹ (773 K-reduced catalyst) likely to correspond to C-O stretching of η^4 -adsorbate. Increase in the intensity by high temperature reduction is reasonably related to the increase in the total population of this species and, consequently, the amount of the products. 1658 and 1654 cm⁻¹ are attributed to the C=C stretching of η^2 (C-O) adsorbate. It may be related to the path of CH₂=CHCHDOD formation.

The active site for the allyl alcohol formation through η^4 -intermediate was proved to be located at the periphery of the migrated support suboxides on the metal surface (chapter 7 and 8). It is consistent to the increasing population of η^4 -adspecies (comparison of Figure 9.2 (a) with (b)) and of CHD=CHCH₂OH and CHD=CHCH₂OD (Table 9.4) that this path proceeds

on the peripheral site of TiO_2 ($x < 2$); this site might exist only on the boundary of the Pt particles and the TiO_2 support in 373 K-reduced catalyst but everywhere on Pt particles in 773 K-reduced catalyst (, assuming migrated TiO_2 is dispersed finely).

$\text{Pt}/\text{Y}_2\text{O}_3$

H/Pt of $\text{Pt}/\text{Y}_2\text{O}_3$ is almost constant against the reduction temperature. h_1 of this catalyst largely changes from 0.66 for 473 K reduction to 0.73 for 773 K reduction. Thus the Pt particles are proposed to be modified in electronic state without coverage of inactive suboxide by high temperature reduction. $\text{Pt}/\text{Y}_2\text{O}_3$ may be more adequate for the elucidation of "pure" electronic effect rather than $\text{Na}/\text{Pt}/\text{SiO}_2$ which has Na on Pt particles.

Consistency of the activation energy for propanal and allyl alcohol, rate of acrolein exchange reaction and isotope distributions of propanal and allyl alcohol suggests that the active sites for these reactions and their environment are not changed by the reduction temperature of the catalyst. This is supported by IR spectra of 473 K reduction, 1672 cm^{-1} (assigned to C=O stretching of $\eta^2(\text{C-C})$), 1618 cm^{-1} (assigned to C=C stretching of $\eta^2(\text{C-O})$) and 1367 cm^{-1} (assigned to C=O stretching of η^1 -adsorbate), which showed little shift into 1673 cm^{-1} , 1619 cm^{-1} and 1367 cm^{-1} , respectively, in 773 K reduction and in which the declining rate of adsorbate by H_2 was not changed.

The site of allyl alcohol formation is suggested to be different from that of propanal, based on the disagreement of $\Sigma d_i / 6\Sigma d_i$, which is similar to Pt/TiO_2 . The production of $\text{CHD}=\text{CHCH}_2\text{OH}$ and $\text{CHDCHCH}_2\text{OD}$ reasonably proposes the path through η^1 -adsorbate for allyl alcohol formation for both reduction

temperature. This species might be formed on the boundary of the conjunction of metal and support oxide. The difference from Pt/TiO₂ is that the contribution of this path become less at 773 K-reduction (Table 9.4). This may be caused by that the oxidation number of yttrium composing this active site is higher than that of dominating yttrium species after 773 K-reduction. This is consistent to the activity decrease by 773 K-reduction in spite of the constant propanal formation rate (Figure 9.1(b)).

As a whole, the electronic modification by the support brought about minor effect on the mechanisms of hydrogenation. The reaction schemes proposed are summarized in Scheme 9.1(a) for propanal, and (b) and (c) for allyl alcohol.

Pt/ZrO₂

Suppression of hydrogen adsorption by 773 K reduction and its regeneration through oxidation followed by 373 K reduction suggests that modification of this catalyst by reduction treatment is similar to SMSI catalysts but its range is small (0.75 to 0.60, Table 9.1).

It is proved by the dis coincidence of $\Sigma i d_i / 6 \Sigma d_i$ between propanal and allyl alcohol that the active site and its reaction environment are different between two products also on this catalysts. The activity, activation energy and isotope distribution for propanal suggest that the site and environment for this product do not depend on the reduction temperature of the catalyst. Further, it is proposed by the lack of CHD=CHCH₂OH and CHD=CHCH₂OD in the isotope distribution of allyl alcohol that the formation proceeds through C=O associative adspecies only. The suppression of the rate of exchange $r_{e, s} / r_{p, a}$ of acrolein (1.3 → 0.8) is caused by the suppression of terminal hydrogen

exchange. (Table 9.2(a), the other species were not decreased much). This intermediate might be related to the band of 1706 cm^{-1} , which is active to hydrogen circulation and absent on 773 K-reduced catalyst. This band should be assigned to C=O stretching of $\eta^2(\text{C-C})$.

1725 cm^{-1} is also assigned to C=O stretching of another $\eta^2(\text{C-C})$ and 1656 cm^{-1} (and shifted to 1649 by 773 K reduction) is attributed to the vinyl stretching of $\eta^2(\text{C-O})$. The increase of the rate of allyl alcohol formation should correspond to the increase in the intensity of this band. The reduction of ZrO_2 maybe results in the contribution to the number of the active site for allyl alcohol accompanied by H/Pt depression and the difference of the oxidation number may relates the activation energy change in Figure 9.1(c).

The proposed D_2 -acrolein reaction mechanism is demonstrated in Scheme 1(a) and (b). There are at least two kinds of site for (a).

Pt/ CeO_2

Pt/ CeO_2 showed SMSI-type hydrogen adsorption suppression but the capacity reduced was only half(0.44 \rightarrow 0.22). In the present study of 773 K reduction, C=O bond was activated for hydrogenation without enhancement of C=C hydrogenation rate. But isotope distributions of acrolein, propanal and allyl alcohol were independent of the reduction temperature in addition to the rate of formation of deuterated acrolein and propanal. Thus the enhancement of C=O deuteration is due to increase of the number of sites for allyl alcohol, which is not active for acrolein exchange reaction, especially in aldehydic hydrogen.

The environment of active site of allyl alcohol are not

completely constant because activation energy significantly increased on 773 K reduced catalyst. It is probably due to that the oxidation number of cerium atom which is a component of the active site is reduced and the energy barrier for deuterium dissociation increases.

References

1. W.F.Turley, R.Adams, *J.Amer.Chem.Soc.*, **47**, 5061 (1925).
2. P.N.Rylander, D.R.Steele, *Tetrahedron Lett.*, 1579 (1969).
3. Y.Nitta, T.Imanaka, S.Teranishi, *Bull.Chem.Soc.Jpn.*, **53**, 3154 (1980).
4. Y.Nagase, H.Hattori, K.Tanabe, *Chem.Lett.*, 1645, (1983).
5. Z.Poltarzewski, S.Galvagno, R.Peitropaolo, P.Staitti, *J.Catal.*, **102**, 190 (1986).
6. M.A.Vannice, B.Sen, *J.Catal.*, **115**, 65 (1989).
7. C.Sudhakar, M.A.Vannice, *J.Catal.*, **95**, 227 (1985).
8. C.Dall'Agnol, A.Gervasini, F.Morazzoni, F.Pinna, G.Strukul, L.Zanderighi, *J.Catal.*, **96**, 106 (1985).
9. R.Szymanski, H.Charcosset, P.Gallezot, J.Massardier, L.Tournayan, *J.Catal.*, **97**, 366 (1986).
10. G.C.Bond, M.A.Duarte, *J.Catal.*, **111**, 189 (1988).
11. Y.J.Lin, D.E.Resasco, G.L.Haller, *J.Chem.Soc., Faraday Trans. 1*, **83**, 2091 (1987).
12. L.Mendelovici, M.Steinberg, *J.Catal.*, **96**, 285 (1985).
13. Y.Hamada, Y.Nishimura, M.Tsuboi, *Chem.Phys.*, **100**, 365 (1985).
14. P.G.Harrison, B.Maunders, *J.Chem.Soc., Faraday Trans. 1*, **81**, 1345 (1985).

Table 9.1 The dispersion of Pt particle (H/Pt) reduced at several temperature.

T_R / K	373	473	773	773-673ox-373
Pt/TiO ₂	0.75		0.001	0.70
Pt/Y ₂ O ₃		0.20	0.19	
Pt/ZrO ₂	0.75		0.60	0.73
Pt/CeO ₂	0.44		0.22	0.40

773-673ox-373 represents 773 K reduction followed by 673 K oxidation and 373 K reduction. The reduction time of catalyst was 60 min and the hydrogen adsorption experiments were carried out at room temperature. The state of Pt on Y₂O₃ reduced at 373 K was oxide.

Table 9.2 (a) The relative ratio of formation and the distributions of *d*-acroleins at the initial stage of D_2 - $CH_2=CHCHO$ reaction on Pt/TiO₂, Pt/Y₂O₃, Pt/ZrO₂, and Pt/CeO₂.

catalyst	TiO ₂		Y ₂ O ₃		ZrO ₂		CeO ₂	
	373 K	773 K	473 K	773 K	373 K	773 K	373 K	773 K
CHD=CHCHO	4	9	5	6	6	6	5	6
CH ₂ =CDCHO	2	6	3	3	3	5	4	4
CH ₂ =CHCDO	2	3	1	1	1	2	2	2
CHD=CDCHO	2	3	2	2	3	1	1	1
r_{ex}/r_{pa}	0.7	2.5	1.2	1.2	1.3	0.8	1.2	1.1

Reactions were carried out at 393 K. $P_{D_2} = 5.2$ kPa, $P_{CH_2=CHCHO} = 1.3$ kPa. Three or four times of samplings were carried out before the total conversion of acrolein reached 15%. $r_{ex} = r_{d_1-ac} + r_{d_2-ac}$, i.e. (total exchange rate)=(the rate for *d*₁-acrolein)+2(the rate for *d*₂-acrolein). r_{pa} : the rate for propanal formation.

Table 9.2 (b) The relative ratio of formation and the distributions of *d*-acroleins at the initial stage of D_2 - $CH_2=CHCHO$ reaction on Pt/Na/SiO₂.

Na / Pt	0.00	0.19	0.75	1.5	2.3	6.1
CHD=CHCHO	5	4	6	7	6	7
CH ₂ =CDCHO	3	3	3	3	4	4
CH ₂ =CHCDO	0	2	6	6	5	6
CHD=CDCHO	0	1	1	0	1	0
r_{ex} / r_{Pa}	0.9	1.3	1.8	1.7	1.9	2.0

Reactions were carried out at 393 K. $P_{D_2} = 5.2$ kPa, $P_{CH_2=CHCHO} = 1.3$ kPa. Three or four times of samplings were carried out before the total conversion of acrolein reached 15%. $r_{ex} = r_{d_1-ac} + r_{d_2-ac}$, i.e. (total exchange rate)=(the rate for *d*₁-acrolein)+2(the rate for *d*₂-acrolein). r_{Pa} : the rate for propanal formation.

Table 9.3 (a) The percentage distributions of *d*-propanals at the initial stage of D_2 - $CH_2=CHCHO$ reaction on Pt/TiO₂, Pt/Y₂O₃, Pt/ZrO₂, and Pt/CeO₂.

catalyst	TiO ₂		Y ₂ O ₃		ZrO ₂		CeO ₂	
	373 K	773 K	473 K	773 K	373 K	773 K	373 K	773 K
d ₀	1	2	1	2	1	3	2	1
d ₁	18	19	18	10	24	22	21	24
d ₂	36	41	47	44	47	50	47	46
d ₃	33	28	25	24	20	19	24	22
d ₄	11	10	9	10	8	6	6	6
$\Sigma id_i / 6\Sigma d_i$	39	38	37	37	35	34	35	34

Reactions were carried out at 393 K. $P_{D_2} = 5.2$ kPa, $P_{CH_2=CHCHO} = 1.3$ kPa. Deuterium was found only on the C=C carbon atoms and no aldehydic deuterium was observed.

Table 9.3 (b) The percentage distributions of *d*-propanals at the initial stage of $D_2 - CH_2=CHCHO$ reaction on Pt/Na/SiO₂.

Na / Pt	0.00	0.19	0.75	1.5	2.3	6.1
<i>d</i> ₀	6	11	19	21	21	19
<i>d</i> ₁	26	27	29	31	30	28
<i>d</i> ₂	45	39	35	32	33	36
<i>d</i> ₃	17	22	17	16	16	17
<i>d</i> ₄	5	1	0	0	0	0
$\Sigma id_i / 6\Sigma d_i$	31	29	25	24	24	25

Reactions were carried out at 393 K. $P_{D_2} = 5.2$ kPa, $P_{CH_2=CHCHO} = 1.3$ kPa. Deuterium was found only on the C=C carbon atoms and no aldehydic deuterium was observed.

Table 9.4 The percentage distributions of *d*-allyl alcohols at the initial stage of $D_2 - CH_2=CHCHO$ reaction on Pt/TiO₂, Pt/Y₂O₃, Pt/ZrO₂, and Pt/CeO₂.

catalyst	TiO ₂		Y ₂ O ₃		ZrO ₂		CeO ₂	
	373 K	773 K	473 K	773 K	373 K	773 K	373 K	773 K
CH ₂ =CHCH ₂ OH	13	14	16	14	18	17	18	17
CH ₂ =CHCH ₂ OD	13	7	11	14	13	17	16	18
CH ₂ =CHCHDOH	11	3	6	8	15	11	13	15
CHD=CHCH ₂ OH	2	6	7	5	0	0	0	0
CH ₂ =CHCHDOD	52	25	28	36	54	55	53	50
CHD=CHCH ₂ OD	9	45	32	23	0	0	0	0
$\Sigma d_i / 6\Sigma d_i$	25	26	24	24	23	23	23	22

Reactions were carried out at 393 K. $P_{D_2} = 5.2$ kPa, $P_{CH_2=CHCHO} = 1.3$ kPa.



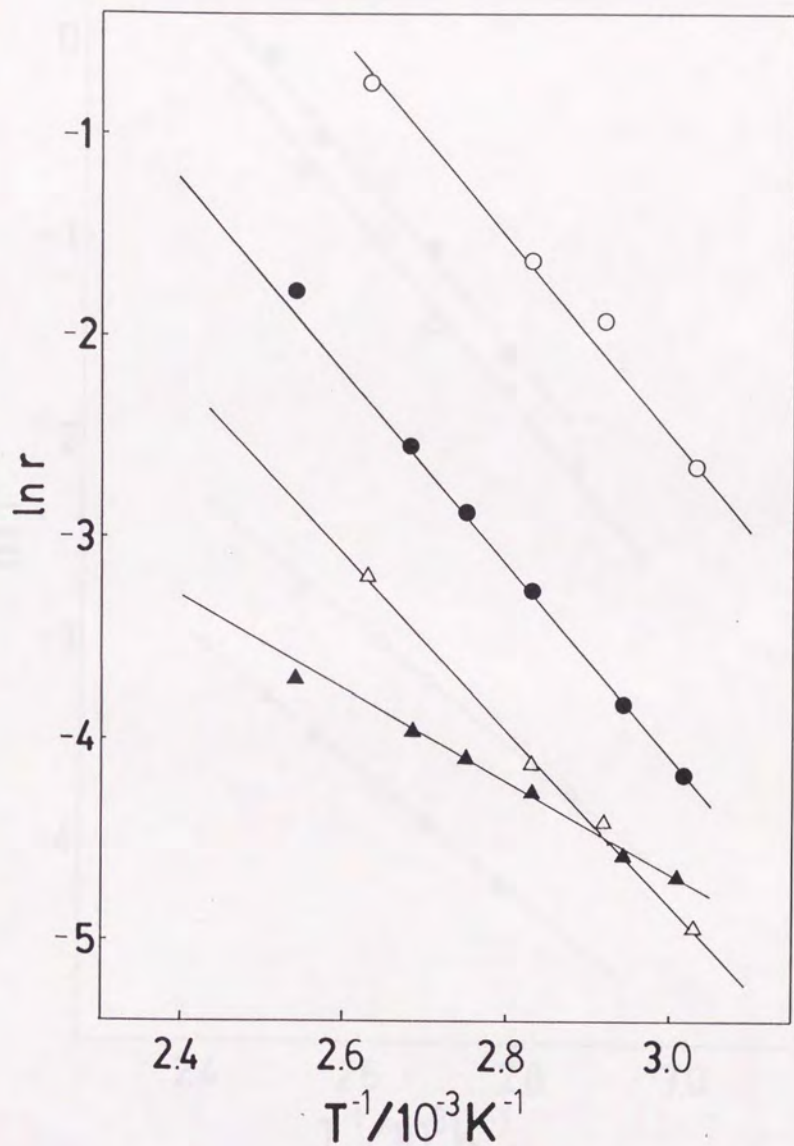


Figure 9.1 (a) Arrhenius plots for D_2 -acrolein reaction on 373 K reduced Pt/TiO₂; ○ : propanal formation, △ : allyl alcohol formation. On 773 K reduced Pt/TiO₂; ● : propanal formation, ▲ : allyl alcohol formation. $P_{\text{D}_2} = 5.2 \text{ kPa}$, $P_{\text{CH}_2=\text{CHCHO}} = 1.3 \text{ kPa}$.

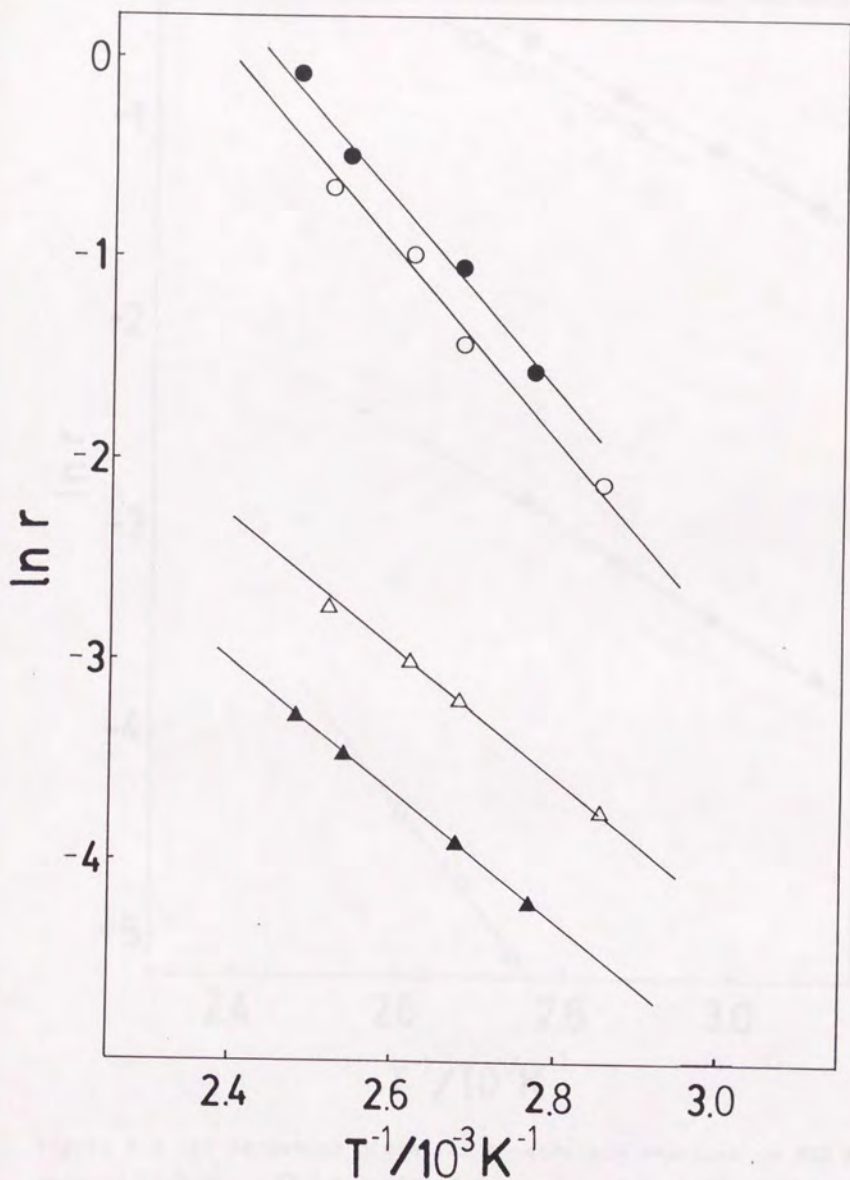


Figure 9.1 (b) Arrhenius plots for D₂-acrolein reaction on 473 K reduced Pt/Y₂O₃; ○: propanal formation, Δ: allyl alcohol formation. On 773 K reduced Pt/Y₂O₃; ●: propanal formation, ▲: allyl alcohol formation. P_{D₂} = 5.2 kPa, P_{C₃H₂=C₃H₃O} = 1.3 kPa.

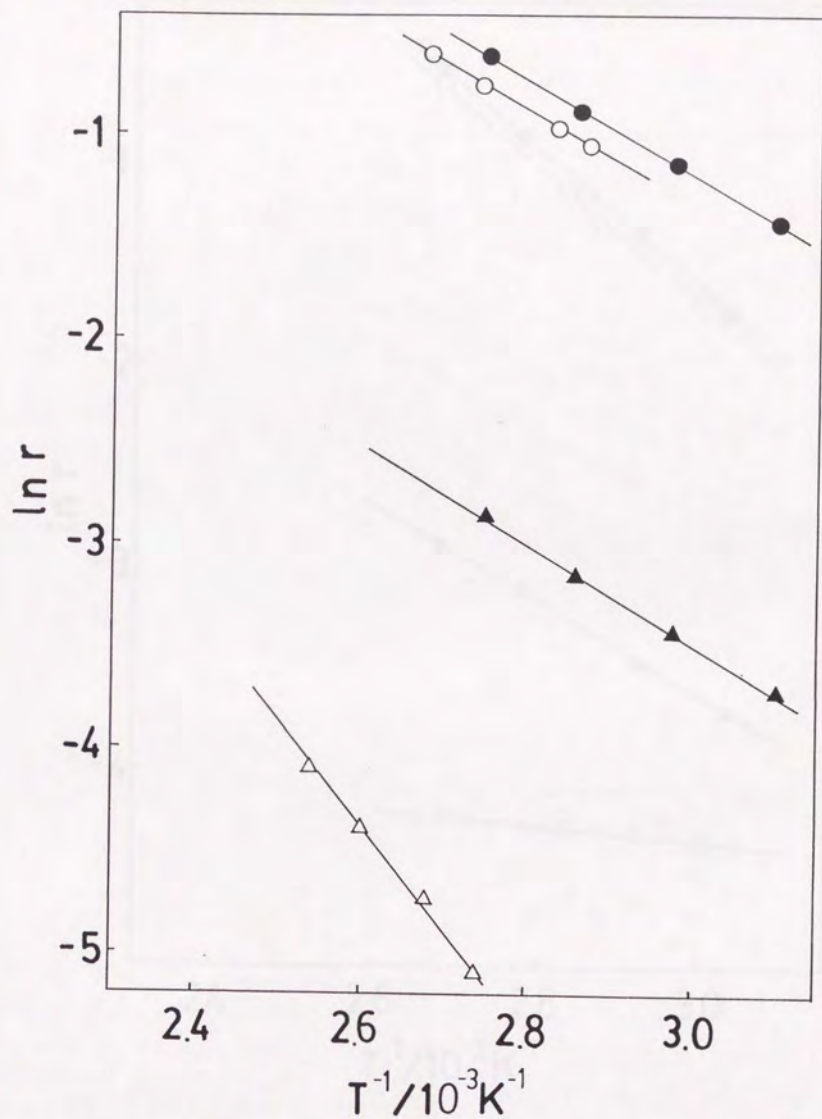


Figure 9.1 (c) Arrhenius plots for D_2 -acrolein reaction on 373 K reduced Pt/ZrO₂; ○: propanal formation, △: allyl alcohol formation. On 773 K reduced Pt/ZrO₂; ●: propanal formation, ▲: allyl alcohol formation. $P_{D_2} = 5.2$ kPa, $P_{CH_2=CHCHO} = 1.3$ kPa.

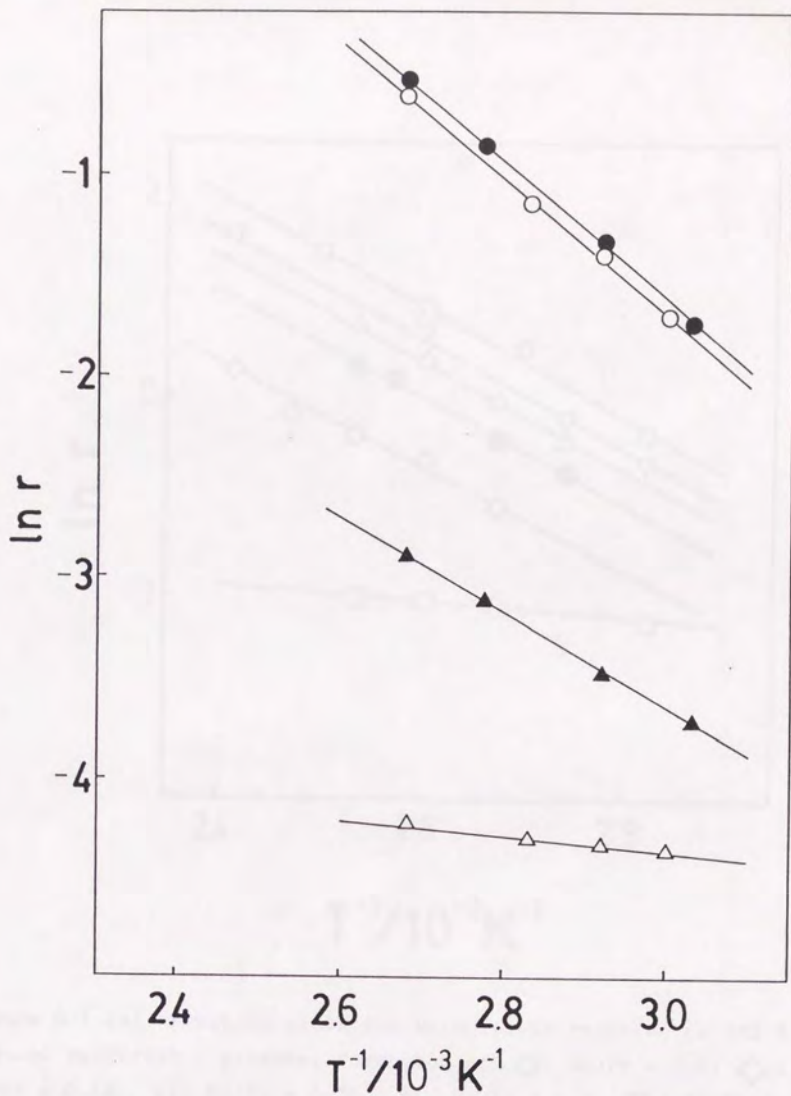


Figure 9.1 (d) Arrhenius plots for D_2 -acrolein reaction on 373 K reduced Pt/CeO₂; ○: propanal formation, △: allyl alcohol formation. On 773 K reduced Pt/CeO₂; ●: propanal formation, ▲: allyl alcohol formation. $P_{D_2} = 5.2$ kPa, $P_{CH_2=CHCHO} = 1.3$ kPa.

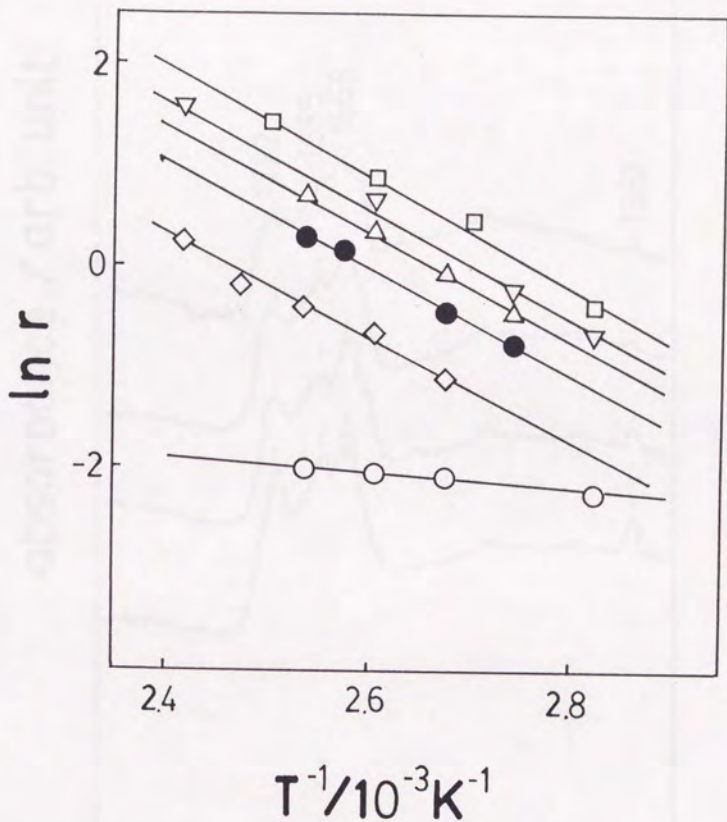


Figure 9.1 (e) Arrhenius plots for D_2 -acrolein reaction on 673 K reduced Na/Pt/SiO₂; propanal formation of ○: Na/Pt = 0.0, ◇: Na/Pt = 0.19, ●: Na/Pt = 0.75, △: Na/Pt = 1.5, ▽: Na/Pt = 2.3, □: Na/Pt = 6.1. $P_{D_2} = 5.2$ kPa, $P_{CH_2=CHCHO} = 1.3$ kPa.

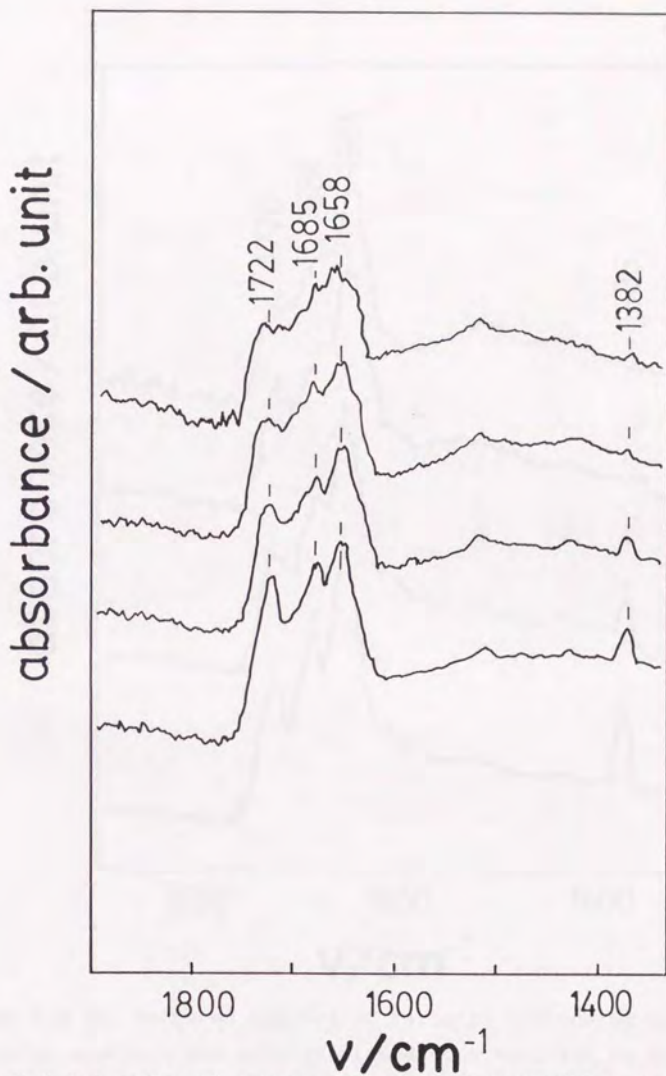


Figure 9.2 (a) Infrared spectra of carbonyl stretching region of adsorbing acrolein and subsequent hydrogen addition on Pt/TiO₂ reduced at 373 K. The spectra are, from bottom to top, after adsorption of acrolein, after 10 min of hydrogen circulation and evacuation of 10 min, after additional 10 min of hydrogen circulation and evacuation of 10 min and further additional 20 min of hydrogen circulation and evacuation of 10 min. Acrolein was adsorbed at 298 K and hydrogen circulation temperature were 353 K.

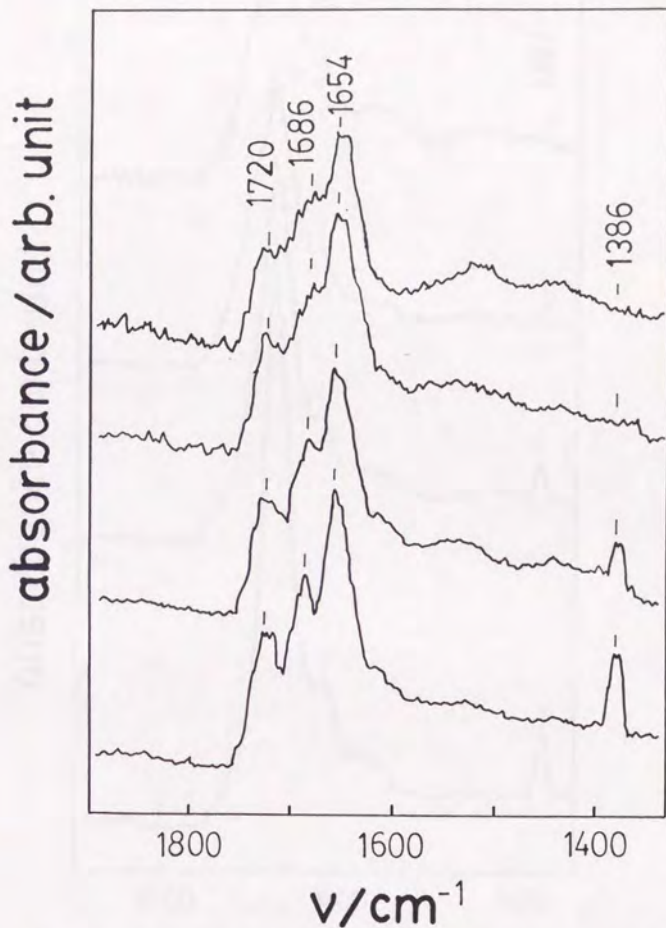


Figure 9.2 (b) Infrared spectra of carbonyl stretching region of adsorbing acrolein and subsequent hydrogen addition on Pt/TiO_2 reduced at 773 K. The spectra are, from bottom to top, after adsorption of acrolein, after 10 min of hydrogen circulation and evacuation of 10 min, after additional 10 min of hydrogen circulation and evacuation of 10 min and further additional 20 min of hydrogen circulation and evacuation of 10 min. Acrolein was adsorbed at 298 K and hydrogen circulation temperature were 353 K.

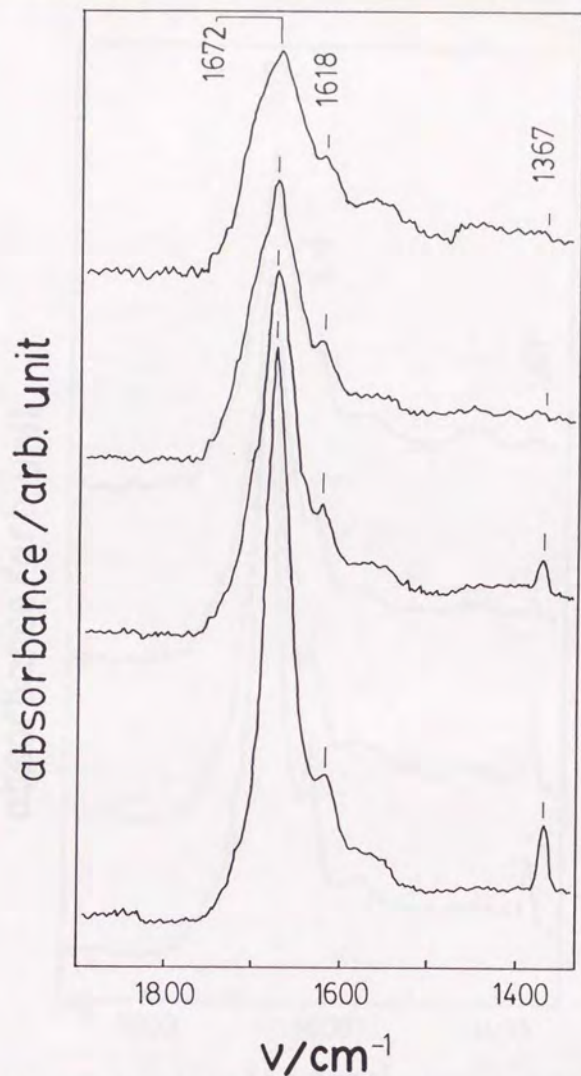


Figure 9.2 (c) Infrared spectra of carbonyl stretching region of adsorbing acrolein and subsequent hydrogen addition on Pt/Y₂O₃ reduced at 473 K. The spectra are, from bottom to top, after adsorption of acrolein, after 10 min of hydrogen circulation and evacuation of 10 min, after additional 10 min of hydrogen circulation and evacuation of 10 min and further additional 20 min of hydrogen circulation and evacuation of 10 min. Acrolein was adsorbed at 298 K and hydrogen circulation temperature were 353 K.

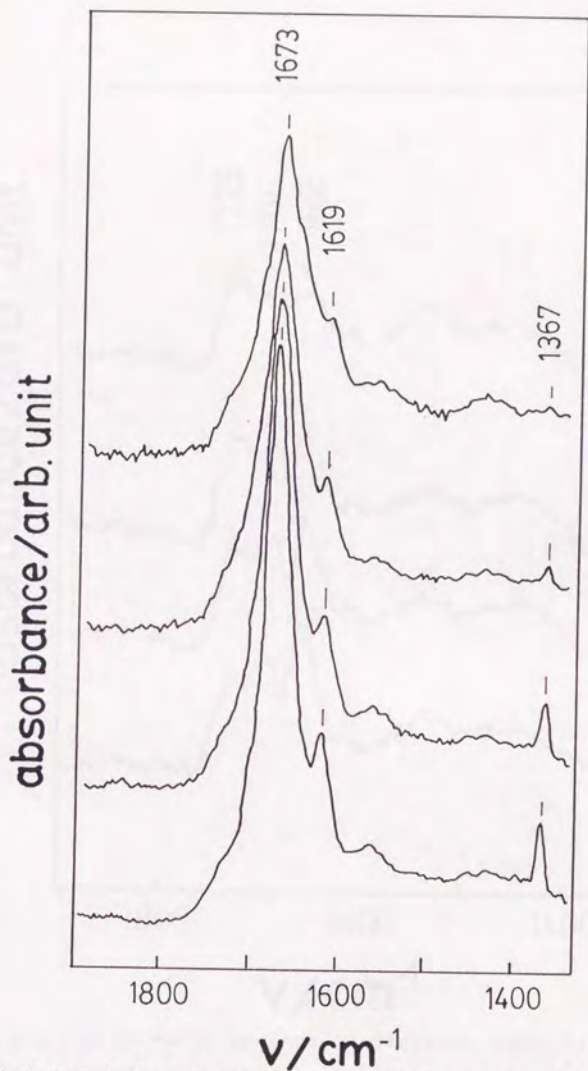


Figure 9.2 (d) Infrared spectra of carbonyl stretching region of adsorbing acrolein and subsequent hydrogen addition on Pt/Y₂O₃ reduced at 773 K. The spectra are, from bottom to top, after adsorption of acrolein, after 10 min of hydrogen circulation and evacuation of 10 min, after additional 10 min of hydrogen circulation and evacuation of 10 min and further additional 20 min of hydrogen circulation and evacuation of 10 min. Acrolein was adsorbed at 298 K and hydrogen circulation temperature were 353 K.

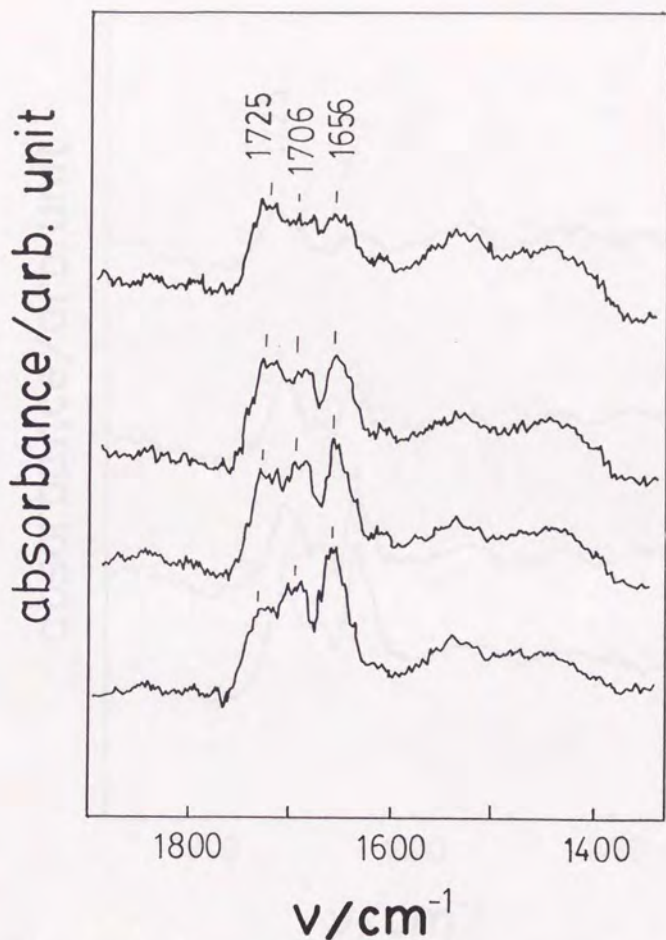


Figure 9.2 (e) Infrared spectra of carbonyl stretching region of adsorbing acrolein and subsequent hydrogen addition on Pt/ZrO₂ reduced at 373 K. The spectra are, from bottom to top, after adsorption of acrolein, after 10 min of hydrogen circulation and evacuation of 10 min, after additional 10 min of hydrogen circulation and evacuation of 10 min and further additional 20 min of hydrogen circulation and evacuation of 10 min. Acrolein was adsorbed at 298 K and hydrogen circulation temperature were 353 K.

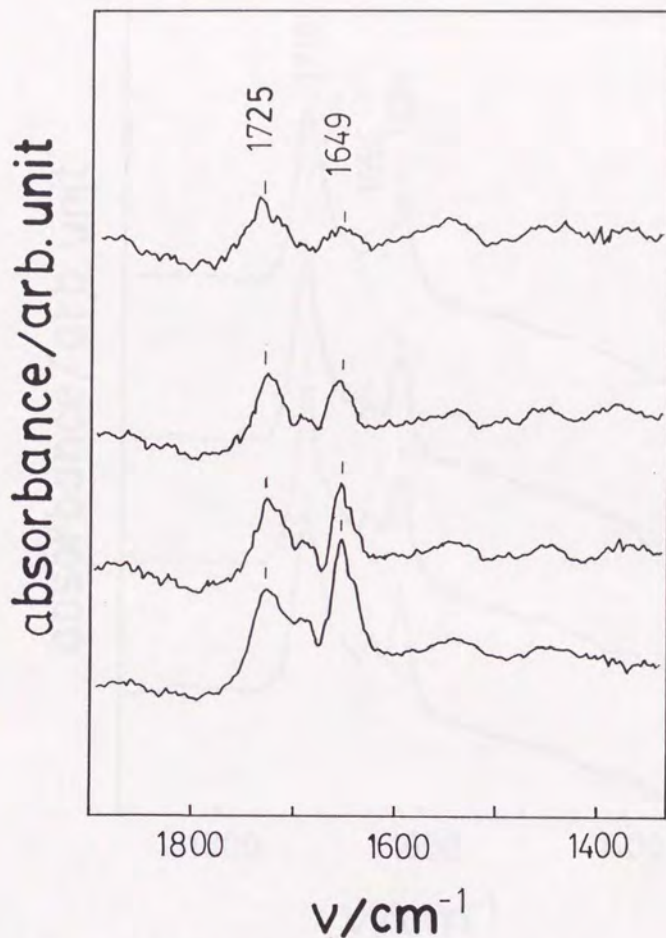


Figure 9.2 (f) Infrared spectra of carbonyl stretching region of adsorbing acrolein and subsequent hydrogen addition on Pt/ZrO₂ reduced at 773 K. The spectra are, from bottom to top, after adsorption of acrolein, after 10 min of hydrogen circulation and evacuation of 10 min, after additional 10 min of hydrogen circulation and evacuation of 10 min and further additional 20 min of hydrogen circulation and evacuation of 10 min. Acrolein was adsorbed at 298 K and hydrogen circulation temperature were 353 K.

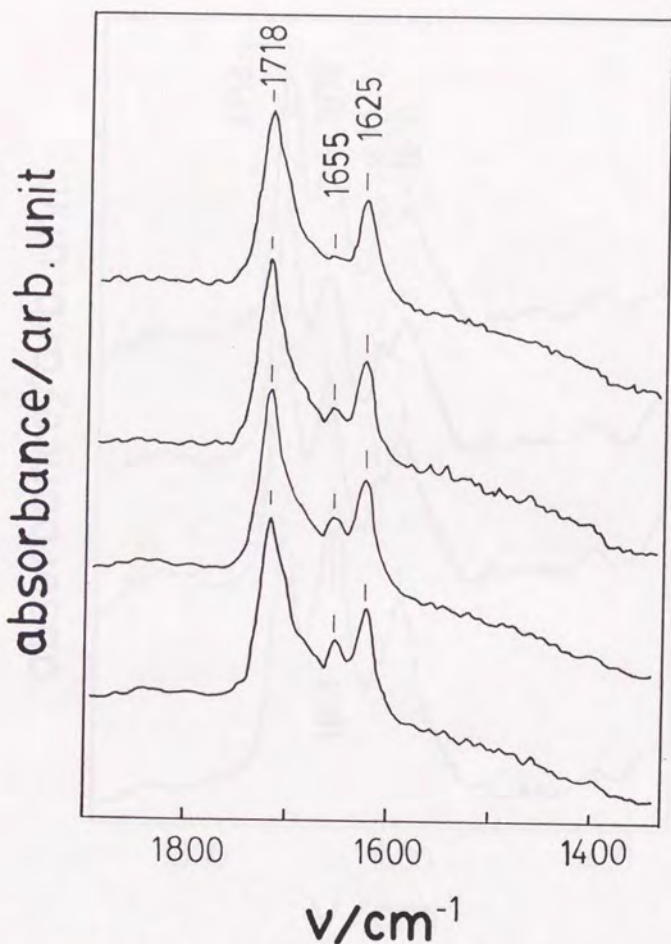


Figure 9.2 (g) Infrared spectra of carbonyl stretching region of adsorbing acrolein and subsequent hydrogen addition on Pt/SiO₂ reduced at 673 K. The spectra are, from bottom to top, after adsorption of acrolein, after 10 min of hydrogen circulation and evacuation of 10 min, after additional 10 min of hydrogen circulation and evacuation of 10 min and further additional 20 min of hydrogen circulation and evacuation of 10 min. Acrolein was adsorbed at 298 K and hydrogen circulation temperature were 333 K.

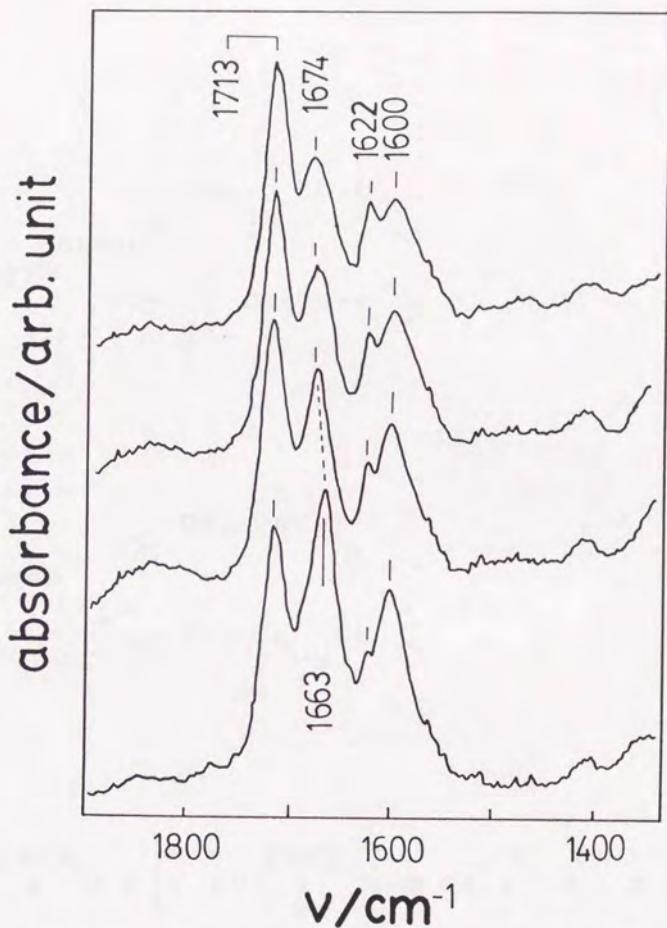
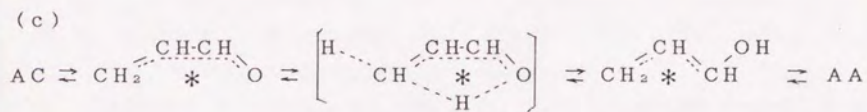
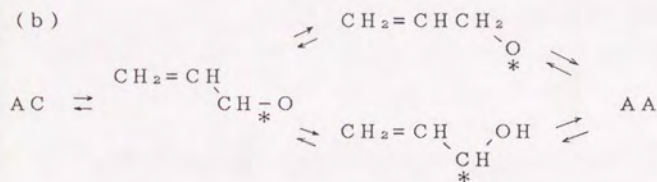
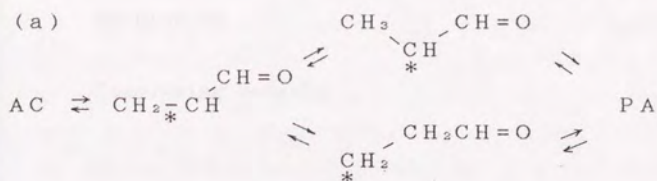


Figure 9.2 (h) Infrared spectra of carbonyl stretching region of adsorbing acrolein and subsequent hydrogen addition on Na/Pt/SiO₂ (Na/Pt = 1.5) reduced at 673 K. The spectra are, from bottom to top, after adsorption of acrolein, after 10 min of hydrogen circulation and evacuation of 10 min, after additional 10 min of hydrogen circulation and evacuation of 10 min and further additional 20 min of hydrogen circulation and evacuation of 10 min. Acrolein was adsorbed at 298 K and hydrogen circulation temperature were 333 K.



Scheme 9.1 Proposed hydrogenation and exchange processes of acrolein on Pt surface. AA, allyl alcohol; AC, acrolein; PA, propanal.

Chapter 10

Concluding Remarks

This thesis deals with several aspects of surface heterogeneity of hydrogenating catalysts in relation to elementary steps. Ethene and substituted ethanes, especially acrolein, are used as probe molecules of the hydrogenation mechanisms to elucidate active sites and their reaction environments.

These reactions are usually treated as "structure insensitive" reactions in comparison with "structure sensitive" reactions as a first test for the catalysts. The comparison of activities is a cheap characterizing method of the catalysts and has been applied in the research of SMSI catalysts. Ethene hydrogenation activity decreases by a few orders of magnitude after low temperature reduction while ethane hydrogenolysis activity decreases by six orders of magnitude. [1] This sort of study includes no reaction mechanisms of surface but the interpretation. It needs the exploitation of the mechanism to elucidate the nature of catalysis on the heterogeneous surface of SMSI catalysts.

In fact, even ethene hydrogenation showed the notable difference in mechanism from the uniform surface --- two kinds of active site and reaction environments were distinguished. Acrolein hydrogenation could probe the heterogeneity further in relation to chemical selectivity. It is interesting also in the view of organic synthesis. Acrolein hydrogenation was quite different from CO hydrogenation in spite of the same kinds of factor ruling the activation apparently. [2]

The electronic effects are dealt with in the thesis but this words are less important in an influence on hydrogenation mechanisms than it seems and is noted everywhere. One reasonable explanation is that the reactant molecules, ethene and substituted ethenes, would be buffer of the electron and the

electronical change in hydrogen adsorption sites is small during the reaction.

10.1 Ethene Deuteration

Chapter 3 to 6 described ethene deuteration mechanisms on noble metal catalysts with "support effects" and "promotion effects." Metal-support interaction was classified by new criteria in chapter 6, electronic modification of metal particles and decoration of the metal surface with support oxides. The density of unoccupied d-state of Pt particle on Pt/ZrO₂ and Pt/Y₂O₃ were elucidated to be controllable by the choice of reduction temperature of the catalysts. The variation of them was larger than that of Pt/TiO₂ and Pt/Nb₂O₅ SMSI-catalysts. On the other hand, the reduction temperature of Pt/V₂O₅ showed no variation of electronic modification on Pt particles at least d-state density but the reversible migration of support oxides on to the metal surface was suggested. VO_x covered metal particle completely by 773 K reduction, as suggested by the deuterioethane distributions in chapter 6, while the SMSI catalysts remained metallic catalysis.

Dual site surface model for ethene deuteration was proposed as to SMSI-Rh/Nb₂O₅, SMSI-Ir/Nb₂O₅, SMSI-Pt/TiO₂ and Na/Pt/SiO₂. Site I (bare metal site) adsorbs CH₂=CH₂ and D₂ and produces d₂-ethane mainly, while site II (peripheral site of NbO_x on metal) adsorbs CH₂=CH₂ only and produces d₀-ethane mainly. Inverse distribution of ethanes formed on site II was reasonably explained by the deuterium supply through surface diffusion and the shuffling by H in adsorbed ethene. It is elucidated that under steady state of deuteration, two kinds of site with

different deuterium environments (surface D/H ratios) permanently exist on metal surface.

Na/Pt/SiO₂ was shown to have two kinds of site but different from those of SMSI catalysts. Site I (bare metal site) bears ethane formation and site II (peripheral site of Na₂O) bears exchange reaction. Electronic disturb of Pt measured by XPS and XANES is rather related with site I because of its large abundant. But the electrons donated by Na was removed by adsorbed ethene which affected little in rate of ethane formation, as demonstrated in chapter 5.

The relation between electronic state measured by XPS or XANES and catalyses needs further consideration. XANES is not surface sensitive and XPS is treated as surface sensitive probe in usual but escape depth is not negligible as for fine particles. Thus, strictly speaking, the conclusion from the result of reaction is a "dynamic state of surface" but from spectroscopic investigations it is a "dynamic state of metal particle." This is one of the largest barrier to understand the nature of catalyst surface and often appears in spectroscopic applications. It can be suggested at most that the bulk electronic alternation reflects changes in surface electronic state. In this context, what is elucidated in chapter 5 is mutual influence between elementary steps of catalyses --- adsorption, surface reactions and desorption --- and metal particle electronic state.

The electronic state of atoms near the conjunction with the support or additives is quite different from the other surface atoms and bulk atoms. The theory states that at thermodynamic equilibrium at the interface the Fermi levels of the metal and the additive must be equal. [3, 4] If the work function of the

electrons in the additive is smaller than in the metal, electrons will flow from the additive to the metal. This explanation holds true to Na, NbO₅ and TiO₅. The screening distance in a metal is quite short; calculations indicate that the electronic perturbation is screened out within two atomic distances as commented in previous chapters. Site II was not spectroscopic detectable in a working state or even in static state.

10.2 Acrolein Deuteration

Acrolein hydrogenation/deuteration is a typical chemoselectivity-related reaction. Chapter 7 to 9 made it clear that this aspect was also useful in the exploitation of the surface in a working state. The characteristics of a simple deuteration, which was elucidated in D₂ - CH₂=CH₂ reaction, remained in acrolein deuteration; dual site mechanism and electronic perturbation influence ruled the reaction similiary. These characteristics appeared in relaiton with the origin of chemoselectivity.

Allyl alcohol formation was observed in Ir/Nb₅O₅, Pt/Nb₅O₅, Pt/TiO₂, Pt/ZrO₂, Pt/Y₂O₃ and Pt/CeO₂. In many cases, peripheral sites were effective for the formation but the intermediates were not $\eta^2(\text{C-O})$, seeming favorable to be polarized by the MO, but $\eta^4(\text{C-C-C-O})$ whose form is a strong electron acceptor. This supports the unusual electron-rich state of metal at the conjunction with additives or supports. And the coordination with electron deficient center of the support oxides, proposed often as to CO hydrogenation on the same kinds of catalysts, was not essential for the carbonyl activation in acrolein.

Deuterium in allyl alcohol is sometimes smaller than propanal which suggests the different deuterium atmosphere. It

is proved with the location of the sites in SMSI-Ir/Nb₂O₅. The sites could not be distinguished between propanal (formed through $\eta^2(\text{C-C})$) and allyl alcohol (formed through $\eta^2(\text{C-O})$) in normal state. On the contrary, SMSI state brought about the differentiation; site I adsorbs D₂ and CH₂=CHCHO (as $\eta^2(\text{C-C})$) to form propanal and site II adsorbs CH₂=CHCHO (as $\eta^4(\text{C-C-C-O})$) only to form allyl alcohol. Normal state of Pt/Nb₂O₅ was similar to Ir/Nb₂O₅. There were two sites on Pt/Nb₂O₅ but site I adsorbs D₂ and site II adsorbs CH₂=CHCHO (as $\eta^4(\text{C-C-C-O})$) to form both propanal and allyl alcohol. $\Sigma d_i / 6 \Sigma d_i$ decreased in SMSI state of Pt/Nb₂O₅.

Pt/ZrO₂, Pt/Y₂O₃ and Pt/CeO₂ formed both products but the selectivity changed less than in SMSI catalysts. But the role of site II (without decoration of MO_x it is situated at the boundary of metal particles on the supports) was proposed. Pt/SiO₂ and Na/Pt/SiO₂ did not produce detectable allyl alcohol under any condition of the previous chapters.

10.3 Other Possibilities and Future Prospect

As mentioned previously, site II is not a large part of catalyst metal particles which is not detectable in spectroscopic techniques usually but plays an important role in catalyses; it often rules whole catalytic performance. This is one of the disadvantages of spectroscopy in the elucidation of the heterogeneity of catalyst surfaces. Spectroscopic studies of electronic states in chapter 4, 5 and 6 are not related with the peripheral sites directly. In such cases, the study through reaction mechanisms takes advantages. It is needless to say that a good combination of spectroscopic techniques with reaction

tests is essential to understanding the nature of catalysis.

It may be expected in general that SMSI catalysts which have many site II are favorable for the formation of less hydrogen-needed products. In fact, CO hydrogenation around site II seems to form higher hydrocarbons more selectively than on site I or LTR catalyst in the data of ref 5 and 6. In acetonitrile hydrogenation on Pt/TiO₂ and Pt/Nb₂O₅, amines are formed in the order, secondary > primary > tertially for LTR catalyst, but tertially > secondary > primary (almost zero) for HTR catalyst. [7] This might be acceptable as a general rule.

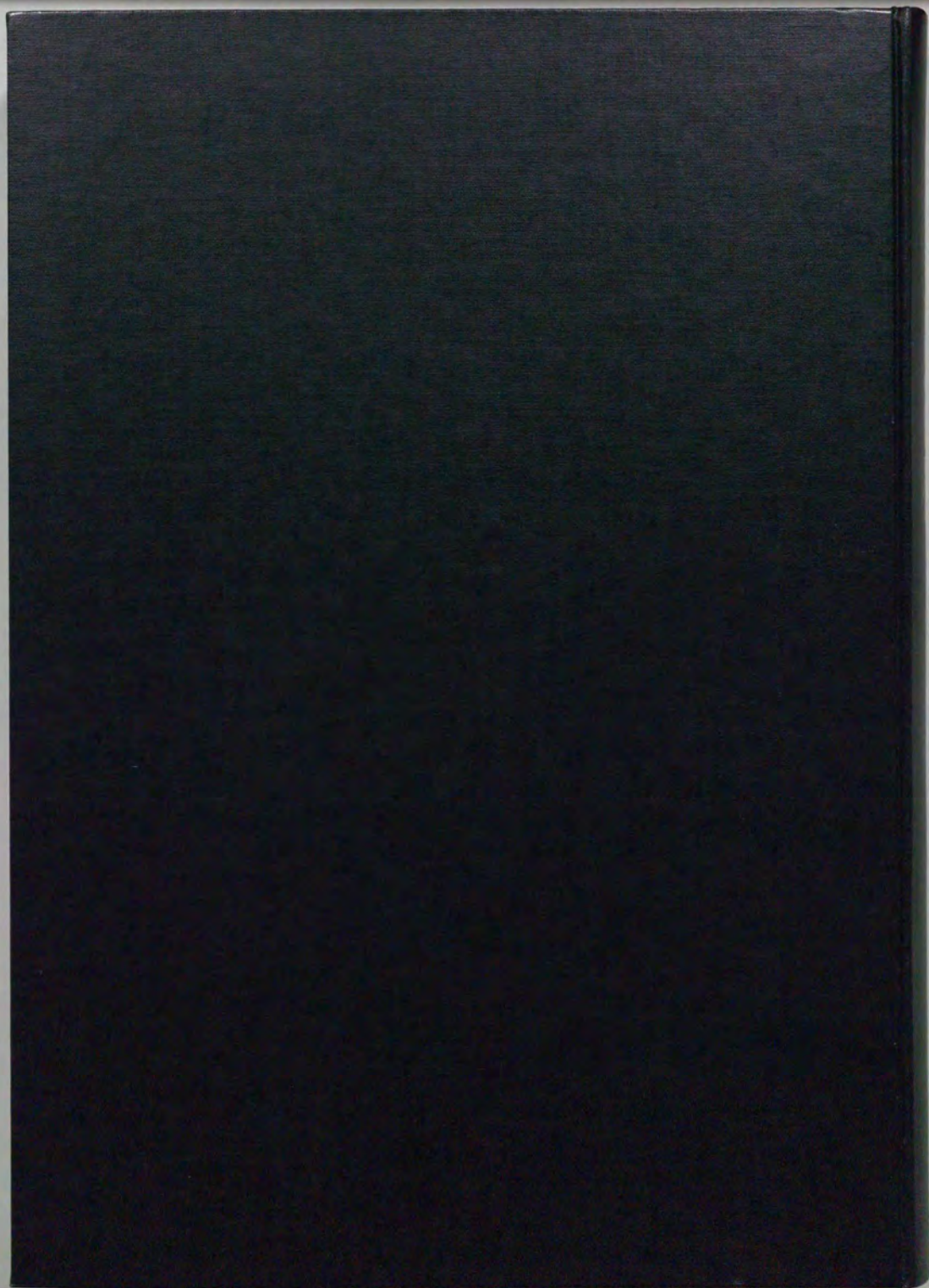
Techniques described in this thesis can be applied to other metal catalysts with metal- or oxide-additives. And these are not the only way to the clarification of metal catalysis.

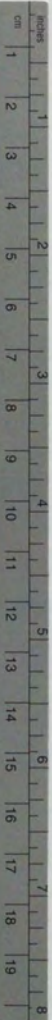
One elementary step can be a probe of metal surface in relation to the design of metal catalysts. It is well known that CO insertion to metal-ethyl bond is a key reaction of ethene hydroformylation. Rh catalysts with several kinds of promoters can be exploited by this reaction. [8] The other kind of approach is design of a intermediate on metal surface as a defined form which is followed by subsequent reactions. The major point of this study is offering a snapshot of the multi-step reaction with considerable amount of intermediates. This technique appeared in a few literature [9] and will contribute to the study of surface heterogeneity.

The methods described above will be useful techniques for chemistry of surface reactions when the elementary steps combine with surface structure originating from surface heterogeneity.

References

1. R.Burch, in "Hydrogen Effects in Catalysis" (P.Zoltan, P.G.Menon, eds.), chapter 13, Dekker, New York, 1988.
2. B.Sen, M.A.Vannice, *J.Catal.*, **113**, 52 (1988).
3. W.Schottky, *Z.Phys.*, **113**, 367 (1939).
4. L.J.Brillson, *Appl.Surf.Sci.*, **11/12**, 249 (1982).
5. M.E.Levin, K.J.Williams, M.Salmeron, A.T.Bell, G.A.Somorjai, *Surf.Sci.*, **195**, 341 (1988).
6. M.E.Levin, M.Salmeron, A.T.Bell, G.A.Somorjai, *J.Chem.Soc., Faraday Trans. 1*, **83**, 2061 (1988).
7. unpublished data of the author.
8. Y.Izumi, K.Asakura, Y.Iwasawa, *J.Chem.Soc., Chem.Commun.*, 1327 (1988).
9. K.Asakura, K.K.Bando, K.Isobe, H.Arakawa, Y.Iwasawa, *J.Am.Chem.Soc.*, **112**, 3242 (1990).





Kodak Color Control Patches

© Kodak, 2007 TM, Kodak



Kodak Gray Scale



© Kodak, 2007 TM, Kodak

A 1 2 3 4 5 6 M 8 9 10 11 12 13 14 15 B 17 18 19

